REPUBLIC OF TÜRKİYE
ANKARA UNIVERSITY
INSTITUTE OF NUCLEAR SCIENCES

MASTER'S THESIS

3D CAD BASED MONTE CARLO SIMULATION TO ESTIMATE SHIELDING EFFECTIVENESS OF AN IRRADIATION UNIT WITH ISO s-^{137}Cs SEALED SOURCES AND INVESTIGATION OF DOSE HOMOGENEITY ON RADIOMETRIC BENCH AND ITS EXPERIMENTAL VALIDATION

Ahmat Harine ABOUBAKAR

DEPARTMENT OF MEDICAL PHYSICS
HEALTH PHYSICS MASTER'S DEGREE PROGRAM

ANKARA
2025

THESIS APPROVAL

The thesis entitled **“3D CAD based Monte Carlo simulation to estimate shielding effectiveness of an irradiation unit with ISO S-$^{137}C_S$ sealed sources and investigation of dose homogeneity on radiometric bench and its experimental validation”** prepared by **Ahmat Harine ABOUBAKAR** was accepted as a **MASTER'S THESIS** in Ankara University Institute of Nuclear Sciences Medical Physics Department by the following jury unanimously/ majority vote on 22/09/2025

Supervisor: Prof. Dr. Haluk Yücel
Ankara University, Institute of Nuclear Sciences

Co-Supervisor: Prof. Dr. Serap Safran
Ankara University, Institute of Nuclear Sciences

Jury Members:

Prof. Dr. Haluk YÜCEL
Ankara University, Institute of Nuclear Sciences

Prof. Dr. Serap SAFRAN
Ankara University, Institute of Nuclear Sciences

Prof. Dr. Mustafa KARADAG
Gazi Faculty of Education, Department of Science Education,
Physics Education

Prof. Dr. OSMAN YILMAZ
Middle East Technical University, Faculty of Sciences,
Department of Physics

Assoc. Prof. Dr. Bahadir SAYGI
Ankara University, Institute of Nuclear Sciences

Approved by

Prof. Dr. Haluk YÜCEL
Director, Institute of Nuclear Sciences, Ankara University

I hereby declare that all information in this thesis has been obtained and presented in accordance with academic rules, code of ethics, and conduct. I also declare that, as required by these rules and conduct, I have fully cited and referenced all material and results that are not original to this work.

22/09/2025

Signature

Ahmat Harine ABOUBAKAR

ABSTRACT

Master's Thesis

3D CAD BASED MONTE CARLO SIMULATION TO ESTIMATE SHIELDING EFFECTIVENESS OF AN IRRADIATION UNIT WITH ISO s-$^{137}C_S$ SEALED SOURCES AND INVESTIGATION OF DOSE HOMOGENEITY ON RADIOMETRIC BENCH AND ITS EXPERIMENTAL VALIDATION

Ahmat Harine ABOUBAKAR

Ankara University
Institute of Nuclear Science
Department of Medical Physics
Health Physics Master's Degree Program

Supervisor: Prof. Dr. Haluk YÜCEL
Co-Supervisor: Prof. Dr. Serap SAFRAN

Gamma irradiation units are increasingly used in scientific, medical, and industrial fields to deliver effective radiation dose to samples and control of dose homogeneity, as well as carrying out radiological dose calibration of the instruments with desired accuracy and precision. The aim of this thesis is to measure and assess both the radiation shielding effectiveness and dose homogeneity on a radiometric bench when a gamma irradiation unit uses ISO s-^{137}Cs sealed sources, which are available at the Institute of Nuclear Sciences at Ankara University. The irradiation unit complying with ISO 4037-1 standard, manufactured by Hopewell Designs Inc., contains two sealed ^{137}Cs sources having nominal activities of 8.58 Ci and 50 mCi as of 14.05.2009. The dose measurements were performed on the radiometric bench and in a concrete shielding room. Then, a detailed 3D CAD model of the irradiation unit was developed considering technical diagrams of the unit, the radiometric bench and the shielded room. A licensed RayXpert® Monte Carlo simulation software was used with this model to estimate dose distributions and shielding performance near the source and within the concrete shielded room. To validate the dosimetric results, dose homogeneity was studied at different distances of 50 cm, 100 cm, 150 cm and 200 cm, respectively, in a 30×30 cm² gamma-ray field area on the radiometric bench by using a PTW 30 cm³ ion chamber. It is found that dose homogeneity is better than 98% on a 30 cm x 30 cm gamma-ray field. In addition, the ambient dose measurements were conducted using both a 450 cm³ ion chamber and a Geiger-Müller detector. For the study of radiation dose homogeneity, the experimental and Monte Carlo simulated results in units of air-kerma values were used to evaluate the dose distribution at several x-y positions. The details of the findings are discussed in the thesis.

This thesis has been *partially* supported by the IAEA Project coded RER0049 and titled "Enhancing the Capacities of Educational Institutions for the Sustainable Use of Nuclear Technologies".

June 2025, 90 pages

Key Words: Dose homogeneity, Irradiation unit, Monte Carlo simulation, 3D CAD Modelling, shielding effectiveness, ^{137}Cs source

ÖZET

Yüksek Lisans Tezi

3D CAD TEMELLI MONTE CARLO BENZETIMI ILE ISO s-$^{137}C_S$ SIZDIRMAZ KAPALI KAYNAKLI BIR IŞINLAMA ÜNITESININ ZIRHLAMA ETKINLIĞININ HESAPLANMASI VE RADYOMETRIK BENÇ ÜZERINDE DOZ HOMOJENLIĞININ INCELENMESI VE DENEYSEL OLARAK DOĞRULANMASI

Ahmat Harine ABOUBAKAR

Ankara Üniversitesi
Nükleer Bilimler Enstitüsü
Medikal Fizik Anabilim Dalı
Sağlık Fiziği Tezli Yüksek Lisans Programı

Danışman: Prof. Dr. Haluk YÜCEL
İkinci Danışman: Prof. Dr.Serap SAFRAN

Gama ışınlama üniteleri; numunelere etkin radyasyon dozu verilmesi, doz homojenliğinin kontrolü ve cihazların istenilen doğruluk ve hassasiyette radyolojik doz kalibrasyonun yapılması için bilimsel, tıbbi ve endüstriyel alanlarda giderek daha fazla kullanılmaktadır. Bu tez, Ankara Üniversitesi Nükleer Bilimler Enstitüsü'nde mevcut ISO s-^{137}Cs sızdırmaz kapalı kaynakları bulunduran radyomtrik bençli bir gama ışınlama ünitesinde, hem radyasyon zırhlanma etkinliğini hem de doz homojenliğini ölçüm ve hesapla değerlendirmeyi amaçlamaktadır. Hopewell Designs Inc. firması tarafından kurulan ve ISO 4037-1 standardına uygun olan bir ışınlama ünitesi, 14.05.2009 tarihi itibarıyla 8,58 Ci ve 50 mCi nominal aktiviteye sahip iki adet ^{137}Cs kaynak içermektedir. Doz ölçümleri, kalın betonla zırhlanmış odasında radyometrik benç üzerinde ve kaynak etrafında gerçekleştirilmiştir.

Daha sonra, ünitenin, radyometrik benç ve zırhlı odanın teknik çizimleri kullanılarak ışınlama ünitesinin ayrıntılı bir 3B CAD modeli geliştirilmiştir. Bu üç boyutlu modelle birlikte lisanslı bir RayXpert® Monte Carlo simülasyon yazılımı kullanılarak kaynak civarındaki ve betonla zırhlı oda içindeki doz dağılımları ve zırhlama etkinliği performansı tahmin edilmiştir. Dozimetrik sonuçları doğrulamak için ayrıca, doz homojenliği, sertifikalı PTW 30 cm³ iyon odası kullanılarak radyometrik tezgah üzerinde 30×30 cm² gama radyasyon alanında sırasıyla 50 cm, 100 cm, 150 cm ve 200 cm'lik farklı mesafelerde incelenmiştir. 30cmx30cm gama ışını alanında doz homojenliğinin %98'den daha iyi olduğu bulunmuştur. Ayrıca, ortam doz ölçümleri hem 450 cm³'lük bir iyon odası hem de bir Geiger-Müller dedektörü kullanılarak gerçekleştirilmiştir. Radyasyon doz homojenliğinin incelenmesi için deneysel ve Monte Carlo simülasyon sonuçları, hava-kerma değerleri biriminde çeşitli x-y pozisyonlarında doz dağılımın değerlendirilmesinde kullanılmıştır. Bulguların ayrıntıları tezde tartışılmaktadır.

Bu tez, UAEA RER0049 kodlu ve "Enhancing the Capacities of Educational Institutions for the Sustainable Use of Nuclear Technologies" başlıklı proje tarafından *kısmen* desteklenmiştir.

Haziran 2025, 90 sayfa

Anahtar kelimler: Dose homojenliği, Işınlama ünitesi, Monte Carlo benzetimi, 3D CAD Modelleme, zırhlma etkinliği , ^{137}Cs kaynak

ACKNOWLEDGEMENTS

I would like to express my sincere gratitude to my first supervisor, Prof. Dr. Haluk YÜCEL, who proposed this research problem relating to my thesis. They have guided and supported me, sacrificing their personal time and energy since the day I started my Master’s education. I also thank my co-supervisor, Prof. Dr. Serap SAFRAN, for her helpful advice and encouragement.

I am gratefully thankful to them for enabling my thesis work in which I benefited from a licensed RayXper® Monte Carlo Simulation Software procured by the IAEA project coded RER0049 and entitled "Enhancing the Capacities of Educational Institutions for the Sustainable Use of Nuclear Technologies”.

I am also grateful to the director of Institute of Nuclear Sciences, Prof. Dr. Haluk YÜCEL for providing the laboratory facilities and measurement equipment of the Institute.

Lastly, I sincerely thank Research Assistant Mr. Ege Can KARANFIL for his valuable collaboration and guidance during the laboratory work as well as other staff in the Institute of Nuclear Sciences.

I would like to express my heartfelt gratitude to my mother, Noura, whose unwavering support and encouragement gave me the strength to pursue my studies. Special thanks to my wife, Amzina, for standing by me and supporting me through every challenge. I am also grateful to my siblings for their constant motivation and belief in me.

Ahmat Harine ABOUBAKAR

2025

CONTENT

LIST OF SYMBOLS AND/OR ABBREVATIONS

Symbol / Abreviation	Description
A	Activity (Bq)
D	Absorbed dose (Gy)
$\dot{D}$	Absorbed dose rate (Gy/h)
E	Photon energy (MeV or keV)
FEP	Full Energy Peak
H	Equivalent dose (Sv)
$\dot{H}^*(10)$	Ambient dose equivalent at 10 mm depth (Sv or Sv/h)
$H_p(10)$	Personal dose equivalent at 10 mm depth (Sv)
HV	High Voltage
HVL	Half-Value Layer
I	Photon intensity (photons/s or photons/cm²·s)
IAEA	International Atomic Energy Agency
IC	Ionization Chamber
ICRP	International Commission on Radiological Protection
ISO	International Organization for Standardization
K_a	Air kerma (Gy)
$\acute{K}_a$	Air kerma rate (Gy/h)
LINAC	Linear Accelerator
MCNP	Monte Carlo N-Particle Code
Monte Carlo	A statistical method used for simulating radiation transport
NCRP	National Council on Radiation Protection and Measurements
PMMA	Polymethyl methacrylate (used in dosimetry phantoms)
QA	Quality Assurance
QF	Quality Factor
RBE	Relative Biological Effectiveness
ROI	Region of Interest
ROI dose	Dose measured in the region of interest
SDD	Source-to-Detector Distance
SS	Source-to-Surface Distance

Symbol / Abreviation	Description
TLD	Thermoluminescent Dosimeter
TVL	Tenth-Value Layer
137Cs	Cesium-137, a radioactive isotope used as gamma source

LIST OF FIGURES

LIST OF TABLES

1. INTRODUCTION

In the last century, the use of ionizing radiation has become an essential topic in modern society, especially in medicine, industry, and scientific research. Gamma irradiation facilities equipped with high-activity radioactive sources, such as Cesium-137 (^{137}Cs) and Cobalt-60 (^{60}Co), are central to applications like material testing, dosimeter calibration, and irradiating biological samples, such as blood irradiation (Yücel and Pomper 2022). Gamma radiation is a very penetrating radiation and poses significant health risks to personnel and the public if one does not take protective measures. Therefore, these facilities require highly effective radiation shielding systems that comply with national and international safety regulations (Republic of Türkiye Official Gazette 2000). Ankara University's Institute of Nuclear Sciences was already set up with a Hopewell-designed sealed Cesium-137 (^{137}Cs) gamma irradiation unit that meets the requirements of ISO 4037-1 standard (ISO 4037-1 2019). This irradiation unit consists of the sealed radioactive sources and it has a special shielding structure, together with a 4 m radiometric bench with a laser alignment, an elevator and the detector's stands and fixing tools. This is used mostly to calibrate radiation detectors, but it is also often used to determine the shielding effectiveness as well as other dose-delivering purposes for any samples (Yücel et al. 2016). In the present irradiation unit, it has two sealed sources with different activities having a high activity source of 8.58 Ci and a relatively low activity source of 50 mCi. These sources are normally dropped freely by gravity in a massive shielding housing structure. However, each of them can be pushed pneumatically to the tungsten(W) collimator position by controlling air pressure from a control console. If necessary, the radiation doses can be reduced at the exit of the collimator by use of any lead-based attenuators or their combinational configurations (x10, x100, x1000 times). Accurate knowledge of the dose distribution around this unit is also a crucial issue for radiological safety. First, it ensures that nearby personnel are adequately protected from radiation exposure by a warning alarm produced from an area monitor inside the 90 cm thick concrete shielding room. This provisional measure is a critical tool as a safety lock when the door of the irradiation room is not opened neither accidentally nor falsely during the irradiation time. Secondly, the scattered radiation from the wall and other equipment inside must be known during irradiation to minimize the additional dose delivered to the samples. According to ISO 4037-1 2019, the contribution due to scattered radiation should be lower than 5% of primary beam Air Kerma rates at experimental distances.

The irradiation unit maintains dose homogeneity at the irradiation positions on the radiometric bench during calibration procedures or other controlled exposures (NCRP No.147 2004, Yücel 2024). Monte Carlo simulation is considered as standard for modelling radiation transport and interactions because it can handle complex geometries and material compositions with high accuracy (Chetty et al. 2007). Here, a licensed RayXpert® software is also used for the comparison with those measured doses. To do this, a CAD based on a Monte Carlo simulation program allows us a detailed 3D modeling of the present irradiation unit. Thus, the calculation of dose distribution in and around shielding structures were performed. Once the simulation results are validated by experimental measurements, they provide an overview of the effectiveness of the shielding system and the uniformity of radiation fields at different distances from the source. This thesis aims to assess the shielding efficiency of the ^{137}Cs irradiation unit at Ankara University Institute of Nuclear Sciences and to evaluate the dose homogeneity at various positions on the radiometric bench.

A CAD model of the irradiation system will be created using the unit's technical diagrams based on physical distance and thickness measurements. Simulations will be performed using RayXpert® software, and the calculated results will be validated with experimental dose measurements taken by a relatively large volume of 450 cm^3 ionization chamber and a calibrated Geiger–Müller (GM) detector having an energy-compensated GM tube. Additionally, the dose measurements will be performed at 30×30 cm^2 target gamma radiation fields using a calibrated PTW 30 cm^3 cylindrical ion chamber. The homogeneity dose results on the radiation field were analyzed at different source-to-detector distances ranging from 50 cm to 200 cm, in order to investigate the homogeneity of the radiation field at a given distance and to achieve over 95% uniformity. For the study of radiation dose homogeneity, the experimental and Monte Carlo simulated results in units of Air-Kerma values were used to evaluate the dose distribution at several x-y positions on the target radiation field. This thesis research is particularly important because it adds to the understanding of radiation protection and how to optimize shielding for facilities using sealed sources. The association of advanced Monte Carlo simulations and real measurements provides a validated model for improving radiation protection standards and shielding design. This thesis study is also in accordance with radiation protection global priorities established by organizations as the International Commission on Radiological Protection (ICRP), the International Atomic Energy Agency (IAEA), and various national nuclear safety regulators.

This thesis consists of 5 chapters. The description of the research problem and the basic literature knowledge are given in the Introduction as the first chapter. The fundamental concepts of gamma radiation and its interaction are briefed in Chapter 2. The third chapter is related to Materials and Methods, which describes the experimental systems and measurement methodologies that are chosen in this thesis. In Chapter 4, the experimental and simulation results are presented with a concise discussion of the obtained results. In Chapter 5, the conclusions are outlined, in which a brief future work discussion is suggested based on experimental and simulated dose results on a radiometric bench equipped with standard sealed sources for the sample irradiation and radiological survey meter calibrations.

The present MSc thesis has been partially supported by the IAEA Project coded RER0049 and titled "Enhancing the Capacities of Educational Institutions for the Sustainable Use of Nuclear Technologies."

2. BASIC CONCEPTS

2.1 Fundamentals of Gamma Radiation and Its Interaction With Matter

The basic interaction processes between radiation and matter are occurred between ionizing radiation and atoms and nuclei. Among the ionizing radiations, gamma radiation is mostly used in practice. It is also known as gamma rays or photons, which are the result of the radioactive decay of atomic nuclei. Its main characteristic is a type of electromagnetic radiation (Dörschell et al. 1995, ICRP No.103 2007). It is characterized by its short wavelength, generally less than 10 picometers, and high frequency (Knoll 2010). Gamma rays consist of alpha and beta particles with no mass or charge, enabling them to pass easily through the most common materials (Attix 1986). Gamma rays can be produced naturally in the decay chains of heavy isotopes such as uranium and thorium, but also intentionally in nuclear reactors and from isotopes used in industrial and medical applications.

The energy of gamma radiation from natural radionuclides ranges from 1 keV to several MeV (Knoll 2010). This high energy means that gamma radiation can ionize atoms and molecules, providing the basis for its biological impact and its use in both imaging and therapy (Malouch et al. 2017). With photons produced at around 662 keV, ^{137}Cs is a gamma emitter widely used for radiotherapy, industrial measurement and calibration (NCRP No. 147 2004). The main modes by which gamma rays interact with matter are the photoelectric effect, Compton scattering and pair formation. They travel at the speed of light (Knoll 2010). The dominant reaction mechanism depends on the photon energy and the atomic number of the material (AAPM TG-108 2006).

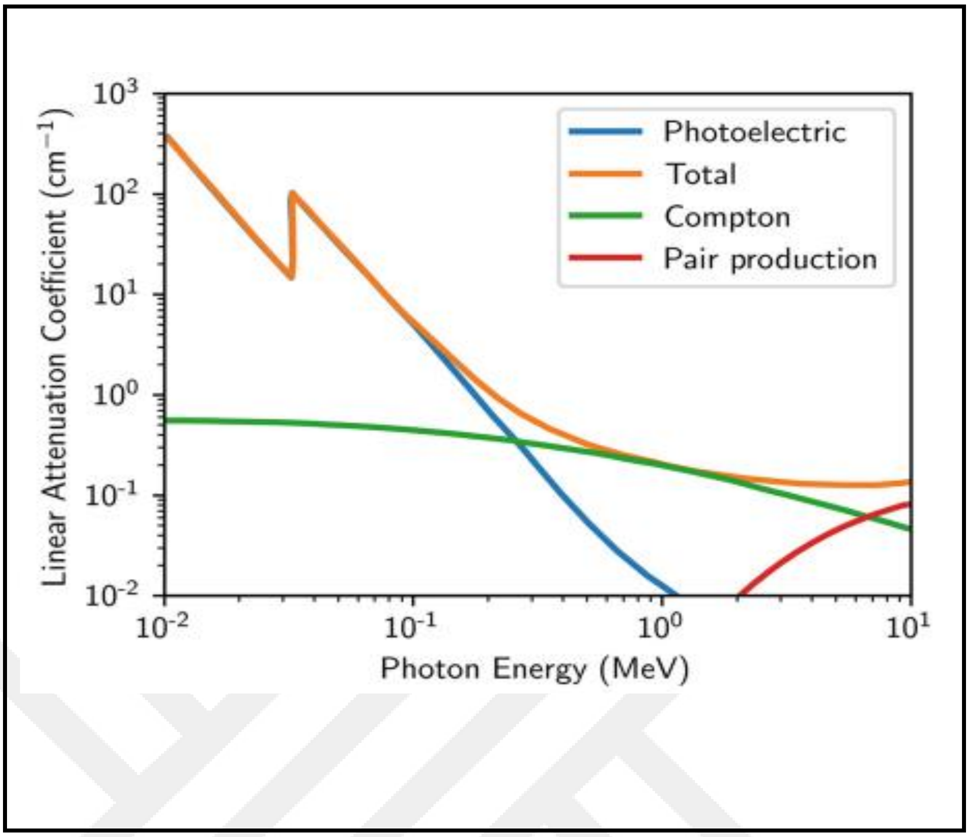

Figure 2.1 Photon interaction mechanisms vs. photon energy: linear attenuation coefficients (Dinescu 2020)

Fig. 2.1 shows the energy dependence of the linear attenuation coefficient (cm^{-1}) for photons in matter, with contributions from the photoelectric effect, Compton scattering and pair production, as well as the total attenuation. Gamma-ray shielding requires materials with a high density and atomic number, such as lead, concrete, and water (McConn et al. 2011). The effectiveness of a material in decreasing the intensity of gamma radiation can be evaluated by its coefficient of linear attenuation, which varies depending on energy and atomic composition (AAPM TG-108 2006). Monte Carlo simulations like the RayXpert® are used for analyzing the trajectory of gamma rays in complex geometries and to assist with constructing safe irradiation facilities with ^{137}Cs sources (Derreumaux et al. 2017, Peyrard et al. 2013).

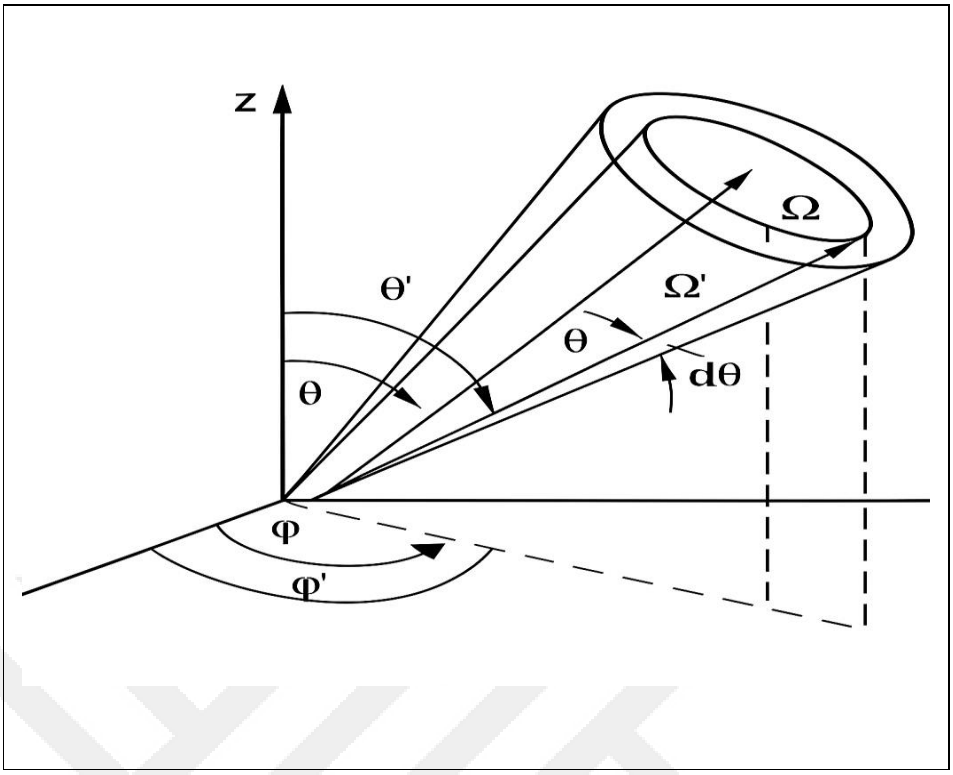

Figure 2.2 Parameters defining the directional change after an interaction (Dörschell et al. 1995)

Fig. 2.2 shows the basic ways that radiation and matter interact, as described by the microscopic cross section (σ). This parameter quantifies the chance of an interaction per atom and is affected by the type of radiation, its energy, and the properties of the target atoms. The most common unit of measurement is the barn (b), equivalent to 10^{-28} m². The concept of the differential cross section, as given in Equation 1, provides more detailed information about the direction particles are scattered in after interaction. (Dörschell et al.1995):

$$\sigma_\Omega(E,\theta) = \frac{d\sigma(E,\theta)}{d\Omega} \quad (2.1)$$

Where Ω is the unit vector in the direction of the particle movement before interaction and $\sigma_\Omega(E,\theta)$ is the differential cross section depending on energy and angle.

Photon interacts with matter. Whenever photons, which include gamma rays, interact with matter through the electromagnetic force, they transfer energy and cause atoms to become excited or ionized (Attix 1986). Compton scattering, ion pair bonding, and the photoelectric effect are the main interaction principles (Knoll 2010).

At energies above 1.022 MeV, pair generation becomes important, Compton scattering develops at intermediate energies, and the photoelectric effect emerges at higher atomic numbers and lower photon energies (Malouch et al. 2017, AAPM TG-108 2006). It is important to better know these processes for radiation detection, shielding and medical imaging applications. Photon interactions can be described using cross-sectional data and mass attenuation coefficients from databases like NIST XCOM. These data are important for Monte Carlo simulations (AAPM TG-108 2006). RayXpert® and similar software use these theoretical models to estimate dose distribution and shielding. To obtain effective experimental results, it is important to validate these models with experimental data and then evaluate the difference (Derreumaux et al. 2017).

2.2.1 Photoelectric Effect

Low-energy photons (usually below 100 keV) and matter interact primarily via their photoelectric effect, especially for high atomic number (Z) materials. The inner-shell electron, usually from the K or L shells, discharges as a result of an atom fully absorbing the input photon. The kinetic energy of the removed electron, also known as the photoelectron, is equal to the photon's energy less the electron's binding energy in the barrel (Attix 1986, Knoll 2010, Podgorsak 2010).

The interaction depends on the photon's atomic number and energy, and the resulting probability depends on the ratio of the atomic number and photon's energy, i.e., the cross section $\sigma \sim Z^{4.5}/E^{3.5}$, where Z is the atomic number of the element and E is the incoming photon energy (Knoll 2010, Heitler 1954). This means that elements from lead and tungsten are highly efficient at absorbing photons at low energies, making them highly appropriate for radiation shielding in irradiation units and medical imaging rooms (ICRP No.103 2007, NCRP No. 147 2004, Shultis and Faw 2000).

In dosimetric considerations, photoelectric absorption plays an important role, resulting in a complete deposition of energy in the absorbing material. The ICRP recommends evaluating strong Z shielding materials for rooms where lower energy photons are used because of this effect (Yücel 2024, Kase et al. 1979).

The following formula is used to calculate the kinetic energy, Ke, of the ejected photoelectron:

$$K_e = E_\gamma - E_b \tag{2.2}$$

Where Eγ is the energy of the incident photon and E_b is the binding energy of the electron in the atom's shell.

According to the following relation, the photoelectric absorption coefficient depended on photon energy E and atomic number Z:

$$\sigma_{Ph} \propto \frac{Z^n}{E^m} \tag{2.3}$$

Essentially, when light shines onto a material, the material transfers its energy to the electrons within it. If that energy is sufficient, the electrons will overcome the forces that hold them to the material and be released as free particles. Electrons emitted in this process are called photoelectrons.

2.2.2 Compton Scattering

Compton scattering is the main interaction mechanism in soft tissues for the majority of diagnostic and therapeutic radiological applications, mainly in the intermediate photon energy range (between 100 keV and 10 MeV) (Knoll 2010, Podgorsak 2010, Sprawls 2017). During this process, an incoming photon strikes with a weakly bound electron of the outer shell, releasing some of its energy to the electron as it is deflected in the process. The scattered photon is reduced in energy and reversed direction, while the ejected electron (Compton electron) carries the remaining energy (Knoll 2010, Klein and Nishina 1929).

The Compton scattering coefficient is proportional to the electron density of the material, and it's relatively independent of atomic number, which makes it important for tissues composed for the most part of low-Z elements such as hydrogen, carbon, and oxygen (Attix1986, Evans 1955). In the field of radiation protection and shielding design, Compton scattering plays a significant role because scattered photons can travel in all directions, causing secondary exposure in closed areas (Yücel 2024, NCRP No. 147 2004, Martin and Harbison 2018).

The Compton formula defines the spectrum variation of the scattered photon:

$$\Delta \cdot \lambda = \lambda' - \lambda = \frac{h}{(m_e\, c)} \cdot (1 - \cos\theta) \tag{2.4}$$

Where λ and λ′ defined as the initial and scattered photon wavelengths, respectively, and define h as Planck's constant, me as the electron rest mass, and c as the speed of light (Knoll 2010, Klein and Nishina 1929).

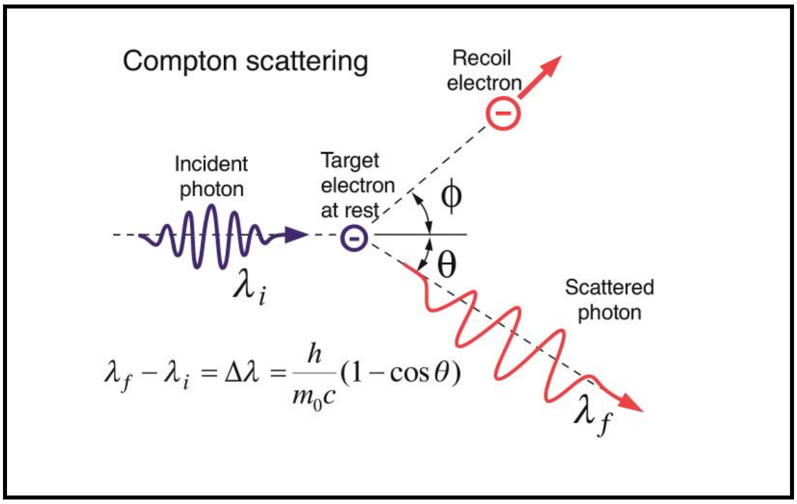

Figure 2.3 Compton Scattering (Sciencefacts, n.d.)

2.2.3 PairProduction

Pair production is produced when high-energy photons with a minimum of 1,022 MeV interact with the strong electromagnetic field of a nucleus, leading to the production of electron and positron pairs (Knoll 2010, Podgorsak 2010, Heitler 1954). The precise pair formation model is important for Monte Carlo simulations of high photon beams from the simulation angle of the photon. These procedures are provided in software programs such as PENELOPE and RayXpert® to obtain precise dose estimates (Derreumaux et al. 2017, Salvat et al. 2011, Berger 1963).

Pair production takes place when a photon with an energy greater than $2m_ec^2$=1,022M_eV, interacts in the proximity of a nucleus and is transformed into an electron-positron pair:

$$\gamma \rightarrow e^- - + e^+ \tag{2.5}$$

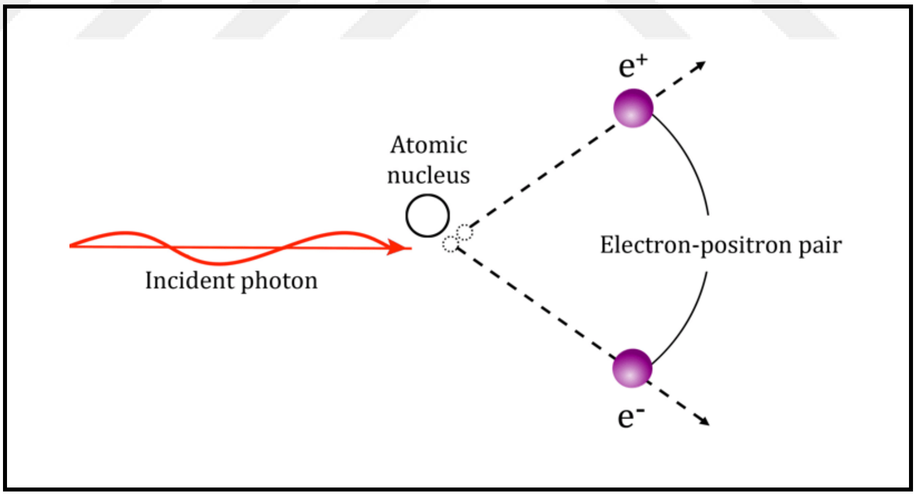

Figure 2.4 Pair production (Omer and Hajima 2018)

The excess energy produced by the photon compared to the energy of the rest mass is transformed into kinetic energy, which is shared between the electron and the positron. The process of positron annihilation with one electron results in the creation of two 511 keV photons, which travel in opposite directions (Podgorsak 2010, Heitler 1954, Evans 1955).

2.2.4 Photon attenuation mechanism

Photograph attenuation, which depends on the attenuation coefficient, refers to the gradual reduction in intensity of a photon beam as it passes through matter. The linear and mass attenuation coefficients reflect the combined effects of photoelectric, Compton, and pair production interactions (ICRP No.103 2007, NCRP No. 147 2004).

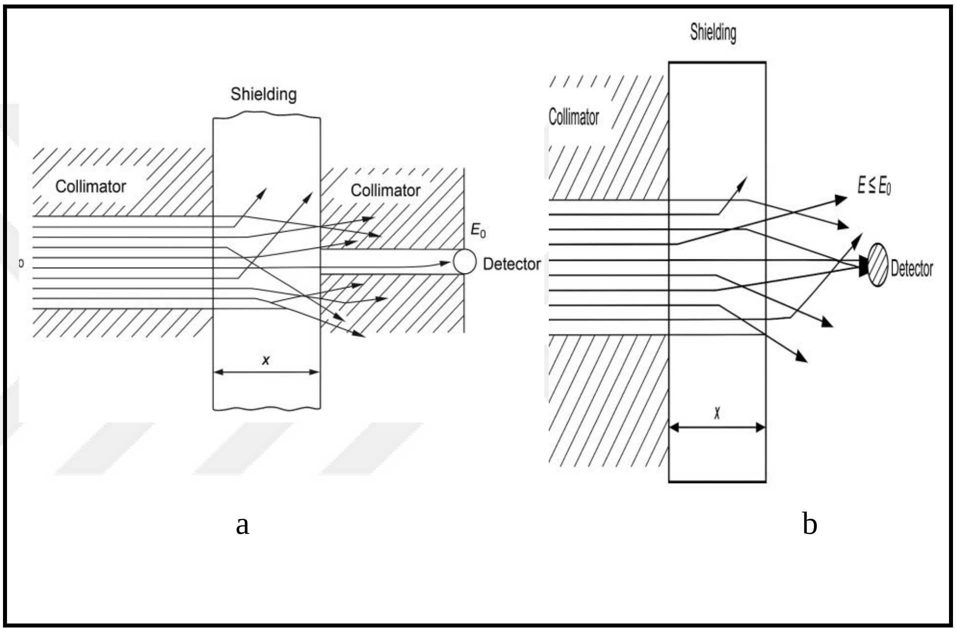

Figure 2.5 Transmission of photons through shielding for source collimation (Dörschell et al. 1995)

Accurate attenuation data for shielding materials like lead, concrete, and tissues is essential. All these elements are estimated using programs such as RayXpert® or obtained from experimental data (Peyrard et al. 2013, McConn et al. 2011). Dense high-Z materials, such as lead, are particularly effective for ^{137}Cs (662 keV) (Knoll 2010). The investigation of the interaction of photons with matter is an important aspect of research in the field of radiation, for diagnostic and therapeutic applications in particular. Attenuation mechanics plays one of the key roles in this field (Pires et al. 2020). Using Monte Carlo simulations to predict the radiation behaviour in different environments. This type of simulation is helpful for radiation room design and shielding planning because it makes it possible to estimate dose rates. Radiation researchers may investigate photon transmission in more detail by using simulation software such as RayXpert®, which allows them to reproduce realistic events (Malouch et al. 2017, Salvat et al. 2011).

The interaction of photons with shielding materials can be described using the radiation transport equation, since this relates photon flux attenuation to material thickness and composition. Assuming a monochromatic photon beam is entering the shield perpendicular to its surface with a thickness of x, the uncollided photon beam density follows an exponential law.

$$\varphi(x) = \varphi_0 \cdot exp[-\Sigma t(E_0) \cdot x] \tag{2.6}$$

The symbol Σ_t(E0) denotes the macroscopic total cross section. In figures similar to those in Figure 2.5.a, collimation is used at both the source and the detector to confirm that only the unscattered photons contribute to the measured flux. When scattered photons are also detected, the equation is modified by introducing a build-up factor B(Σt x), as shown in Figure 2.5.b.

$$\varphi(x) = B(\Sigma_t x)\varphi_0 exp[-\Sigma t(E_0)x] \tag{2.7}$$

The build-up factor is influenced by photon energy, the geometry of the shielding, and the properties of the material. For this reason, it is important to design the shielding precisely and to assess the dose accurately (Dörschell et al. 1995).

In industrial or medical fields, the use of gamma radiation sources requires a precise assessment of photon attenuation. This helps to ensure people and equipment are protected from radiation. Shielding designers and medical physicists could create safer, more efficient shielding solutions thanks to a clear understanding of how photons are absorbed or scattered by different materials (Republic of Türkiye Official Gazette 2000).

2.2 Radiation Units and Dosimetric Quantities

Radiation is the energy that moves through space in the form of electromagnetic waves, for example, gamma rays, X-rays, or particles, for example, alpha and beta particles. To ensure safety and effectiveness in the domains of medical physics and radiation protection, accurate radiation measurement is important. This is achieved by using a system of standardized units and dosimetric quantities, which help professionals measure exposure, energy deposition, and biological effects (Smith and Stabin 2012).

The most basic concept in radiation measurement is exposure, which refers to the amount of ionization produced by X-rays or gamma rays in air. It is measured in coulombs per kilogram (C/kg), though the older unit, the roentgen (R), is still used in some texts (Knoll 2010). While exposure is useful for characterizing radiation beams in air, it does not describe how much energy is absorbed by a material or tissue.

The definition of the absorbed dose is the method to address such issues. The energy deposited by ionizing radiation in each unit mass of a substance is measured, and the unit of measurement is the gray (Gy). One Gy is equal to one joule per kilogram (Podgorsak 2010). However, not all types of radiation cause the same amount of harm for the same absorbed dose. For this reason, the equivalent dose is calculated by applying a radiation weighting factor (W_R), which accounts for the differing effects of different types of radiation. The unit remains the sievert (Sv), providing a better estimation of biological harm.

The effective dose is determined by multiplying the equivalent doses received by various organs by tissue weighting factors (WxT), according to the sensitivity of each organ to effects induced by radiation. This provides a way of estimating the overall health risk from partial or whole-body exposure using a single number (ICRP No.103 2007).

In practical radiation protection, operational quantities are used for monitoring purposes. These include the ambient dose equivalent H*(10) and personal dose equivalent Hp(10), which are designed to be conservative estimates of actual tissue doses (Martin and Harbison 2018). These quantities are especially important in the calibration of personal dosimeters and environmental monitoring devices.

Another quantity that needs to be defined is KERMA, which is short for "Kinetic Energy Released per unit Mass". This is the initial kinetic energy transferred from photons to charged particles in a medium. Kerma is important in dosimetry for evaluating the interaction between high-energy photons and tissues or detectors (Attix 2004).

Understanding these quantities is essential in a variety of applications, including shielding design, radiological protection, medical imaging, and radiation therapy. A correct interpretation of these units ensures not only compliance with safety regulations but also optimizes the clinical outcomes in patient treatment (Boone et al. 1997, Bushberg et al. 2012).

2.2.1 Air kerma and dose rate concepts

Air Kerma is a fundamental dosimetric parameter widely used in medical physics and radiation protection. The amount of kinetic energy transmitted to small particles of charged air by uncharged ionizing particles is referred to. These particles are mostly made up of photons, such as X-rays and gamma rays. It has been used in nuclear safety assessment, radiation, and diagnostic imaging for determining exposure levels for both patients and staff. The amount of energy absorbed per kilogram of air is equal to 1 Gy, that is, the SI unit of Air Kerma (1 Gy = 1 J/kg). This value is used as a reference point in calculations of absorbed dose and in the establishment of radiation protection guidelines by international regulatory bodies, including the IAEA, NCRP, and ICRP (ICRP No. 103 2007, Attix 1986, Pratt 2004).

The rate of Air Kerma ($\dot{D}$) quantifies the intensity of radiation at a particular point and is given by:

$$\dot{K} = \frac{dK}{dt}(\text{Gy/s}) \tag{2.8}$$

In the case of spot sources like ^{137}Cs, kerma rates in the air at a distance from the source are determined according to the following formula (Knoll 2010) :

$$\dot{k} = \frac{\Gamma.A}{d^2} \tag{2.9}$$

Where:
Γ is the Air Kerma rate constant (for ^{137}Cs, Gy·m²/(Bq·s)),
A is the source activity in becquerels,
d is the distance from the source (m).

Depending on the radiation physics principle called the "inverse square law," the strength of radiation decreases as the square of the distance from the source increases. This principle is key to the construction and safety evaluation for irradiation rooms, particularly when it comes to determining where control rooms must be located and how to set up operational zones. Personnel working nearest to irradiators or higher-level sources have to be more secure from the radiation source. Even when the source is running at high intensity, plant engineers may make sure the radiation dose in control rooms is below permitted bounds by using the inverse square law (AAPM TG-108 2006).

The inverse square law provides the basis for planning and safety design in locations where workers can be present during irradiation procedures. This method facilitates the establishment of shielding requirements and distance-based limit of safety by providing easy numerical calculations of the expected dosage at various distances. This concept lets radiation protection officers and health physicists to estimate exposure levels to use effective safety precautions, especially physical barriers. Facilities may comply with regulatory dose limits, reduce radiation exposure to staff, and increase overall operational safety by utilizing this standard (AAPM TG-108 2006, Martin and Harbison 2018).

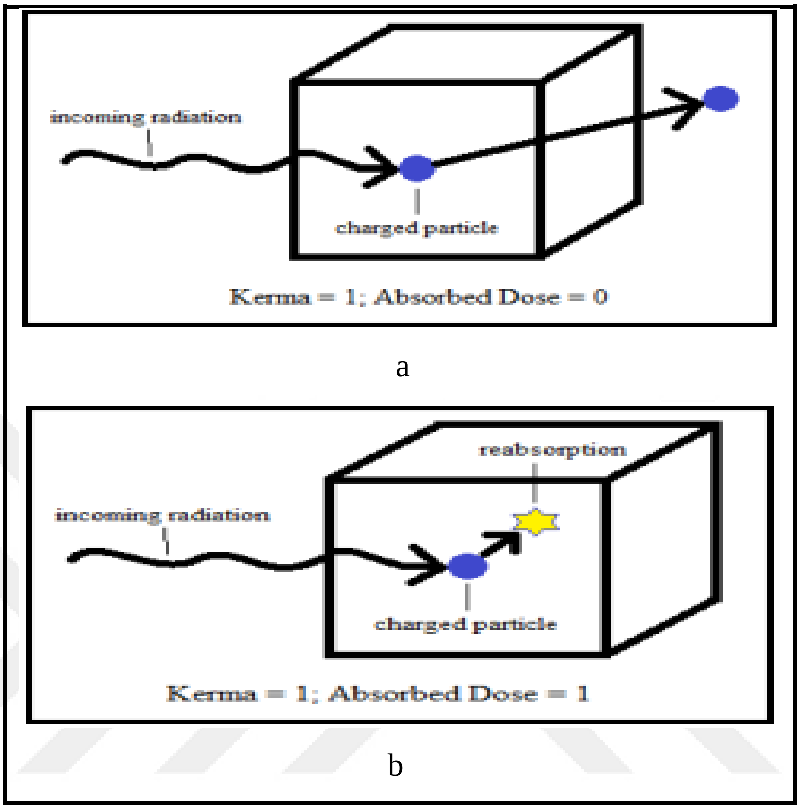

Figure 2.6 (a) presents an illustration of an ion produced within a material by ionizing radiation. (b) illustrates how an ion generated within the material is subsequently absorbed, contributing to Air Kerma and absorbed dose

Air Kerma is used as the foundation for calculating the barrier thickness necessary to satisfy controlling exposure limitations in the Hopewell ^{137}Cs shielding design (Republic of Türkiye Official Gazette 2000, NCRP No. 147 2004, ISO 4037-1 2019).

2.2.2 Dose homogeneity and uniformity criteria

Uniform dose is important for the safety and efficiency of processes like plastics processing, food preservation and product sterilization in industrial irradiation, specifically for Hopewell's ^{137}Cs units. The basic principle of ^{137}Cs systems is the delivery of ionizing radiation to a target volume by the emission of gamma rays from sealed ^{137}Cs sources. The dose rate delivered by the irradiation unit has to be uniform;

for example, the absorbed radiation has to be uniformly distributed throughout the material or the test specimen. When doses are not uniformly distributed, there may be areas that do not receive sufficient dose, reducing the effectiveness of the irradiation. On the other hand, regions that receive excessive radiation may sustain damage, degradation, or unnecessary exposure, all of which can have a negative impact on the safety and quality of products (Yücel 2024, AAPM TG-108 2006, Derreumaux et al. 2017, NCRP No.151 2005).

Permissible 95% according to ISO 4037-1 standard.The goal is to minimize this ratio while maintaining regulatory compliance and operational efficiency (ISO 4037-1 2019, Kase et al. 1979).

2.3 Radiation Shielding Principles

When it comes to radiation protection, the fundamental principle in the field is radiation shielding, particularly when dealing with ionizing radiation such as gamma sources. Minimizing the amount of radiation to levels determined safe for both the general public and occupational workers is the primary aim of shielding. There are several kinds of radiation, for example, gamma, X-ray, and neutron. The level of energy source activity, occupancy factors, and facility design impact the manner in which shielding is designed (Arafah et al. 2017).

In this thesis, the shielding will be studied near the source as well as in the surrounding area and the control room, where the shielding effectiveness and dosage distribution of a Hopewell ^{137}Cs Irradiation Unit are evaluated. The International Commission on Radiological Protection (ICRP) and the National Council on Radiation Protection and Measurements (NCRP) generate the most important radiation protection guidelines. NCRP No. 147 is utilized for diagnostic X-ray shielding, and NCRP Report No. 151 provides high-energy and therapeutic systems (NCRP No. 147 2004, NCRP No. 151 2005).

The radiation shielding evaluation is based on the linear attenuation model describes the exponential decrease in radiation intensity as it passes through a material (Knoll 2010): This relationship is described by the law of exponential attenuation:

$$I = I_0 e^{-\mu x} \tag{2.10}$$

In this equation, I represents the intensity of the transmitted radiation, I_0 denotes the initial (incident) radiation intensity. The parameter μ is the linear attenuation coefficient of the shielding material, expressed in cm^{-1}, and x(cm) is the thickness of the shielding material. The term e refers to the base of the natural logarithm.

This equation assumes a narrow beam geometry and homogeneous material, that commonly used in preliminary shielding calculations for medical imaging and radiation therapy facilities. To account for the contribution of scattered radiation, the buildup factor (B) is introduced into the linear attenuation model. The modified form of the exponential attenuation law becomes:

$$I = \mathrm{I}_0 \mathrm{B} e^{-\mu x} \tag{2.11}$$

In this context, I represents the intensity of the transmitted and scattered radiation, while I_0 denotes the initial or incident radiation intensity. The buildup factor, B, is a dimensionless quantity that accounts for the contribution of scattered photons reaching the detector. The linear attenuation coefficient of the shielding material, μ, is expressed in cm^{-1}, and x corresponds to the thickness of the shielding material in centimeters. Finally, e represents the base of the natural logarithm.

The buildup factor depends on several parameters is including the photon energy, material composition, and geometry. It is significant in broad beam conditions and thick shielding, where secondary (scattered) photons contribute appreciably to the total radiation dose beyond the shielding barrier (Yücel 2024a).

These guidelines ensure the dosage limitations specified by global safety regulations (ICRP No.103 2007, ISO 4037-1 2019) are respected. The utilization of primary and secondary barriers, shielding materials, and build-up factors for ^{137}Cs gamma rays is investigated in the sections that follow.

2.3.1 Primary and secondary barriers

The direct beam from the source of radiation has been designed to be attenuated by primary obstacles. The beam from the source is directly impacted on the shielding walls of the irradiation chamber in the particular case of the ^{137}Cs irradiation unit used in this thesis. The gamma rays with the characteristic of Cs-137 at 662 keV will be attenuated by these barriers (Yücel 2024a).

For primary barriers the required shielding thickness t can be calculated by using NCRP 147 formula as below:

$$B_P(x_{barrier} + x_{pre}) = \left(\frac{T}{P}\right)\frac{d^2P}{K_P \cdot U \cdot N} \tag{2.12}$$

Where: B_P is the transmission factor for the primary barrier, $x_{barrier}$ is the thickness of the main shielding barrier (cm), x_{pre} is the thickness of the pre-shielding (cm), T is the occupancy factor representing the fraction of time the area is occupied, P is the design dose limit (mSv/week), d is the distance from the source to the point of interest (m), K_P is the Air Kerma per unit workload at 1 m from the source (mGy/Gy), U is the use factor representing the fraction of workload directed toward the barrier, and N is the number of sources or beams contributing to the dose **(**NCRP No. 147 2004).

2.3.2 Secondary barriers

Leakage and distributed radiation are reduced by secondary barriers. The causes of this radiation in the control room or nearby corridors are: scatter from materials exposed to radiation, leakage from building penetrations, or shielding interactions (Yücel 2024a).

The secondary shielding calculation complies with NCRP standards and often applies similar parameters, it takes into account:

- Workload leakage,
- Photon energy scattered,
- Use decreased (U ≥ 1)

Because of the prolonged occupancy (T =1), the dose equivalent from secondary radiation can be smaller but still considerable. The suggested formula is:

$$t = \text{TVL}\left(log_{10}\left(\frac{\text{P}.d^2}{0.001.W.U.T}\right)\right) \tag{2.13}$$

Where: TVL : is the tenth-value layer (cm), P : is the design dose limit (mSv/week), d : is the distance from source to point of interest (m), W : is the workload (Gy/week), U : is use factor, T : is the occupancy factor. For ^{137}Cs sources the TVL values depend on shielding materials: Lead: TVL = 0,7 cm, Concrete: TVL = 6,6 cm from Iso 4037-2019.

A factor of 0,001 allows for the overall proportion of source leakage to be taken into account; this calculation ensures that shielding in spaces of control rooms meets the ICRP public exposure limit of 1 mSv/year or the ICRP occupational limit of 20 mSv/year for an 8.58 Ci ^{137}Cs source (ICRP No.103 2007, NCRP No. 147 2004).

The lead shielding inside the Hopewell unit achieves over 99% attenuation at 662 keV, according to primary and secondary barrier modeling in Monte Carlo simulations using RayXpert®. To confirm the modeling results, ion chamber and GM counter measurements are proposed.

2.3.3. Shielding materials and buildup factors

Shielding performance depends on thickness, material composition, and buildup factors. Buildup factors consider secondary radiation from Compton scattering, photoelectric absorption, and pair production. These effects raise photon flux downstream of the shielding, particularly at high energies or in thick materials (NCRP No. 147 2004, Shultis and Faw 2000).

- Common Shielding Materials:

The commonly used shielding materials are presented in Table 2.1.

Table 2.1 Radiation Shielding Properties of Common Materials for 662 keV of ^{137}Cs

Material	Density(g·cm^{-3})	TVL for 662 keV of ^{137}Cs (cm)	Use Context
Lead	11.34	0.7	Primary shielding, collimation
Concrete	2.35	6.6	Structural walls, control rooms
Steel	7.87	2.4	Support structures, vaults
Barite	3	5	High-density panels

- Buildup Factor Fundamentals

Buildup factors (B) account for re-scattered radiation beyond exponential attenuation:

$$I = I_0 e^{-\mu x} B(x, E) \tag{2.14}$$

For example, the typical buildup factor for 662 keV of 137Cs is given in Table 2.2.

Table 2.2 Buildup factors for 662 keV (ISO 4037-1 2019, Martin and Harbison 2018, NCRP No. 147 2004).

Material	Material Thickness (cm)	Mean Free Path (MFP) (no unit)	Buildup Factor (B) (no unit)
Lead	5	5,0	1,1
Lead	10	10,0	1,2
Concrete (std)	15	3,5	1,25
Concrete (std)	30	7,0	1,45
Steel	10	5,0	1,15
Steel	20	10,0	1,35

MFP is the linear attenuation coefficient (cm^{-1}) multiplied by thickness (cm).

The RayXpert® Monte Carlo code, which is licensed for this thesis, considers both macroscopic cross-sections and buildup factors for precise dose mapping. Simulation data matches well with empirical buildup data from ISO 4037-1 and NCRP.

- Selection of Shielding Material

Material selection is influenced by factors such as the energy of the incident radiation (662 keV for ^{137}Cs), spatial constraints, and budgetary as well as environmental considerations. Lead is preferred for compact shielding because of its high atomic number (Z=82), which raises the probability of photoelectric interaction. Concrete, while less dense, is cheaper and easier to install in large volumes.

RayXpert® combines PNNL material libraries and NIST-XCOM cross-section data. This enables simulations of specific compositions to reinforce concrete and laminated lead-steel shielding. The thesis includes simulations with both standard concrete and lead panels to examine dose reduction at the control room boundary.

2.4 Gamma Radiation Emitted by Radionuclides

The properties of the reference gamma radiation emitted by radionuclides, in addition to the methodology and requirements for generating this radiation field for a designated radiation quality with an objective value of the expanded overall uncertainty (k = 2) of approximately 6% to 10%. All reference fields created using gamma radiation emitted by radionuclides are treated in the same way, regardless of whether they are matched or characterised reference fields. The reason for this is the weak variation of the conversion coefficients from Air Kerma to phantom-related quantities with photon energy. This variation is within the range of 600 keV to 1400 keV. These coefficients range from 1.06 to 1.22 for all phantom-related quantities and, for applicable phantoms, remain consistent. According to this standard, all reference radiation fields shall be produced using collimated sources.

2.4.1. Radionuclides used for the production of gamma radiation

The calibration of dosemeters and dose rate meters is to be achieved using gamma radiation emissions from the following radionuclides, as shown in Table 2.3.

Table 2.3 Radionuclide Properties (ISO 4037-1 2019)

Short name	**Radionuclide**	**Radiation energy (keV)**	**Half-life (a)**	**Air kerma rate constant[1] (µGy·h⁻ ¹·m²·MBq⁻ ¹)**
S-Cs	^{137}Cs	661.7	30.05 ± 0.08	0.079
S-Co	^{60}Co	1173.3 1332.5	5.271 ± 0.0008	0.31

The Air Kerma rate constant is only valid for an unshielded point source. This is as stated in ICRU Report . The purpose of this text is to serve as a guide, not as a tool for calculating Air Kerma rates.

2.4.2 Specification of radiation sources

The source needs to be as small as possible, so it is essential to use sources made of a radioactive substance with sufficient mass-related specific activity. The Air Kerma rate arising from the primary radioactive isotope must not exceed 1% of that caused by the radiation emitted by the isotope.

Table 2.4 Specific activity and chemical form of nuclides

Radioactive nuclide	Specific activity ($Bq \cdot kg^{-1}$)	Recommended chemical form
^{137}Cs	$8.51 \cdot 10^{14}$	Chloride
^{60}Co	$3.7 \cdot 10^{15}$	Metal

NOTE:
^{60}Co is particularly well-suited for generating sources with high specific activity related to their mass.
As newly made sources of ^{137}Cs may contain significant amounts of ^{137}Cs, decay corrections should account for the different half-lives associated with these two cesium isotopes. Therefore, the use of older ^{137}Cs sources is recommended, and the source manufacturer should provide specifications for any impurities.

2.4.3 Encapsulation

The standard to which the sources should comply is the ISO 2919 document (ISO 4037-1 2019). Outside the collimated beam, the Air Kerma rate is ensured not to exceed by 5%. The capsules must be able to absorb the beta radiation from the sources, i.e., the surface density must be 0.2 g·cm-2 for ^{60}Co and 0.5 g·cm-2 for ^{137}Cs.

The secondary standards used for all measurements shall be of high sensitivity. For the energy range of interest, the variation in response to Air Kerma due to the energy and direction of radiation should be small and known. This can be found, for example, in ISO 4037-1 2019. The Air Kerma rate is guaranteed to be no more than 5% higher than the collimated beam. Radiation from outside the collimated beam is due to scattered radiation from the environment, as well as leakage radiation from the source safety shield and collimator. Therefore, the radiation contained within the collimated beam comprises radiation scattered from the source cap, the source shielding, and the collimator.

2.4.4 Collimated geometry installation

In Figure 2.7, the principal characteristics of an example collimator, particularly applicable in the case of ^{60}Co and ^{137}Cs, are shown schematically.

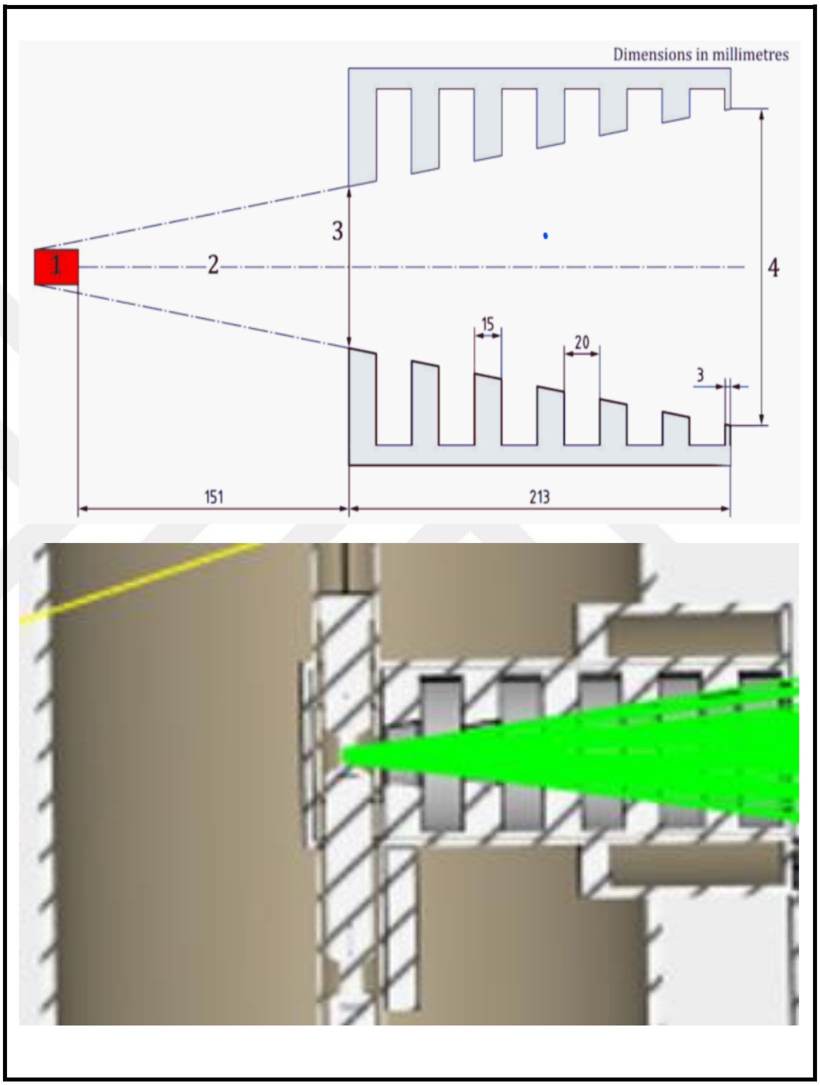

Figure 2.7 Example of a Collimator (ISO 4037-1 2019)

The maximum percentage of scattered photons produced by this type of installation is 5% for ^{137}Cs, and a lower percentage for ^{60}Co. The safety enclosure must be made out of lead or similar materials with enough thickness to decrease the level of Air Kerma rate of the undesired type of radiation that is able to penetrate the interior of the enclosure to reach a thousandth of the primary beam. The lead is 12.5 mm thick for ^{60}Co

and 6.5 mm thick for ^{137}Cs. It may be necessary to increase these values to ensure that users are exposed to safe levels.

Figure 2.7 shows the shape and dimensions of the primary photon beam as defined by a collimator. The collimated installation illustrated in the figure consists of a conical collimator containing the radiation source at its widest point. It consists of a series of six apertures, each with a thickness of 15 mm. These apertures are separated by 20 mm and act as trapping points for photons that are scattered at the edges of the previous aperture. The final aperture has been made to have a thickness of 3 mm with a diameter that is larger than the size of the beam's cross-section at that location. They are manufactured from a tungsten alloy.

Table 2.5 Example of composition used in the aperture alloy of the collimator shown in Figure 2.7

Element	**Content by Mass (%)**
Tungsten	89
Nickel	7
Copper	4

2.5 Monte Carlo Simulation Technique for ^{137}Cs Irradiation Room Shielding

Monte Carlo simulation is a type of computational analysis that uses repeated, systematic random testing to find solutions to complex physical and mathematical problems that cannot be solved using analytical methods, assuming they are deterministic in theory (ICRP 2007). In the field of radiation physics, MC simulations are used to study the movement of particles (for example, photons, electrons and neutrons) through matter by modeling their random interactions with atomic structures (Faddegon et al. 1990, RayXpert® Manual 2022).

RayXpert® is a cross-platform application, compatible with both Windows and Linux, that utilizes a Computer-Aided Design (CAD) interface for three-dimensional geometry modeling and performs Monte Carlo simulations with continuous energy calculations.

2.5.1 Principle of Monte Carlo simulation in radiation transport

Monte Carlo simulation is used in radiation transport models to describe particle paths as they interact with matter, accounting for all potential physical causes, including pair production, Compton scattering, and the photoelectric effect. Probabilities derived from physical data on the effective cross-section dictate each particle's behavior (Kawrakow 2000). Sample a particle source, track the particle path, and identify interaction types. The core formula for estimating the result is as follows, Q using MC is:

$$Q = \frac{1}{N}\sum_{i=1}^{N} q_i \tag{2.15}$$

Where q_i represents the result obtained from the particle with index i in the simulation sequence, and N denotes the total number of particles simulated. (Derreumaux et al., 2017). To improve statistical accuracy with fewer records, RayXpert® uses variance reduction approaches to calculate photon and neutron transit (McConn et al. 2011). The stochastic process uses probability density functions that are derived from the following to determine interaction types and free path lengths (λ):

$$P(x) = \mu e^{-\mu x} \tag{2.16}$$

The linear attenuation coefficient is represented by the value μ (Andreo, 1991). This method ensures correct simulation of photon attenuation in shielding materials (Nelson et al. 1985). RayXpert® combines physical modelling with CAD geometry, providing authentic simulations with automatic mesh generation that show challenging buildings and materials (Nelson et al. 1985). It is important that the device can show how the dosage is spread and make the most of the shielding.

2.5.2 Application of Monte Carlo in shielding calculation

The use of Monte Carlo simulations is for determining shielding in LINAC rooms, diagnostic radiology, and medical facilities (Verhaegen and Seuntjens 2003). In order to determine dosage distribution and detect potential leakage regions, the computations must simulate the radiation sources, material composition, and configuration of the geometry (Kramer et al. 2004). The radiography room's walls, doors, lead windows, and equipment are all included in the 3D virtual model that RayXpert® generates. The program examines particle interactions on all surfaces and models photon emission. The resulting dose maps help optimize wall thickness and material selection by highlighting shielding weak areas (IAEA No.47 2006).

The dose rate D at given location is estimated as:

$$D = \frac{1}{N}\sum_{i=1}^{N} E_i . W_i \tag{2.17}$$

where W_i is each particle's statistical weight and E_i is the deposited energy per time (ICRP No.103 2007). RayXpert® allows it to be less difficult to meet with regulation dose limits by simulating doses in μSv/h or Gy/h for various positions (Faddegon et al. 1990).

Particularly in rooms with multiple radiation sources or mixed structures, Monte Carlo offers significant benefits over analytical techniques (RayXpert® Manual 2022). Monte Carlo accounts for secondary radiation and scattering, in contrast to analytical methods based on tenth-value layers (TVLs). Shielding in clinical practice must safeguard the public as well as medical personnel. The ionizing leakage using walls and penetrations (cables, ducts, and doors) is kept within the acceptable limits specified by ICRP and NCRP standards by using MC simulations (Rogers 2006). For automated compliance checks, RayXpert® incorporates these standards (Kawrakow 2000).

Furthermore, Monte Carlo allows for the evaluation of the overall dose over time, which is crucial for workload calculations in high-use facilities like LINAC rooms (Hubbell

2006). This ensures cost-effectiveness and safety by avoiding over-designing barriers (Andreo 1991).

2.5.3 Statistical uncertainty and convergence in Monte Carlo

The most significant feature of MC simulation is statistical uncertainty due to the random sampling of particle histories (Peyrard et al. 2013). As the number of particles N increases, the precision of simulation results rises as well, albeit at the cost of computational time (Nelson et al. 1985).

The uncertainty of the estimated result is frequently expressed using the relative standard deviation:

$$\sigma_r = \frac{\sigma}{\bar{Q}} = \frac{\sqrt{1\frac{1}{N}\sum_{i=1}^{N}(q_i - \bar{Q})^2}}{\bar{Q}} \qquad (2.\ 18)$$

Where $\bar{Q}$ is the score for each time and q_i is the mean result (Sánchez-Doblado et al. 2005).

Until the relative uncertainty level for all collected zones falls below the user-specified uncertainty thresholds, which may be 5% (Verhaegen and Seuntjens, 2003). To ensure the quality of the simulation, the software provides assigned colors, uncertainty maps, and convergence indicators (Kramer et al. 2004). It's necessary to make sure that biases are not introduced by variance reduction strategies like Russian roulette and importance sampling (IAEA No.47 2006). These procedures are automated by RayXpert®, which also offers logs to confirm convergence (Ma and Jiang 1999). If the convergence process in shielding design does not occur, the radiation exposure may be overestimated or underestimated, resulting in either dangerous exposure shielding expenses. Therefore, before the results of simulations are verified, an uncertainty analysis needs to be conducted (Podgorsak 2010).

2.5.4 Benefits of Monte Carlo over analytical models

MC experiments have many benefits over conventional analytical models, for example, NCRP Report No. 49 or IAEA shielding standards (ICRP No.147 2007). Simplified assumptions, including point sources, unlimited foundations, and monoenergetic beams, are the foundation of analytical models, which hardly ever accurately depict clinical situations (Faddegon et al. 1990).

Monte Carlo enables:

Modeling heterogeneous geometries, such as spaces with ducts, multiple barriers, or asymmetrical layouts (RayXpert® Manual 2022). For polyenergetic X-ray tubes, energy spectrum inclusion is crucial (Attix 1986). Assessment of scattering, encompassing secondary radiation and backscatter (Rogers 2006). Accurate spatial analysis is made possible by realistic dose distribution maps (Kawrakow 2000). Shielding a LINAC room with multiple entrances and an internal labyrinth is an example of this. In this configuration, the MC recreates neutron transport and buildup and the analytical models might underestimate neutron leakage (Hubbell 1982). Mixed shielding can be studied using both neutron and photon transport physics modules with RayXpert® (Andreo 1991). Analytical techniques are limited when graded shielding (for example, lead + concrete) or composite materials are utilized. Monte Carlo allows for the precise design of layered barriers by tracking every interaction (Peyrard et al. 2013).

In order to find economical solutions without affecting safety, MC allows for optimization, in this case by comparing multiple scenarios (material types, wall thickness) (Malouch et al. 2017). This is helpful when improving LINACs or renovating hospitals (Verhaegen and Seuntjens 2003).

Since MC simulations might be more computationally demanding, software applications like RayXpert® optimize processing through GPU acceleration and multithreading, making them suitable for clinical and laboratory use (Kramer et al. 2004).

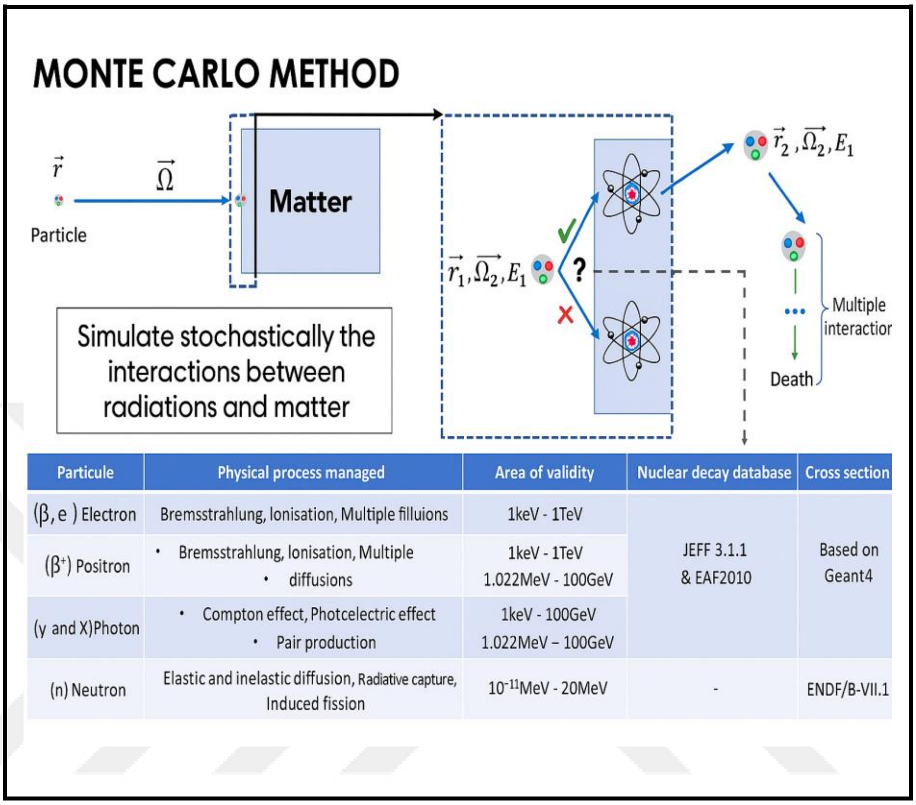

Particule	Physical process managed	Area of validity	Nuclear decay database	Cross section
(β, e) Electron	Bremsstrahlung, Ionisation, Multiple filluions	1keV - 1TeV	JEFF 3.1.1 & EAF2010	Based on Geant4
(β⁺) Positron	• Bremsstrahlung, Ionisation, Multiple • diffusions	1keV - 1TeV 1.022MeV - 100GeV		
(γ and X)Photon	• Compton effect, Photcelectric effect • Pair production	1keV - 100GeV 1.022MeV – 100GeV		
(n) Neutron	Elastic and inelastic diffusion, Radiative capture, Induced fission	10^{-11}MeV - 20MeV	-	ENDF/B-VII.1

Figure 2.8 Monte Carlo method for Simulating radiation-matter interactions (RayXpert® Manual 2022)

3. MATERIALS AND METHODS

3.1 Hopewell Designs G10 Gamma Beam Irradiator System Overview

Hopewell Designs, Incorporated G10-2 model gamma beam irradiator with two sealed ^{137}Cs sources is a relatively sophisticated, multipurpose device mainly used for radiation dosimetry and calibration of radiation detection equipment. By means of sensitive engineering, including source design, shielding, and beam collimation, it provides a horizontal gamma radiation beam.

With options that cover manual to fully automated control, single and dual source configurations, it has been designed to provide both flexibility and safety. It is housed in a shielded structure made of tungsten and stainless steel and contains radioactive sources of ^{137}Cs with different levels of activity. Up to 2,600 Ci of radioactive material can be supported by the G10, depending on its configuration (Facure et al. 2007)

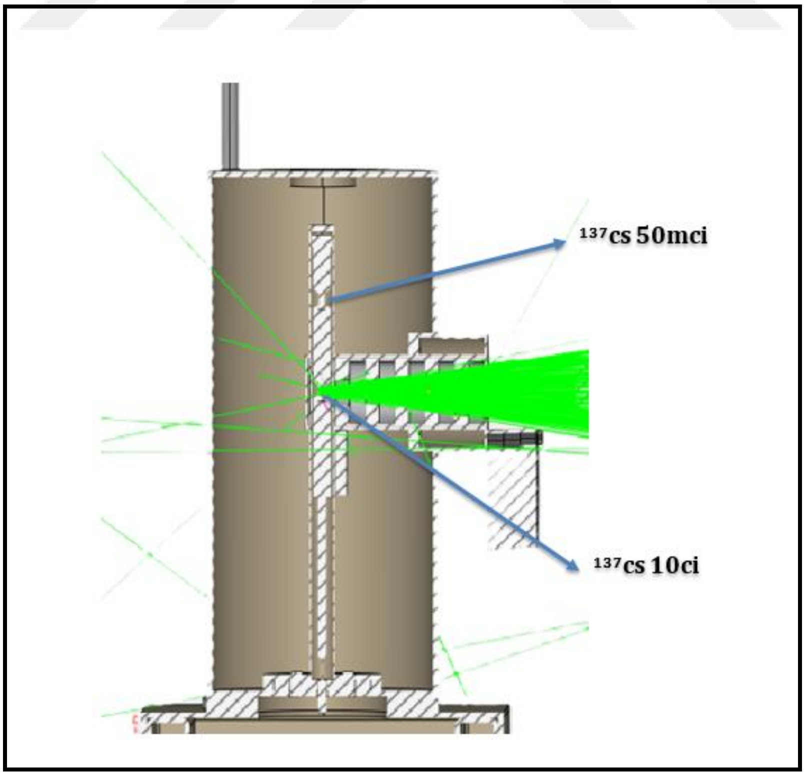

Figure 3.1 Placeholder: cross-section of dual source gamma beam irradiator

3.2 Technical Features and Source Handling

Two radioactive sealed ^{137}Cs sources (Serial No: 2737G, Model:CDC.711M and Product Code No: CDC38210) provided by QSA Global, Inc (Burlington, MA 01803) have been loaded in the present gamma irradiator, where ^{137}Cs source is classified as ANSI/ISO Classification No: C66646 with a sealed capsule type X3814. Special form certificate number is USA/0363/S-96. The measured dose rate is 6,866 nGy/s (at the activity of 8.58 Ci) *as of 14.05.2009*. Since Air Kerma Rate ($\dot{K}_a$) is given in unit of nanograys per second at one meter distance, to convert Air Kerma Rate ($\dot{K}_a$) to equivalent activity (Ci) by a factor of 1.25. The irradiator includes a lead shield enclosed in steel, with a beam centerline one meter above the ground. A pair of position sensors coupled to a pneumatic air cylinder allows for the safe manipulation of radiation sources, providing accurate exposure placement. Using a tungsten shielding reduces inter-source coupling in dual-source models by enabling separate exposure of sources with low and high activity.

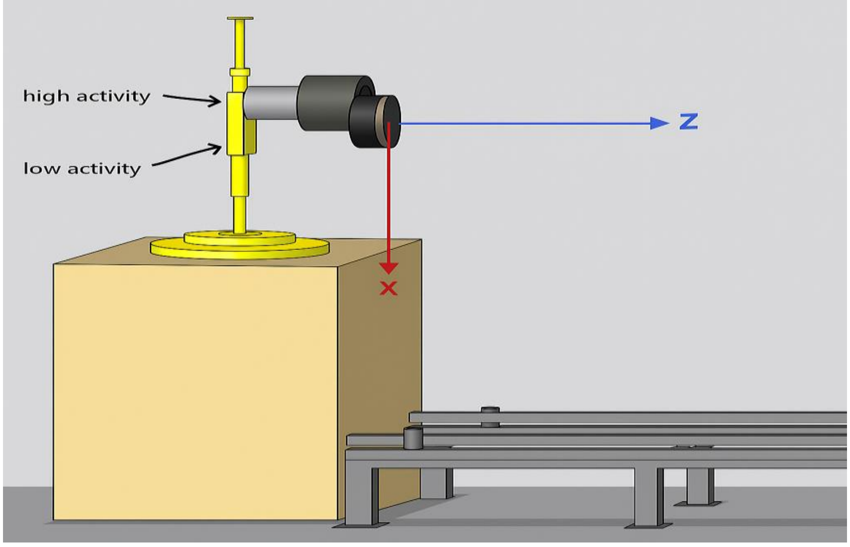

Figure 3.2 Dual source configuration showing high activity ^{137}Cs and low activity ^{137}Cs source

In accordance with strict international safety standards (ANSI/HPS N43.3 2018, NCRP Report 88 1986), the radiation shielding design provides assurance that the system emits less than **5 mR/h** at a distance of 12 inches from the shield's surface when in the shielded position.

Collimator: The beam geometry is defined by a tungsten beam collimator, which serves to restrict the solid of the radiation field to a maximum angle of 16 degrees. It is ensured by this precise collimation that radiation exposure is restricted to the intended calibration volume, with unnecessary scatter being prevented and measurement accuracy being maintained.

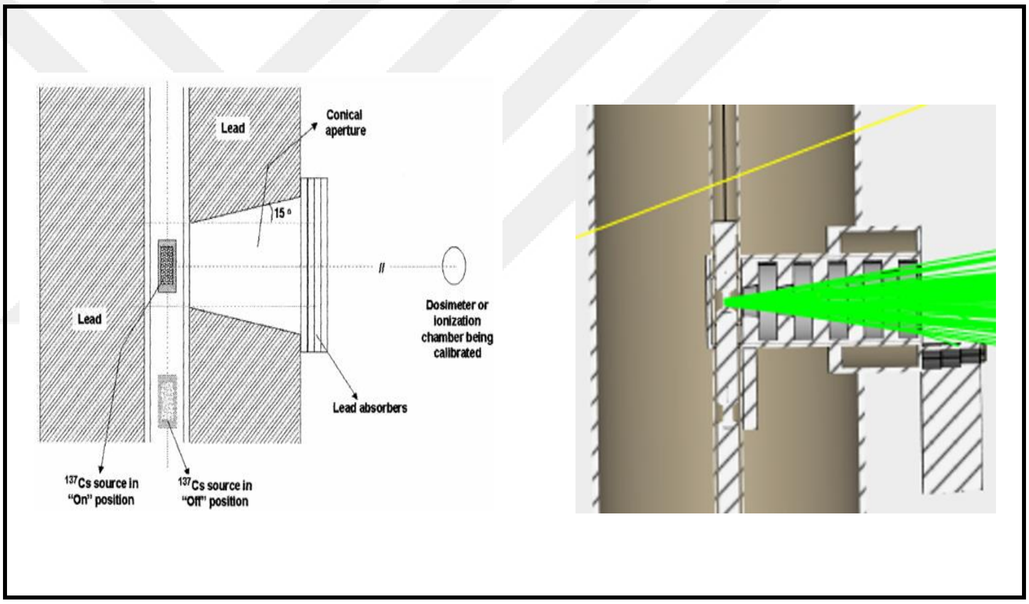

Figure 3.3 Collimator schema

3D Modeling with CAD Software:

Construction of the Simulated Collimated Reference Radiation Field Using ^{137}Cs Source:

In compliance with the requirements of the ISO 4037-1 2019 standard for collimated reference radiation fields, a photon-based simulation model was constructed to study the gamma dose distribution produced by ^{137}Cs sources (Montgomery 2013). The geometry of the simulation is identical to that of the laboratory irradiation room at the Ankara

University Institute of Nuclear Sciences. The dimensions of the room are 5 m (length), 4 m (width), and 5 m (height) (Hopewell 2021), which were used to model the actual space in SolidWorks.

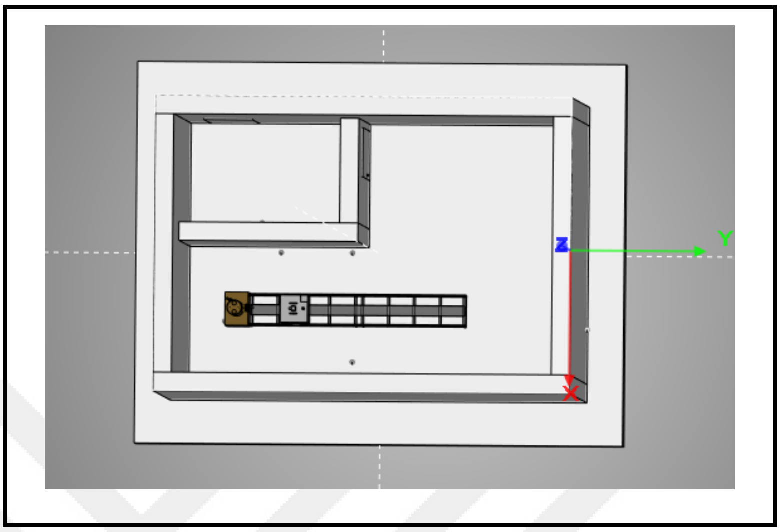

Figure 3.4 3D SolidWorks model of the irradiation room and ^{137}Cs source unit

Hopewell Designs Inc.'s 137Cs irradiation unit's 3D design was created in SolidWorks using the manufacturer's technical handbook as a guide. To ensure accuracy between the real unit and the 3D model, all internal component dimensions and specifications, including those of the collimator, attenuators, shielding, and housing, were precisely matched to the technical sheet (RayXpert® Manual 2022). Using the actual spatial arrangement of the unit in the lab, the entire room and irradiation unit assembly were modeled. The STEP file format was then exported to RayXpert® for Monte Carlo simulation (NCRP No. 147 2004).

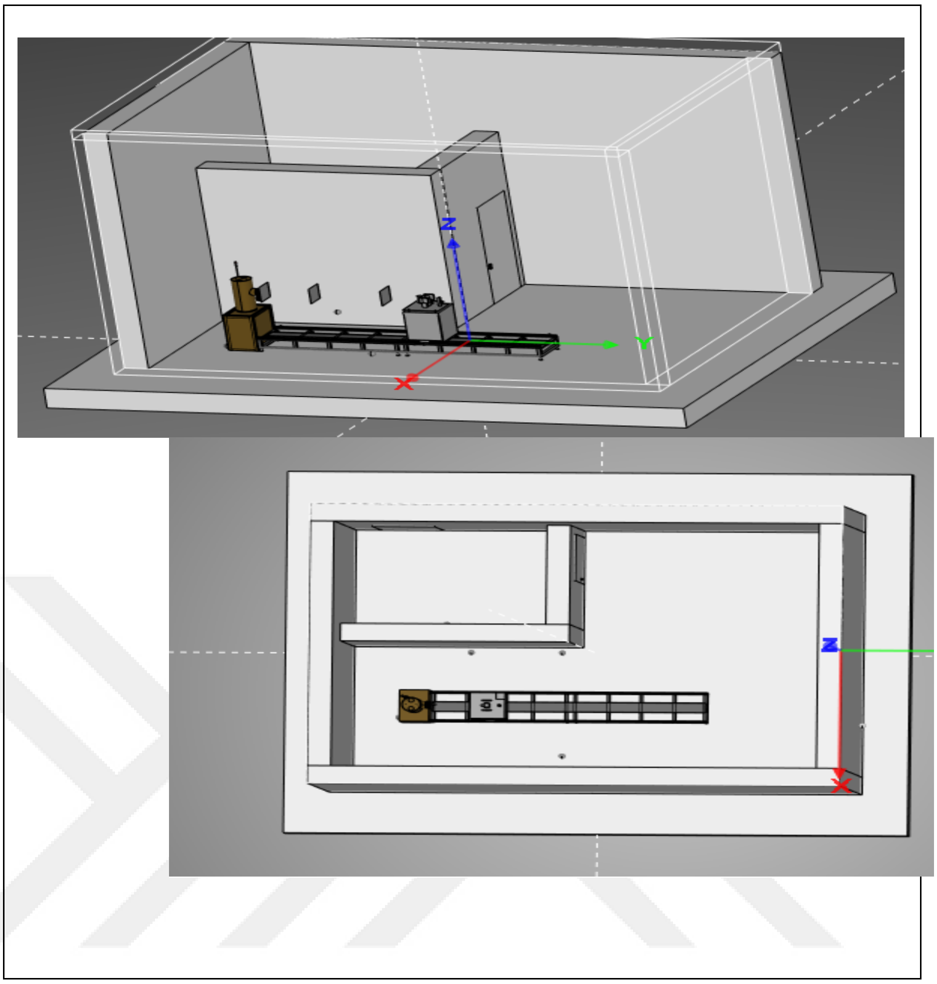

Figure 3.5 R ayXpert® interface showing the imported 3D model

In RayXpert®, material definitions were assigned for each component: the collimator was modeled as a tungsten composite, the attenuator as lead, and the room walls and floor as concrete, which is consistent with radiation shielding design practices (ICRP No.107 2008). The simulation used only photon transport, as ^{137}Cs is a gamma-emitting isotope with a principal photon energy of 662 keV and negligible particle emission under normal conditions (Sempau et al. 2002).

The source of ^{137}Cs is located at the geometric center of the Hopewell rod and is aligned with the conical collimator aperture. The geometry adhered to the reference configuration of a typical collimated radiation field, in which the detector is positioned at predetermined separations from the source along the central beam axis (Montgomery 2013). The detectors were placed at 50 cm, 100 cm, 150 cm and 200 cm from the source

^{137}Cs for the 10 mCi. This configuration allows precise measurement of the dose rate profile near the source, where dose gradients are highest and calibration accuracy is important (Sempau et al. 2002).

To calibrate and evaluate the beam properties, lead attenuators of varying thicknesses were added directly after the collimator exit. These attenuators help modulate the Air Kerma rate without changing the source activity, which is a common practice in metrological calibration fields (Montgomery 2013). The separation between the radioactive source and the final collimator opening was maintained at 36.4 cm, in accordance with ISO specifications (Montgomery 2013).

Detectors were placed at multiple positions:

- Near the irradiation unit to measure direct beam dose and scatter,
- On-axis positions (including the two detectors at 50 cm and 100 cm) to characterize the primary field,
- Behind the wall to evaluate shielding efficiency and verify that the dose rate 30 cm beyond the wall does not exceed 2.5 µSv/h, a safety limit referenced in radiation protection guidelines (RayXpert® Manual 2022).

The spatial coordinate system was defined as follows:

- X-direction: Direction from the source to the detector. The source-to-test point distance was defined as D, from aperture to detector as D1, from the test point to the wall as D2, and from the source to the back wall as D3.
- Y-direction: Room width (W = 4 m)
- Z-direction: Room height (H = 5 m)

The cylindrical detector, with a sensitive volume measuring (Φ10 cm × 30 cm) and enclosed in a 2 mm thick aluminum shell, was positioned along the beam's central axis. In accordance with ISO 4037 requirements for uniform irradiation of the entire sensitive volume, the beam cone angle was set to 16°, ensuring that its cross-section exceeded the detector's volume (ISO 4037-1 2019).

The Monte Carlo technique was utilised to model photon fluence and establish the distribution of the dose rate throughout the central axis of the beam. Dose mapping was performed both with and without detectors in place to examine the impact of scattering and attenuation. The spatial dose rate distribution was influenced by both the room geometry and materials, as well as the scattering contribution from the detector volume. The results serve as a reference field for calibration studies, with the field dimensions and shielding designed to meet international radiation protection standards (Montgomery 2013, ICRP No.103 2007).

3.3 Monte Carlo Simulation Setup with RayXpert®

In this section, the simulation setup is described in detail using the RayXpert® Monte Carlo code to evaluate the shielding effectiveness and dose homogeneity of a gamma irradiation unit. The system modelled is the Hopewell ISO-S-^{137}Cs Gamma Irradiation Unit, equipped with sealed 137Cs sources of nominal activities 8.58 Ci and 50 mCi (reference date: 14.05.2009). This unit is currently installed in the G-1 Laboratory at the Institute of Nuclear Sciences of Ankara University. The simulations aim to support the theoretical component of this thesis by modelling the experimental setup as accurately as possible in RayXpert®, a commercial CAD-based Monte Carlo software (License No: *259603454, UNIV TURKIYE, Ankara Üniversitesi*). The results obtained will later be compared with experimental measurements made using a 450 cm^3 ion chamber and a Geiger-Müller detector.

Source Definition and Placement: In this study, two sealed ^{137}Cs sources were employed. The first was an 8.58 Ci source, typically utilized for routine high-dose irradiation applications. The second was a 50 mCi source, intended for low-dose and close-proximity measurements. In the RayXpert® simulation environment, the source configuration interface was accessed and each source was defined as a decay source. The selected radioisotope was ^{137}Cs from the JEFF 3.1.1 database, using only photon emissions. Electrons and other emissions were deactivated in order to focus only on gamma interactions. The space configuration was defined as a point source positioned inside the source capsule, aligned with the location in the irradiation unit. The direction of emission was configured to match the axis of the collimated beam.

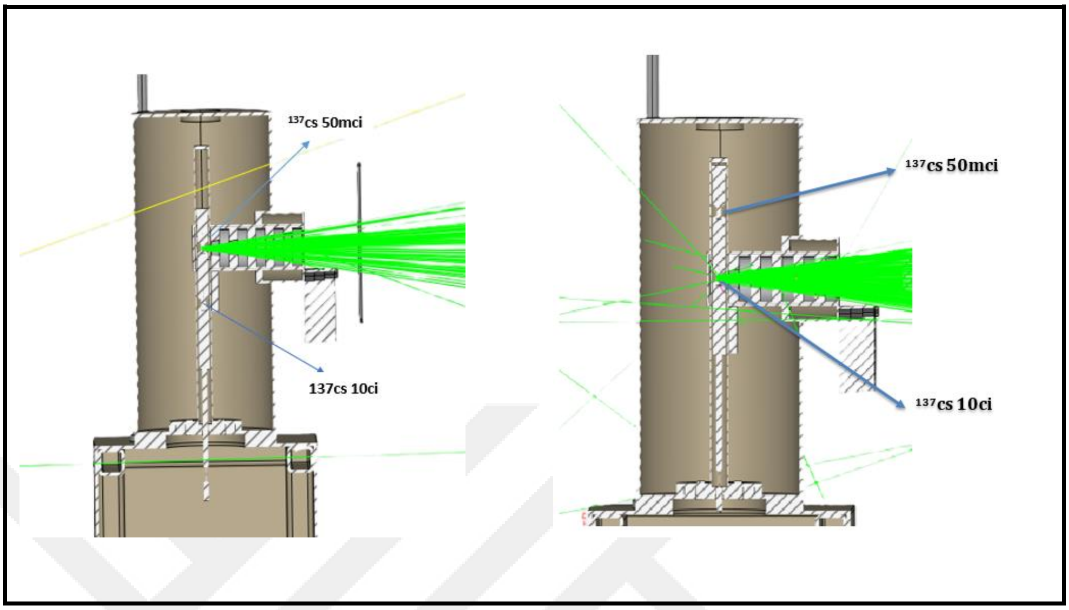

Figure 3.6 Source configuration for 8.58 Ci and 50 mCi ^{137}Cs sources

Detector Configuration: The simulation employed multiple virtual detectors (sensitive volumes) to evaluate dose rates at various locations. Two linear detectors were positioned along the main beam axis at distances of 50 cm and 100 cm from the source. Additional detectors were placed near the shielding structure to assess potential radiation leakage in the near field, and one detector was located behind the wall inside the control room to monitor occupational exposure levels. These detectors were modeled to represent ion chamber volumes, using either cylindrical air-equivalent geometries or spherical sensitive volumes.

Evaluation of dose homogeneity at target distances for consistent irradiation of samples and detectors is one of the thesis's goals. Setting up 2D grid maps, or mapping surfaces, at specific intervals along the beam axis allowed for this to be accomplished. The grids were defined as 30 cm x 30 cm square planes. The following distances were used to position each grid perpendicular to the beam axis: At 50 cm, 100 cm, and 150 cm for the 50 mCi ^{137}Cs source, at 50 cm, 100 cm, and 200 cm for the 8.58 Ci ^{137}Cs source. These positions were selected in order to evaluate the uniformity of the distribution of the dose and to identify areas where the dose variation remains within 5% (homogeneity ≥ 95%).

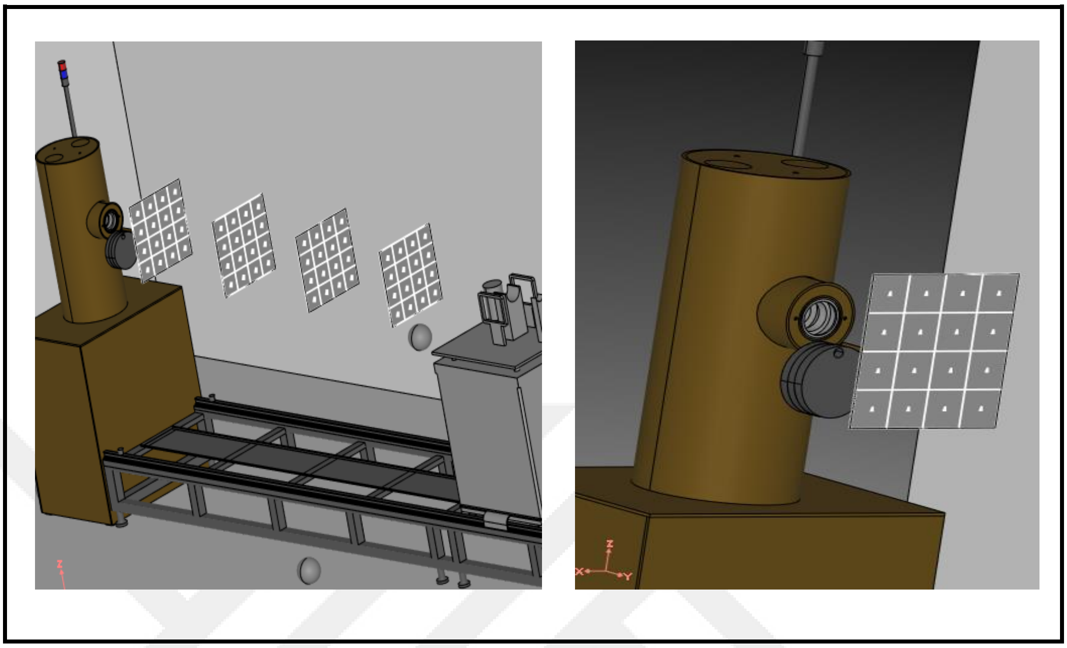

Figure 3.7 2D grid mapping setup at 50 cm, 100 cm, 150 cm, and 200 cm for both sources.

Monte Carlo Computation Setup: The Monte Carlo simulation was set up computation parameters after completing the geometry and detectors. The RayXpert® standard transport algorithms were used, and the physics was configured to only use photon transport.

The calculation parameters were set as follows: the number of particle trajectories was $1x10^7$; no variance reduction techniques were applied; the observable of interest was the ambient dose equivalent, *H*(10), as defined by ICRP 74; multithreading was enabled using 8 processor cores; and the stopping criterion was a relative statistical error of less than 5% per detector volume (X-5 Monte Carlo Team 2003).

Three key dosimetry quantities were selected for evaluation:

- Flux (particles/cm²/s): The following quantity represents the particle fluence rate, showing the number of photons traversing the unit region per second. It delivers information about photon field strength at various locations.
- Air Kerma (Gy or µGy/h): The Air Kerma defines the kinetic energy distributed in air by photons, that has relevant for dosimetry in free-air limitations. This figure was calculated on the detector surfaces and in the mapping dose.
- Ambient Dose Equivalent H(10)*: The following is the operational quantity proposed by the ICRP for evaluating the dose from the outside gamma radiation. It represents the effective dose measured at a tissue depth of 10 mm, which is used for radiation protection assessments. The progress of the simulation was monitored using the built-in convergence features. When the simulation was done, the dose maps and detector data were exported for analysis.

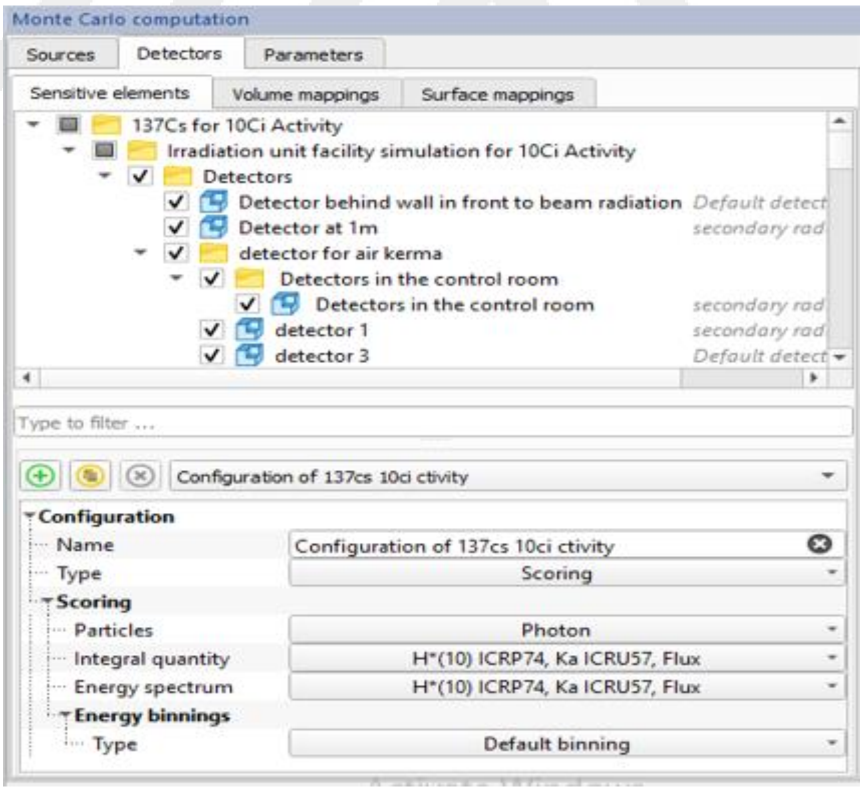

Figure 3.8 Configuration and detector setup for Monte Carlo simulation of ^{137}Cs (10 ci) irradiation facility (RayXpert® Manual 2022)

Monte Carlo computation settings and convergence indicators were monitored throughout the simulation. For post-processing and data analysis, RayXpert®'s tools were used to extract and visualize the results. This included dose rate measurements (in μGy/h or mGy/h) at each detector, two-dimensional dose distribution maps for each mapped surface, and the associated statistical uncertainties and standard deviations.

These variables simulation outputs will be compared with experimental measurements conducted using a calibrated ion chamber and Geiger-Muller detector placed at identical locations.

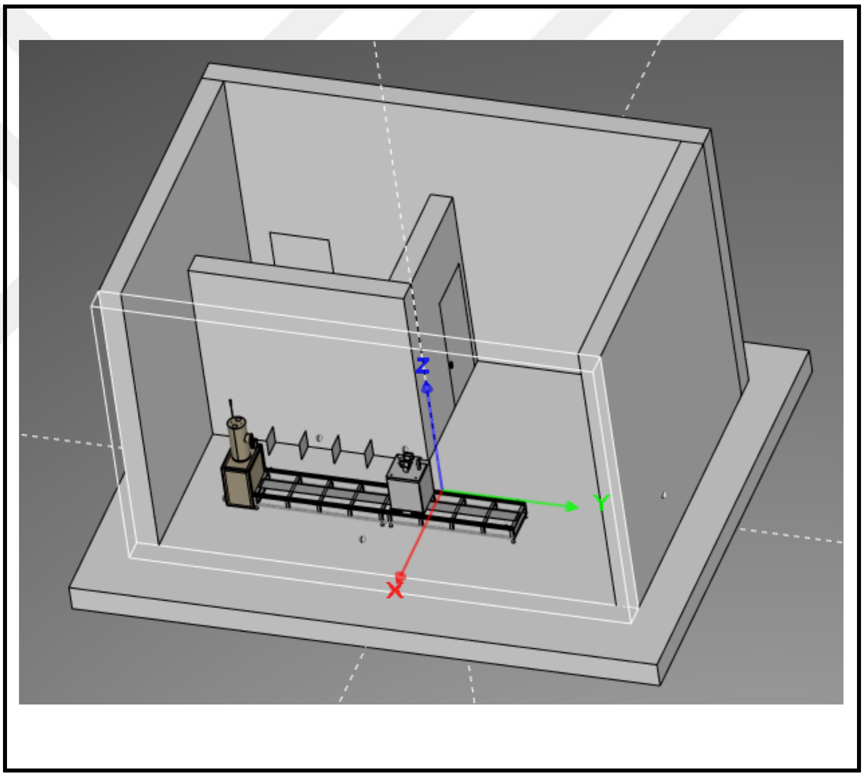

Figure 3.9 Dose map visualizations and extracted detector values

By analyzing both the shielding performance and the dose homogeneity, this simulation supports a comprehensive theoretical evaluation of the irradiation unit, which is validated through practical experiments at the Ankara University Institute of Nuclear Sciences.

4. RESULTS

4.1. Dose Rate Investigation

4.1.1 Background radiation assessment near a ^{137}Cs irradiation unit (source not exposed)

Figure 4.1 Radiation Surveymeters a)NEB G-M Detector, b)SmartIon Chamber

A certificated G-M counter(Model NEB.211 S/N 162) and a 450 cm^3 sensitive volume *SmartIon* Mini Instruments Detector (Model MFG507 and Serial No. M0004993) were regularly used in the irradiation unit laboratory for dose rate measurements as well as environmental dose measurements. During calibration, another PTW 28cm^3 sensitive volum cylindrical ion chamber detector connected to a PTW UNIDOS Webline electrometer is carefully positioned at fixed distances from the source. The detector measures units is Gy/h, mGy/h, µGy/h.

The Dose Rate Meter (ÇNAEM: NEB.211,) is a manually operated radiation detector that is used every day in the laboratory to monitor background radiation levels. The function of this detector is to verify ambient radiation dose rates and ensure safe working conditions within the irradiation unit. It measures various units, for example R/h, mR/h and µR/h, for precise assessment of dose rates from low to high. Regular calibration and use of this device are important for maintaining radiation safety standards and detecting abnormal changes in radiation levels in the laboratory.

Figure 4.2 PTW TM23361 Model Cylindrical Ion Chamber

The TM23361Model(S/N:0535) is a precision air-filled ionization chamber designed for use in radiation dose measurements in calibration laboratories, radiological protection, and medical physics applications. This detector works by collecting the ion pairs produced when ionizing radiation, gamma rays from sources like ^{60}Co or ^{137}Cs, passes through the chamber's air. It is recognized for its stability, linear response, and energy independence over a wide energy range. The chamber offers precise measurements of quantities like ambient dose equivalent or Air Kerma. It needs to be connected to a high precision electrometer in order to measure the resulting ionization current, the chamber is important instrument for high accuracy dosimetry in standard and reference measurements.

Background Radiation Assessment Around ^{137}Cs Irradiation Unit (Source Not Exposed Position):

Before the operational use of a ^{137}Cs irradiation unit, it is critical to assess the ambient radiation levels around the unit with the radioactive source in the shielded position. This step ensures that the environment remains within safe radiological limits even when the source is not actively irradiating. These evaluations conform to the international safety guidelines on radiation exposure limits for occupational and public settings, as defined by organisations (NCRP No.147 2004).

In this study, 10 measurement points were selected in proximity to the irradiation unit, and radiation dose rates were recorded using calibrated instruments. The readings, originally in milliroentgens per hour (mR/h), were converted to milligray per hour (mGy/h) to standardize dosimetric assessment.

Table 4.1 Background radiation levels around an inactive irradiation unit when in its shielding

Point	**Dose Rate (mR/h)**	**Dose Rate ($\mu Gy/h$)**
1	22.0	0.193
2	24.0	0.210
3	40.0	0.351
4	31.0	0.272
5	17.4	0.153
6	14.0	0.123
7	28.0	0.246
8	31.0	0.272
9	25.0	0.219
10	20.0	0.175
Average		**0.221±9.52%**

The correlation coefficient (R) is estimated to be 0.999, and the standard deviation (σ) for the dose rate measurements(n=10) is to be 0.0632 μGy/h, however, experimental standard deviation is to be 0.0211 μGy/h.

Background Dose Rate Measurements Near the Irradiation Unit (Source Not Active):

The measured dose rates ranged from 0.123 μGy/h to 0.351 μGy/h, with an average value of 0.221 μGy/h. Although these levels are relatively low, they reflect: Standard safety guidelines state that when the source is in storage (unexposed) position, the ambient dose rate in areas that are accessible to personnel must not exceed 0.5 μGy/h (ICRP No.103 2007). The room possibly be safely occupied in non-operational conditions because the average dose rate of 0.221 μGy/h found in this study is below acceptable safety limits.

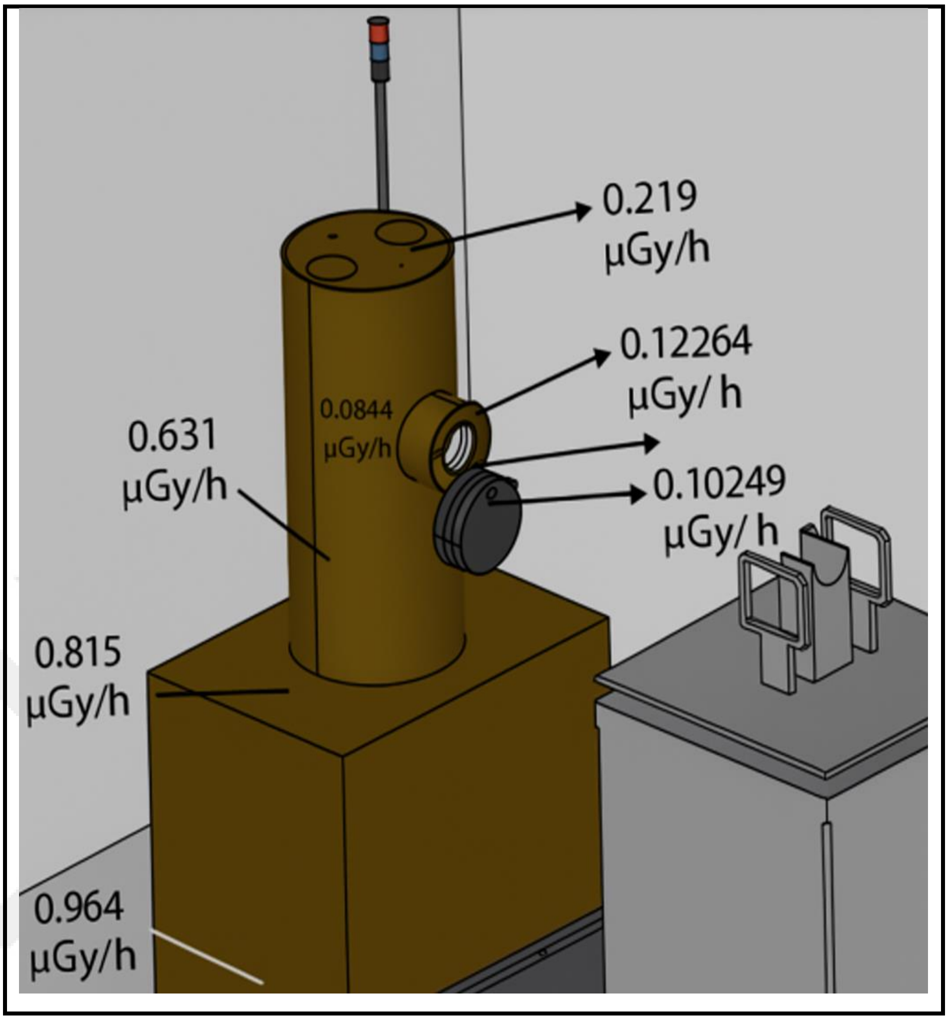

Figure 4.3 Measurements of dose rates across the 10 measurement points around the ISO s-^{137}Cs source irradiation unit

The dose rate (Air Kerma) was manually measured near the ISO s-^{137}Cs irradiation unit in Institute of Nuclear Sciences of Ankara University to assess the radiation levels and evaluate the effectiveness of the unit's shielding. These measurements are crucial for ensuring safety and compliance with radiation protection standards.

4.1.2 Dose rate measurements at 100 cm distance

The dose rate was measured at a distance of 100 cm from the ^{137}Cs source in the experimental setup. For the 10 Ci activity, the recorded dose rate was 15,7 mGy/h, while for the 50 mCi source, the measured value was only 87 μGy/h. Given the significantly lower dose rate of the 50 mCi source, it was evaluated as negligible in terms of its contribution to the irradiation process and was excluded from further analysis. The aim, therefore, remained on the highly radioactive 10 Ci source, which is representative of the operational dose levels relevant to irradiation treatment and safety assessments.

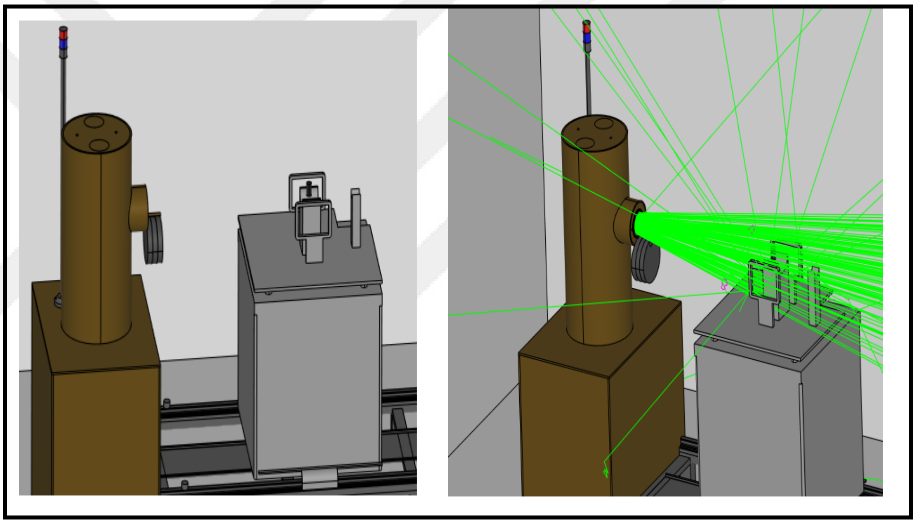

Figure 4.4 Simulation RayXpert® at 1m from the source

By using Monte Carlo simulation with the RayXpert® software to estimate the theoretical dose rate under the same geometric and material conditions. The simulation provided a dose rate of 18.2 mGy/h at 100 cm, slightly higher than the experimental value. This difference of approximately 2.5 mGy/h can be attributed to idealized assumptions in the simulation, such as perfect geometry, uniform emission from the source, and the exclusion of environmental factors that reduce scattering. the simulated and experimental values agree well, showing the validity of the Monte Carlo model and its applicability for other studies on shielding and dose distribution.

4.2 Experimental Dose Homogeneity Evaluation

ISO 4037-1 standard stipulates that the Air Kerma rate at each test point must differ by no more than 5% across the entire cross-sectional area of the detector's sensitive volume or the full area of the phantom. Hence, in order to assess the dose distribution around the Hopewell ^{137}Cs irradiation unit, experimental measurements were carried out using a 30 cm × 30 cm grid, subdivided into 16 points (from position 1.1 to 4.4) with 10 cm spacing between each line. At each grid point, a 28 cm^3 sensitive volume TM23361(S/N:0535) ionization chamber was positioned and exposed to radiation for a period of 60 seconds. The objective was to analyze the homogeneity of the dose field at four distinct source-to-detector distances: 50 cm, 100 cm, 150 cm, and 200 cm.

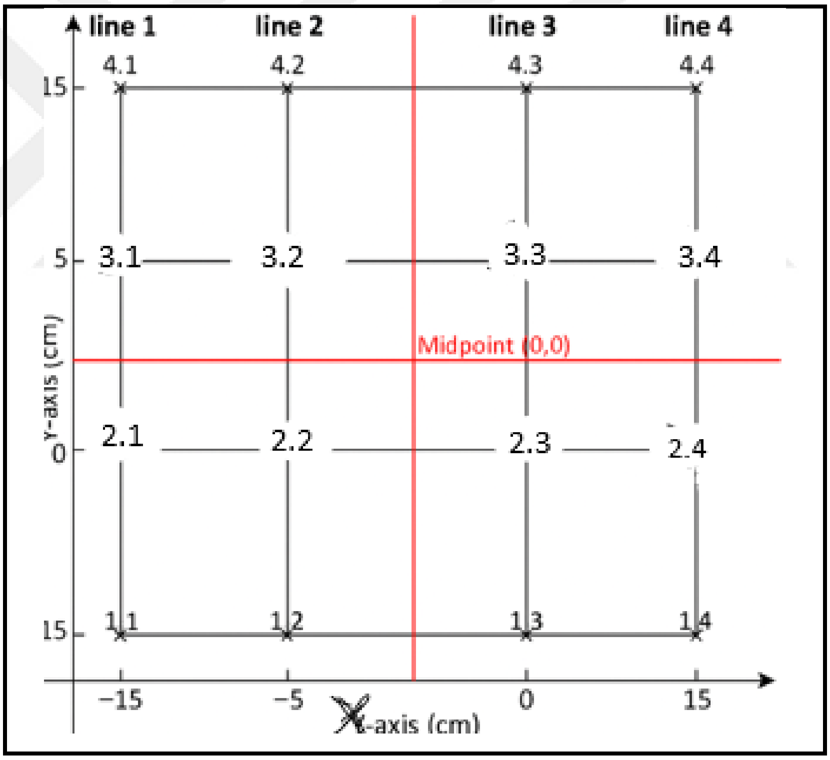

Figure 4.5 Model of dose homogeneity measurement points in a two-dimensional grid

The aim of this grid mapping is to assess the uniformity of the dose rate. It is a 30 cm × 30 cm measurement area centered at (0,0). The grid consists of 16 points from 1.1 to 4.4, distributed symmetrically around the center in a 4x4 matrix, positioned at ±15 cm and ±5 cm on both the X and Y axes. The points are spaced 10 cm from each other, starting 5 cm from the center. The detector placed manually at each labelled point to measure the Air Kerma dose rate. The dose rate measured for 60 seconds at position 1.1, then moved the detector sequentially through each position 1.2, 1.3, and so on until the final point 4.4, to ensure consistent measurement conditions across the entire grid. This precise, repeated process enables us to analyse the uniformity of the radiation field.

Dose homogeneity within this target irradiation area is studied at distances of 50 cm, 100 cm, 150 cm, and 200 cm.

Table 4.2 Dose Distribution Measurements at Varying Distances from ^{137}Cs Source

Position	Measured 50cm mGy/h	Measured 100 cm mGy	Measured 150cm mGy/h	Measured 200 cm mGy/h
1.1	0.162	0.747	5.714	3.777
2.1	0.378	9.501	6.741	3.870
3.1	0.591	12.200	6.807	3.855
4.1	0.513	4.491	6.777	3.825
4.2	1.056	14.870	6.906	3.912
4.3	1.332	15.260	6.957	3.921
4.4	0.600	5.820	6.873	3.906
3.2	51.51	15.860	7.065	3.957
3.3	62.48	16.060	7.092	3.969
2.2	47.58	15.720	7.062	3.987
2.3	60.84	15.750	7.071	3.975
1.2	0.618	10.670	6.765	3.885
1.3	0.447	11.140	6.750	3.903
1.4	0.177	0.732	5.754	3.816
2.4	0.531	9.495	6.855	3.909
3.4	1.155	15.330	7.074	3.954

Measurement period is 60s for all measurements.

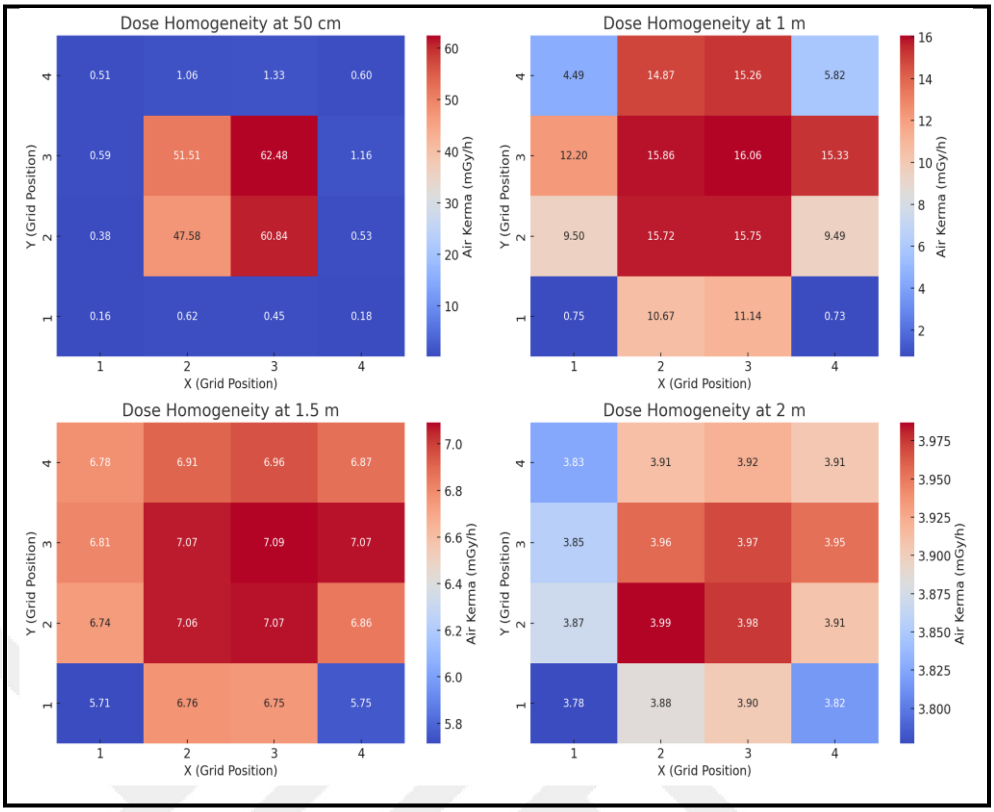

Figure 4.6 Experimental dose homogeneity

At 50 cm, the dose distribution displayed good homogeneity only in the central region of the grid. The highest Air Kerma values were recorded at: 2.2, 2.3, 3.2, 3.3 points.

Table 4.3 The maximum dose rate values 50 cm

Position n in the grid	**Measured Air Kerma rate (mGy/h)**
Point 2.2	47.58
Point 2.3	51.51
Point 3.2	60.68
Point 3.3	62.73

These values formed a central high-dose plateau, with only about 10% variation, indicating a localized area of homogeneity. However, beyond this central zone, the dose rate decreased sharply. For example, peripheral positions such as 1.1 and 4.4 showed values as low as 0.16–1.33 mGy/h, illustrating the collimation effect of the 16° beam angle. This steep dose gradient is typical at short distances due to the strong angular confinement of the beam.

At a distance of 100 cm, dose homogeneity improved over a broader portion of the grid. Although the central values decreased due to beam divergence, they remained within a moderate range:

Table 4.4 Dose rate measurements at 100 cm distance

Position n in the grid	**Measured Air Kerma rate (mGy/h)**
Point 2.2	15.72
Point 2.3	14.76
Point 3.2	15.75
Point 3.3	16.06

An average of around 15.5 mGy/h was shown by these central values, the dose inhomogeneity was continued to be shown by edge positions like 1.3 (12.2 mGy/h) and 4.1 (0.73 mGy/h) by increasing the distance for a wider irradiated area, improving uniformity, it was not yet fully homogeneous.

At 150 cm, the dose field demonstrated considerable uniformity across the entire grid. Measured Air Kerma values ranged from approximately 5.71 mGy/h to 7.09 mGy/h, with variations of less than 15% across all 16 points. This suggests that beyond this distance, the collimator's influence diminishes and the field becomes effectively homogeneous.

At 200 cm, uniformity was confirmed once more, with all measured values ranging between 3.78 mGy/h and 3.99 mGy/h. These results confirm that full dose homogeneity is achieved beyond 150 cm. Such data are essential for selecting source-to-detector distances for calibration and dosimetry applications, ensuring reliable and uniform exposure.

It is worth noting that the reference Gamma radiation emitted by radionuclides and the method and requirements by which a laboratory can produce a reference radiation field for a selected radiation quality, with a target value of the expanded overall uncertainty (k = 2) of the dose(rate) value of about 6 % to 10 %. (ISO 4037-1 2019). In this the estimated maximum overall uncertainty is 7% at a 95% confidence level.

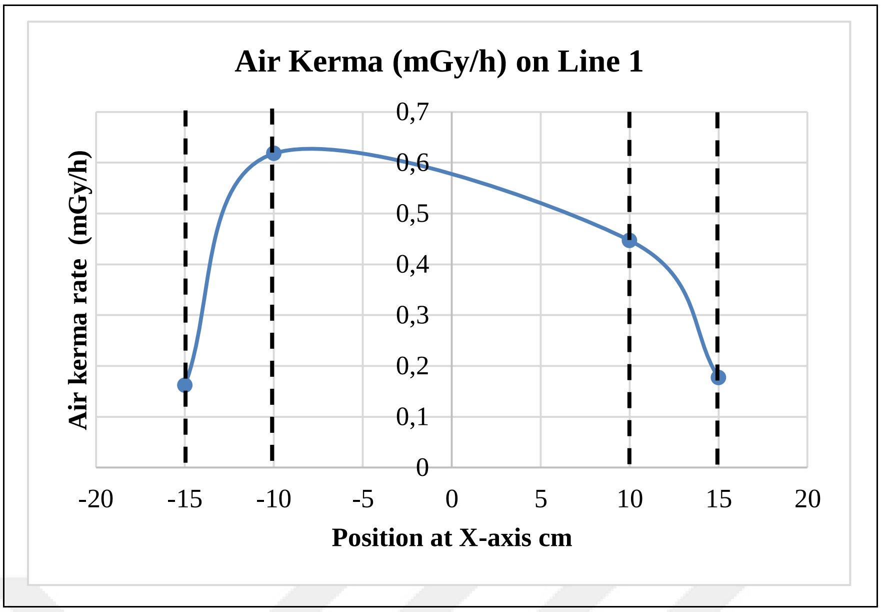

Figure 4.7 Air Kerma measured on line 1 at 50 cm

Line 1 shows a gradual rise in Air Kerma rate from the periphery 0.1 mGy/h to the central beam axis 0.6 to 0.7 mGy/h. This reflects the peripheral exposure and partial coverage of the primary beam. Dose distribution close to the source is highly non uniform due to scatter contribution and sharp beam edges (Attix 2004).

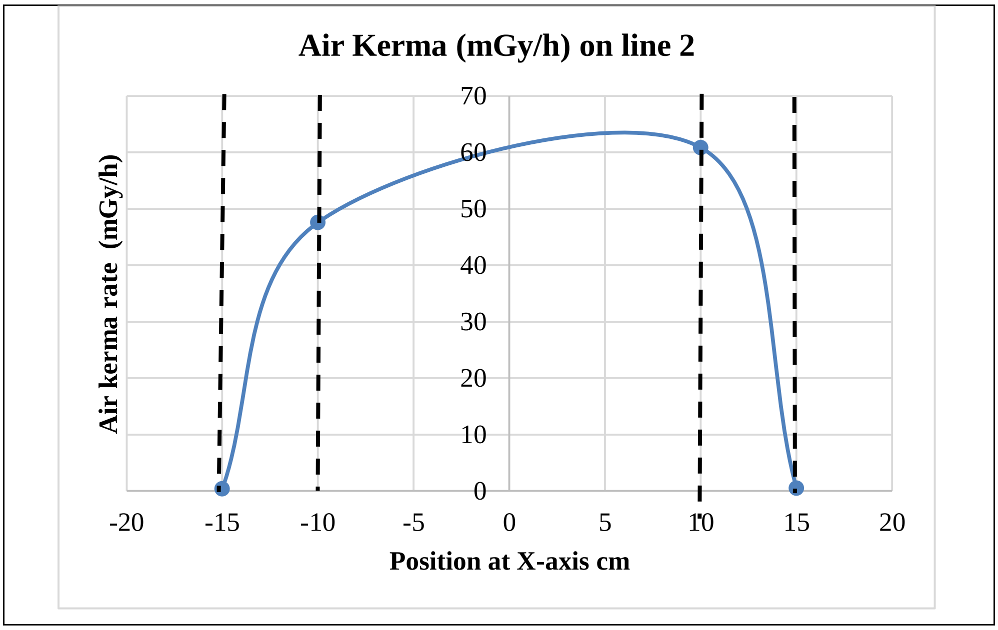

Figure 4.8 Air Kerma measured on line 2 at 50 cm

Line 2 demonstrates the strongest maximum 60 mGy/h to 70 mGy/h at the central axis. This corresponds to the direct exposure region where beam intensity is maximum, the primary radiation field, dominated by unattenuated photons (Bushberg et al. 2012).

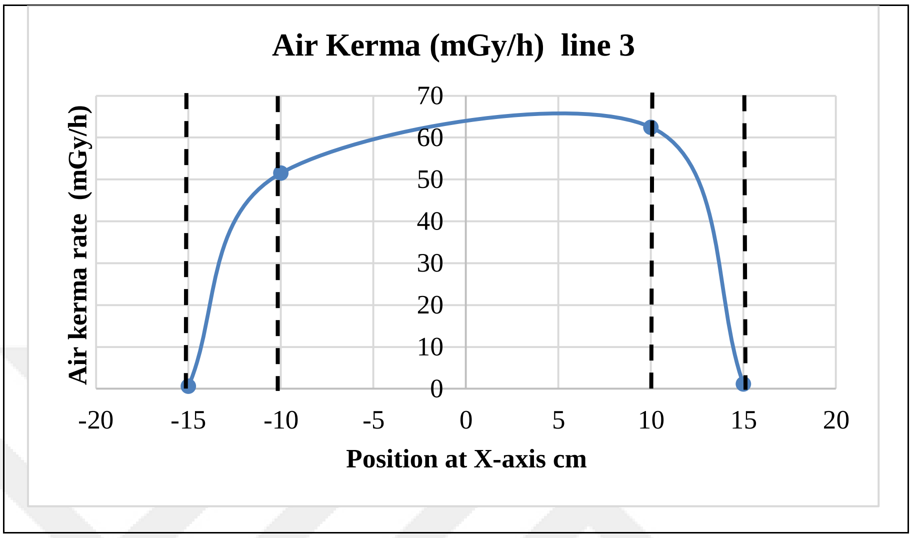

Figure 4.9 Air Kerma measured on line 3 at 50 cm

Line 3 has an intermediate maximum 40 mGy/h to 50 mGy/h, indicating partial overlap with the central field but with slightly reduced intensity. Lateral displacement from the central axis reduces measured Air Kerma due to inverse square geometry and beam divergence (El-Sersy et al. 2012).

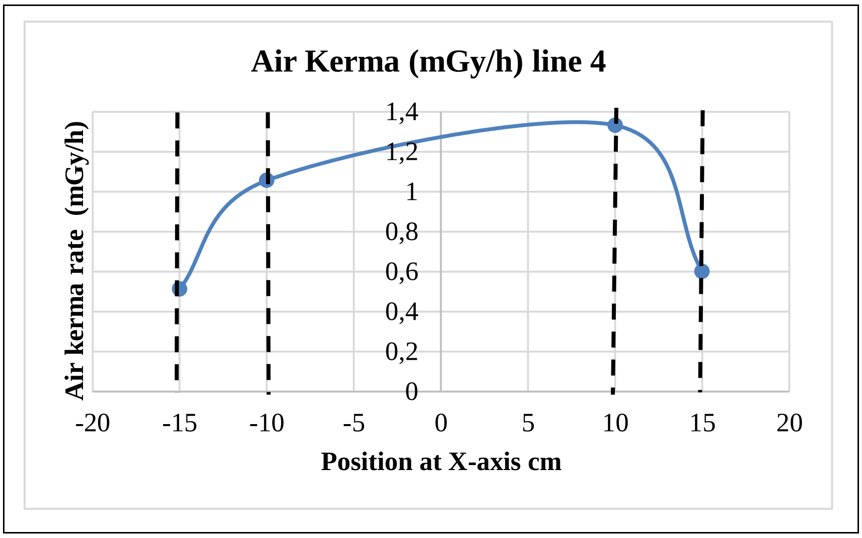

Figure 4.10 Air Kerma measured on line 4 at 50 cm

Line 4 records only 1.2 mGy/h to 1.4 mGy/h at maximum, showing it mostly lies outside the intense primary beam. Peripheral dose profiles at short distances reflect mostly scatter radiation with minimal primary contribution (AAPM TG-108 2006).

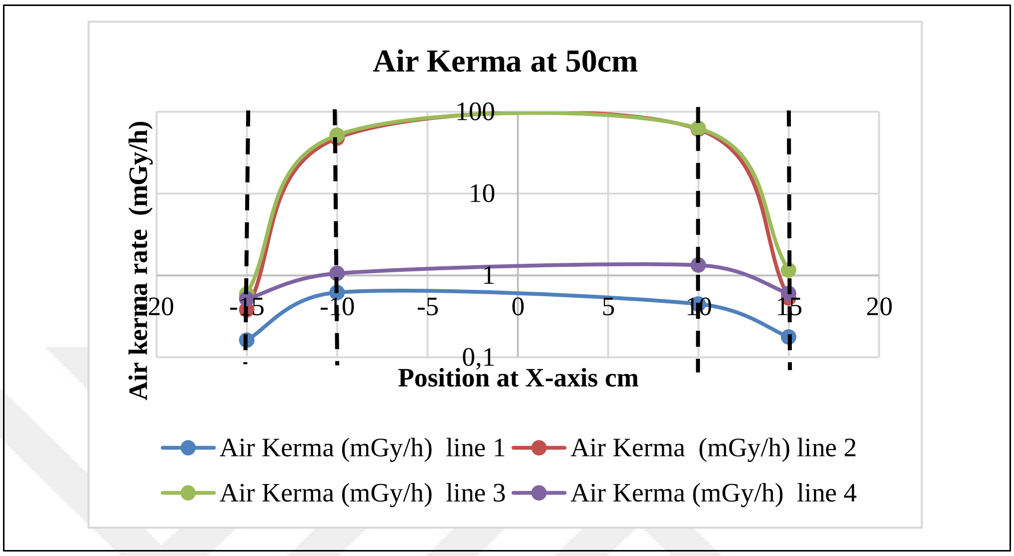

Figure 4.11 Air Kerma measured on line 1 , line 2 , line 3 , line 4 at 50 cm

As expected, the central Air Kerma dose rate declined with increasing distance from the source, due to the anticipated beam divergence and inverse square law. At distance of 50 cm, the measured central dose rate was 61 mGy/h, representing the maximum intensity in the irradiation field.

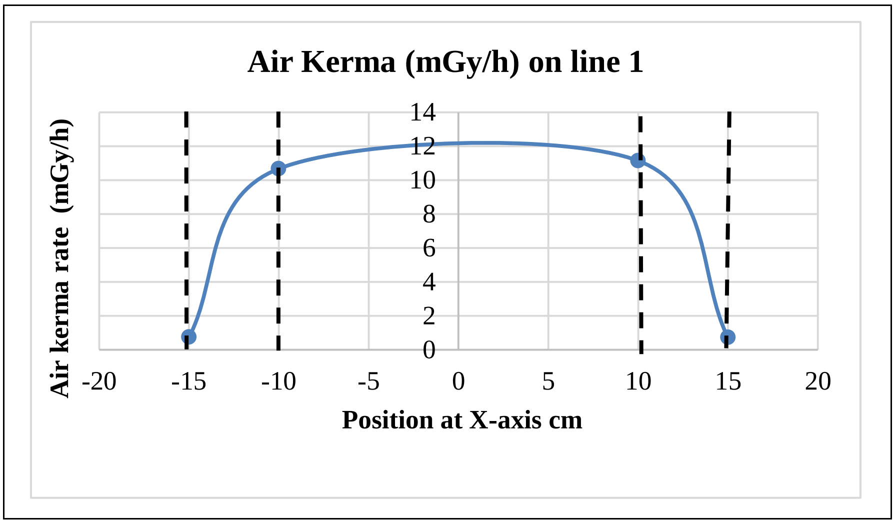

Figure 4.12 Air Kerma measured on line 1 at 100 cm

Line 1 increases from 12mGy/h to 14 mGy/h at the beam center, illustrating dose decrease with distance. The dose profile at 1 m becomes broader and smoother compared to short distances (Dörschell et al. 1995).

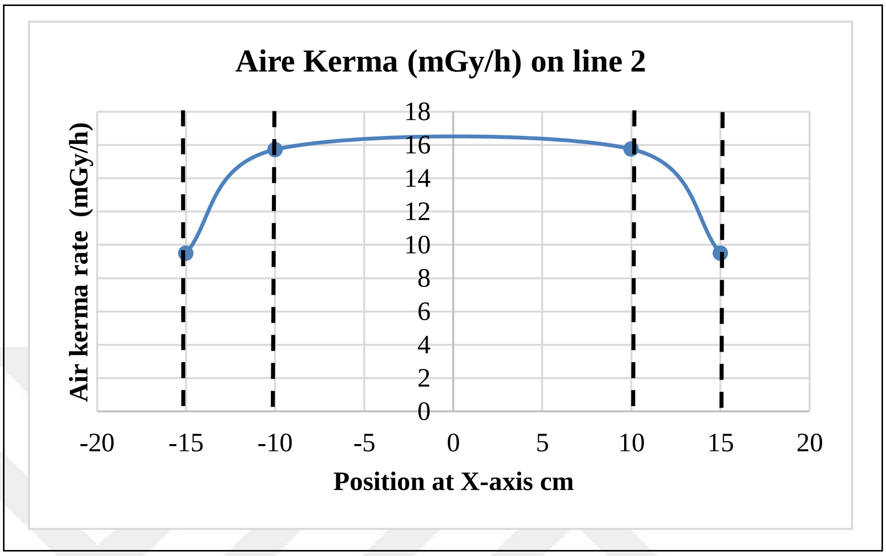

Figure 4.13 Air Kerma measured on line 2 at 100 cm

Line 2 reaches the highest intensity 16 mGy/h, confirming its alignment with the central axis. Literature indicates that at 1 m, the central maximum is still visible but less sharp than at 50 cm (Yang et al. 2023).

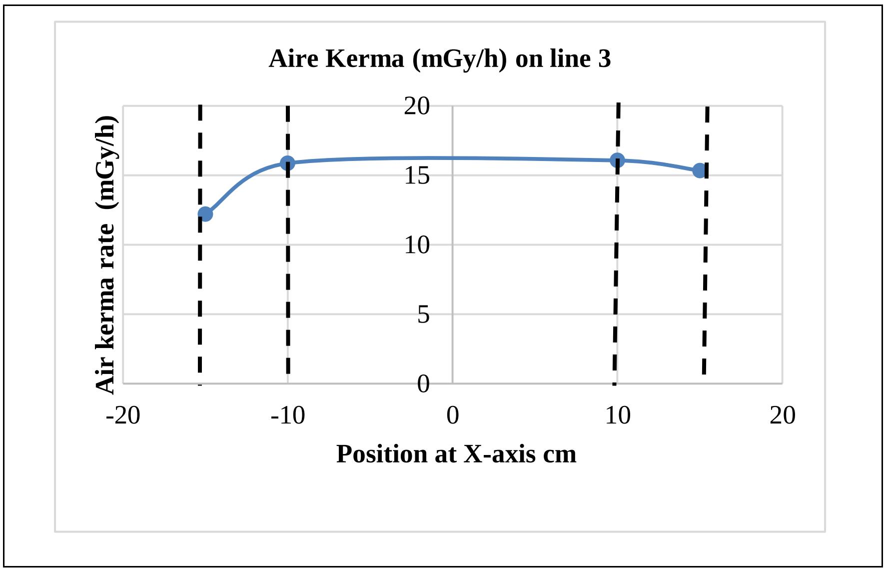

Figure 4.14 Air Kerma measured on line 3 at 100 cm

Line 3 maximum at 14mGy/h to 15 mGy/h, nearly symmetric to line 2 but slightly lower. This reflects lateral spread of the beam as predicted by the inverse square law and beam divergence.

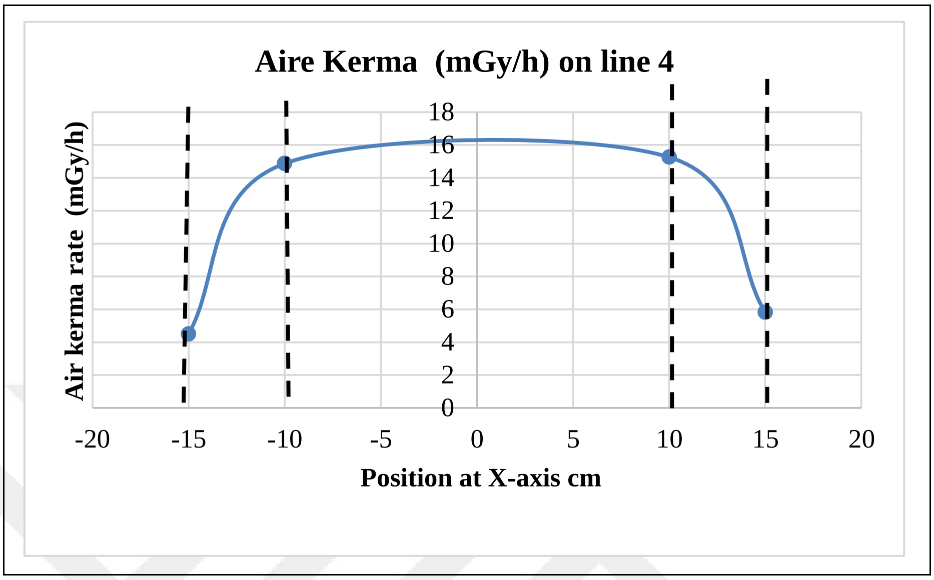

Figure 4.15 Air Kerma measured on line 4 at 100 cm

Line 4 is flatter 13mGy/h, 14 mGy/h maximum, suggesting more uniform exposure. At mid range distances, lateral scatter smoothens dose variation across measurement lines (Bushberg et al. 2012).

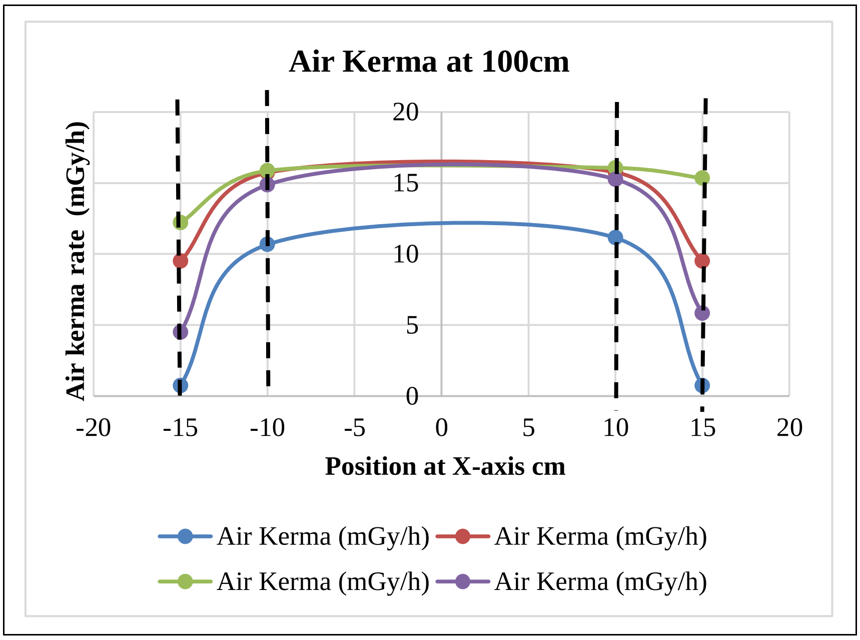

Figure 4.16 Air Kerma measured on line 1, line 2 , line 3 , line 4 at 100 cm

As the detector is moved to 100 cm distance, the dose rate dropped to 15 mGy/h, indicating a sharp 75.4% reduction. This considerable decrease is primarily due to the narrow collimation angle and the concentrated nature of the beam at shorter distances.

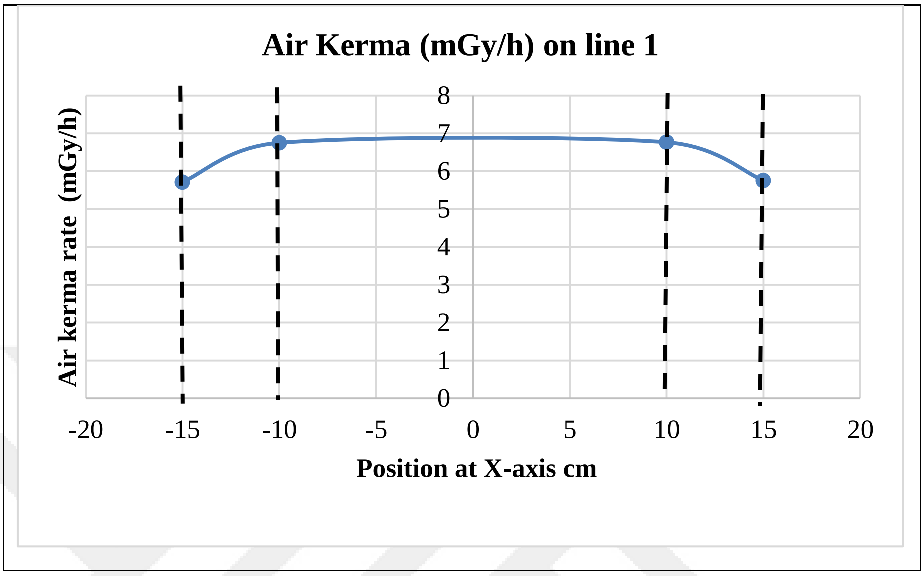

Figure 4.17 Air Kerma measured on line 1 at 150 cm

Line 1 shows nearly constant dose is 7 mGy/h. Beam homogenization with distance, where primary and scattered components blend (Attix 2004).

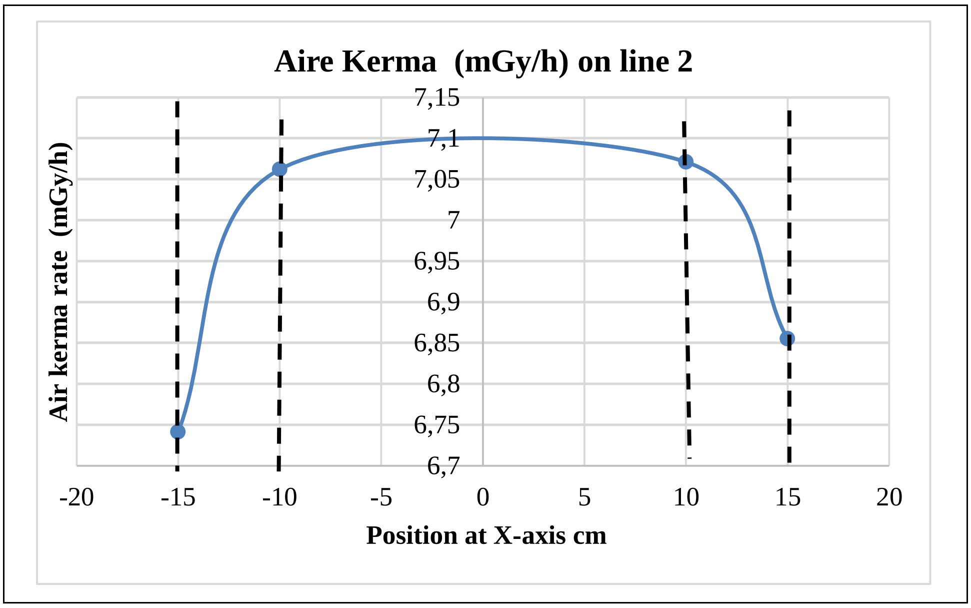

Figure 4.18 Air Kerma measured on line 2 at 150 cm

Line 2 values 6.9 mGy/h 7.1 mGy/h show minimal fluctuation, confirming beam uniformity. This is consistent with NCRP guidelines, which note that beyond 150 cm, dose profiles stabilize due to geometric broadening.

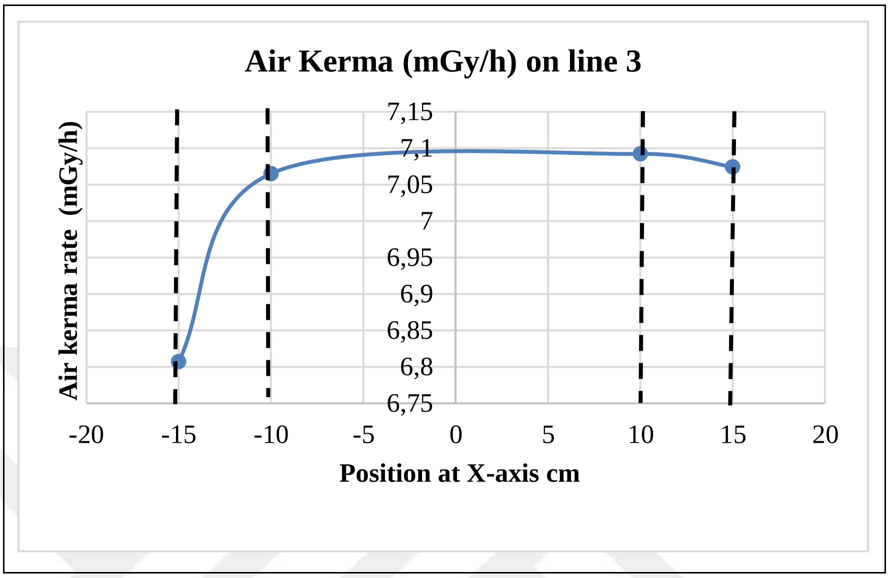

Figure 4.19 Air Kerma measured on line 3 at 150 cm

Line 3 follows a similar trend 6.8 mGy/h to 7.1 mGy/h. Differences between lines decrease as distance increases, since the divergence smoothens lateral variations (El-Sersy et al. 2012).

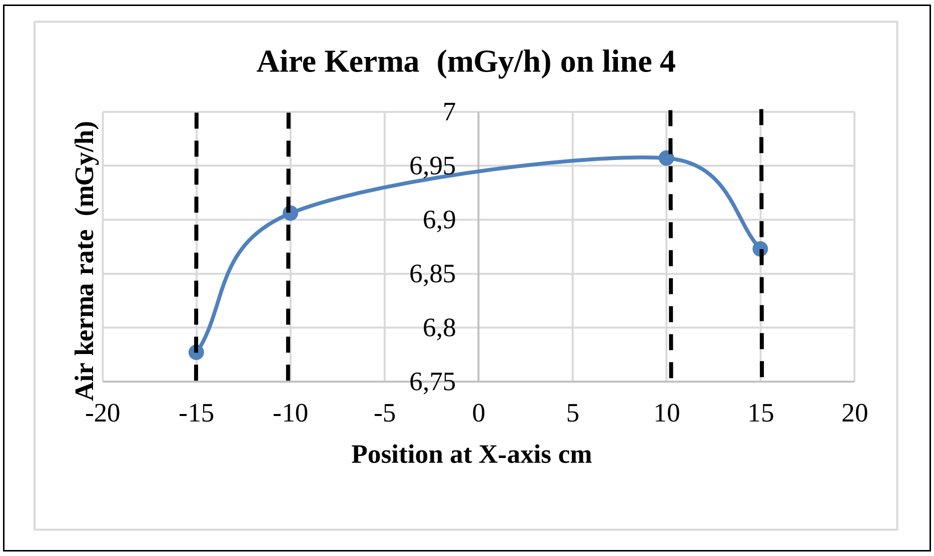

Figure 4.20 Air Kerma measured on line 4 at 150 cm

Line 4 remains between 6.76 mGy/h to 6.96 mGy/h, with negligible variation. This uniformity demonstrates the transition from localized hot spots (seen at 50 cm) to broad uniform fields at longer distances.

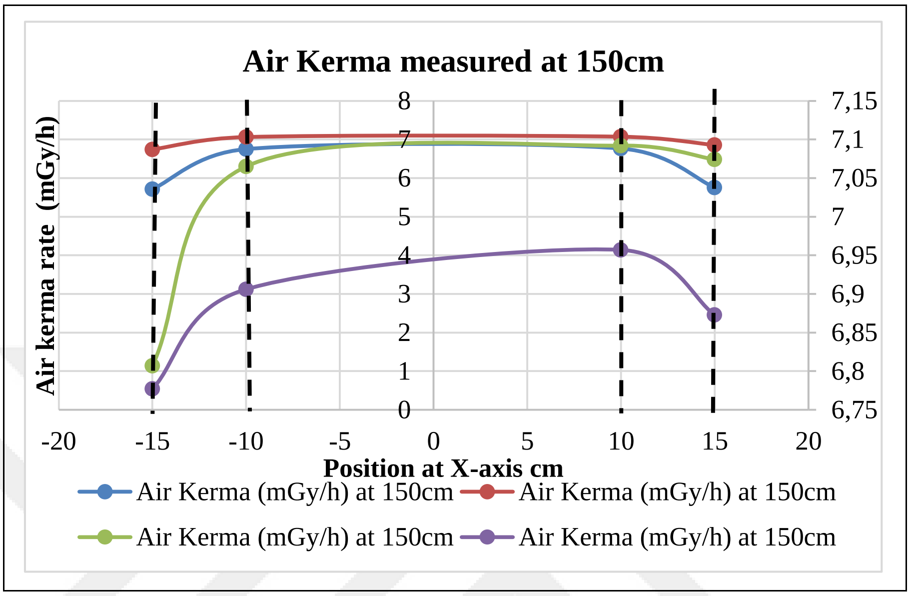

Figure 4.21 Air Kerma measured on line 1 , line 2 , line 3 , line 4 at 150 cm

At 150 cm Figure 4.21 shows the dose rate continued to decline to 7.092 mGy/h, corresponding to an additional 52.7% decrease from the 1 m measurement. The gradient of dose reduction became less steep beyond this point.

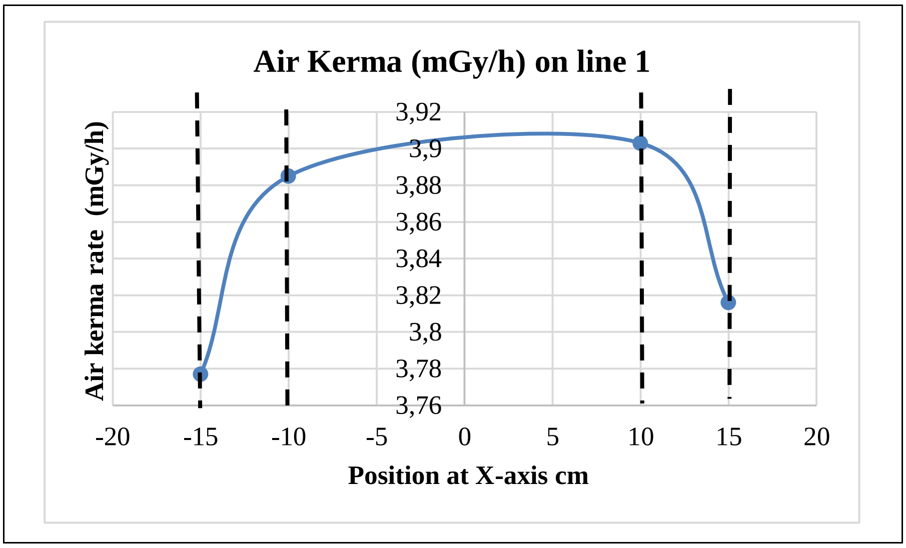

Figure 4.22 Air Kerma measured on line 1 at 200 cm

Line 1 values 3.76 mGy/h and 3.9 mGy/h reflect stable dose distribution. Literature confirms that at long distances, the beam profile becomes nearly flat (Bushberg et al. 2012).

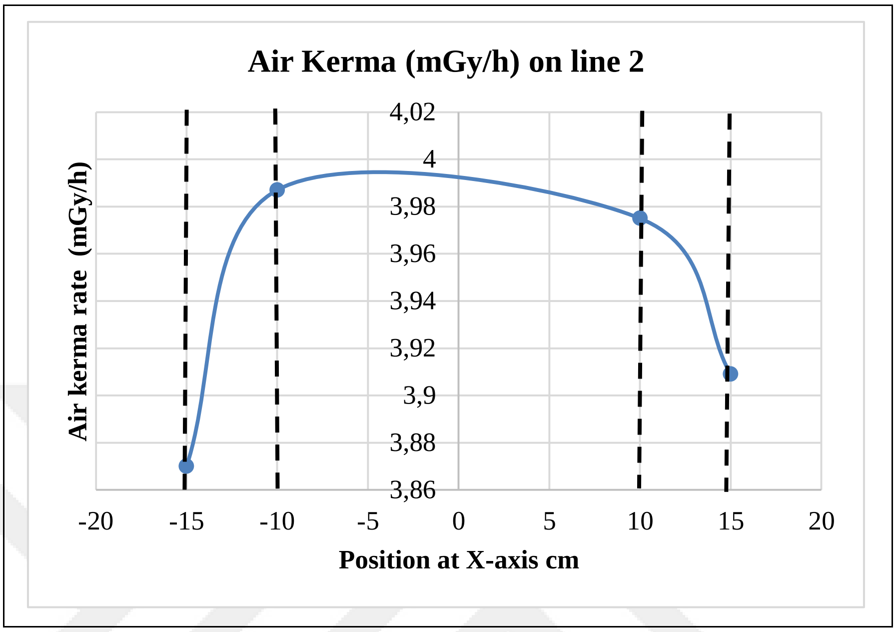

Figure 4.23 Air Kerma measured on line 2 at 200 cm

Line 2, (3.86 mGy/h to 4.02 mGy/h) shows slightly higher readings but almost uniform. Long distance profiles reflect mostly geometry and less field irregularity.

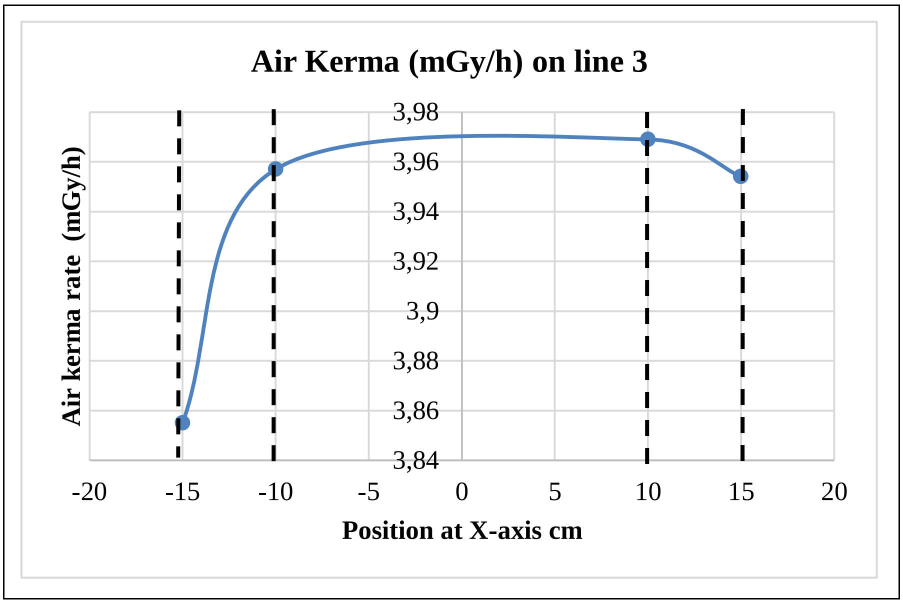

Figure 4.24 Air Kerma measured on line 3 at 200 cm

Line 3 (3.84 mGy/h to 3.98 mGy/h) overlaps with Line 2, confirming reproducibility which emphasizes field consistency at extended measurement distances.

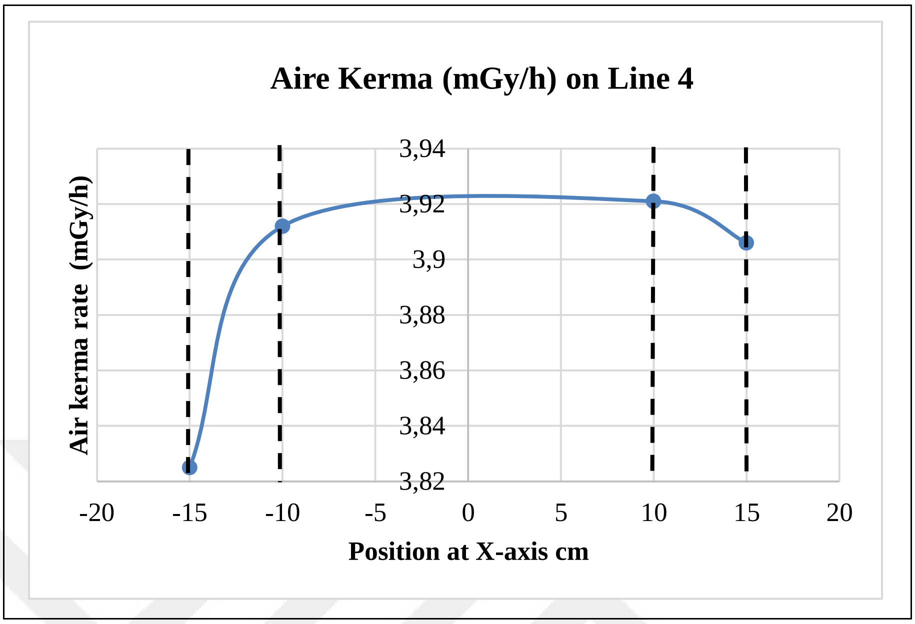

Figure 4.25 Air Kerma measured on line 4 at 200 cm

Line 4 (3.82 mGy/h to 3.94 mGy/h) is nearly identical to the others, confirming beam uniformity.

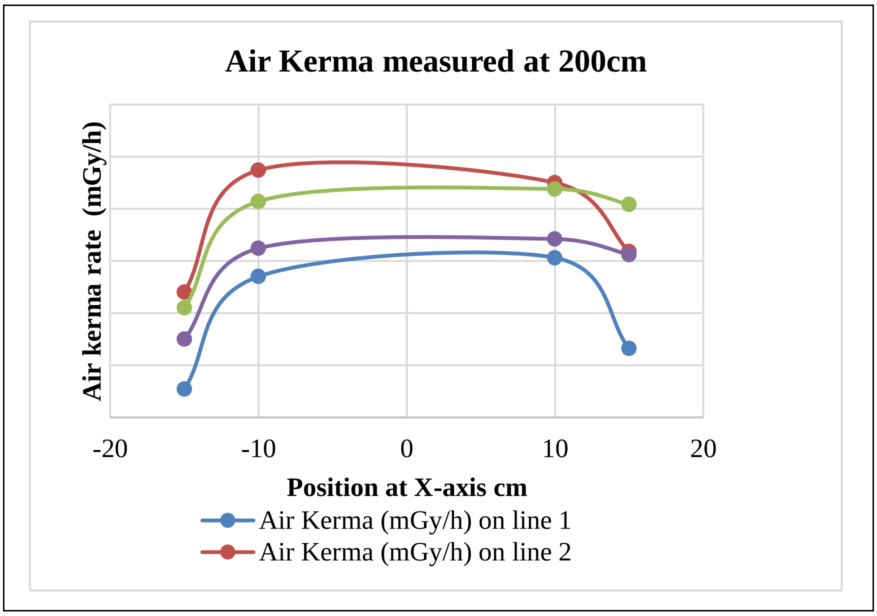

Figure 4.26 Air Kerma measured on line 1 , line 2 , line 3 , line 4 at 200 cm

Figure shows that at 200 cm, the central dose was measured at 3.9 mGy/h, a 45.0% decrease from the value at 150 cm. This gradual flattening of the dose rate with increasing distance reflects a transition toward a more uniform and stable irradiation field. Beyond 150 cm, the reduction in dose becomes more linear and the field more homogeneous, confirming that distances ≥1,5 meters are more suitable for applications requiring uniform exposure, such as calibration or dosimetry measurements. These observations are consistent with beam behavior governed by geometrical spread and partial attenuation due to collimation, and they align with recommendations outlined in ISO 4037 for reference radiation fields (ISO 4037-1 2019).

Table 4.5 Percentage Decrease in Central Dose Rate

Distance Interval	Percentage Decrease in Dose rate (%)	Comment
50 cm → 100 cm	75.4	Rapid intensity loss due to strong beam collimation and the inverse square law.
100 cm → 150 cm	52.7	Beam divergence continues; dose reduces at a slower rate.
150 cm → 200 cm	45.0	The field becomes flatter and more homogeneous.

Percentage Decrease in Central Dose Rate

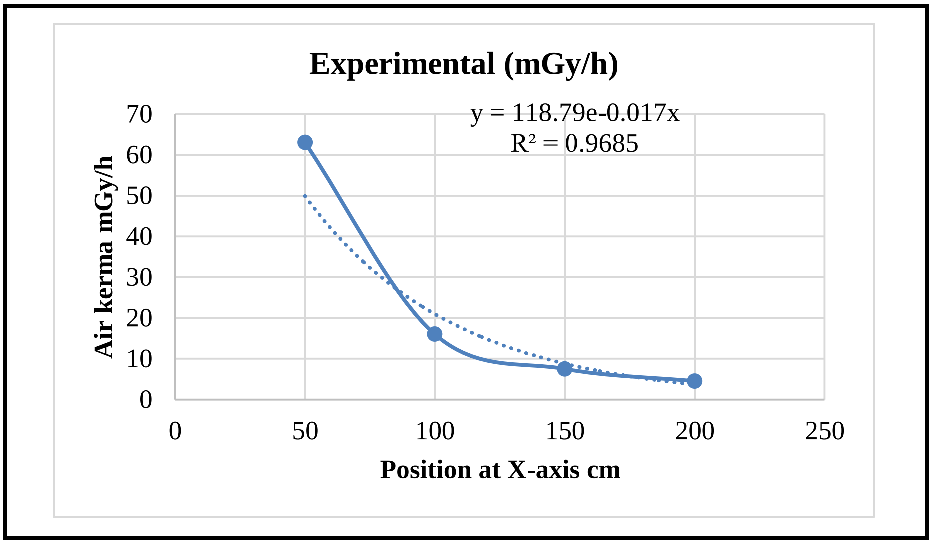

Figure 4.27 Experimentally measured Air Kerma rates and their fit values versus distance

This curve shows that the highest dose rate measured by experiment becomes lower as the distance from the source increases. At 50 cm, the dose is around 62.7 mGy/h, which is the highest. When moving to 100 cm, it drops to about 16,1 mGy/h. At 150 cm, it goes down to 7.6 mGy/h, and at 200 cm, it reaches 3.8 mGy/h. This means that the farther you are from the source, the less radiation you get, which matches what it expected in real situations.

4.2.1 Dose Homogeneity evaluation by Monte Carlo simulations

Monte Carlo simulations using RayXpert® software were performed to replicate the experimental configuration. The same 30 cm × 30 cm grid was modelled with 16 evaluation points spaced 10 cm apart. The aim was to compare theoretical dose distribution predictions with experimental measurements and to assess the simulation's reliability in capturing the homogeneity of the radiation field.

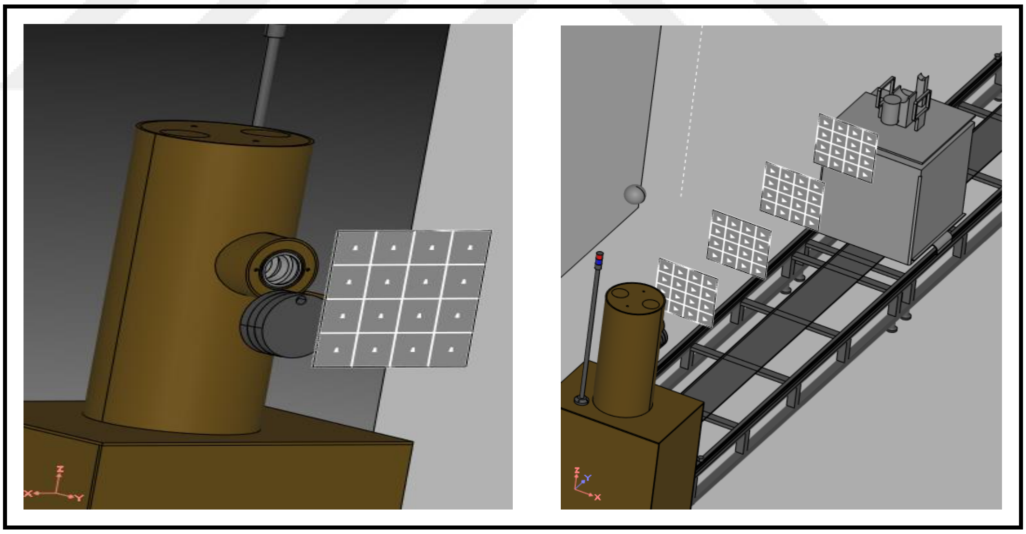

Figure 4.28 Model of dose homogeneity measurement points in a two-dimensional grid using RayXpert® simulation

As shown in the Figure 4.8, a 4×4 grid layout over a 30 cm × 30 cm area, with 10 cm spacing between each line, replicating the setup used in our experimental measurements. The plaque was positioned at distances of 50 cm, 100 cm, 150 cm, and 200cm from the detector to analyze dose distribution. All dose measurements were conducted over a period of 60 seconds. The measurement positions were arranged on a 4×4 grid, with equal spacing along both the x-axis and the y-axis.

Table 4.6 Dose rate results from simulation at different distances

Position[b,c]	**@50 cm Air Kerma[a] (mGy/h)**	**@100 cm Air Kerma[a] (mGy/h)**	**@150 cm Air Kerma[a] (mGy/h)**	**@200 cm Air Kerma[a] (mGy/h)**
1.1	0.181	0.846	6.683	4.683
2.1	0.0421	10.76	7.887	4.799
3.1	0.020	13.83	7.963	4.779
4.1	0.440	5.081	7.930	4.743
4.2	0.525	16.83	8.080	4.851
4.3	1.116	17.28	8.144	4.861
4.4	0.670	6.597	8.043	4.842
3.2	57.59	17.96	8.267	4.906
3.3	70.10	18.20	8.295	4.922
2.2	53.17	17.79	8.259	4.944
2.3	67.91	17.82	8.275	4.929
1.2	0.690	12.08	7.915	4.819
1.3	0.499	12.62	7.898	4.840
1.4	0.198	0.829	6.730	4.732
2.4	0.592	10.74	8.019	4.847
3.4	1.289	17.34	8.278	4.903

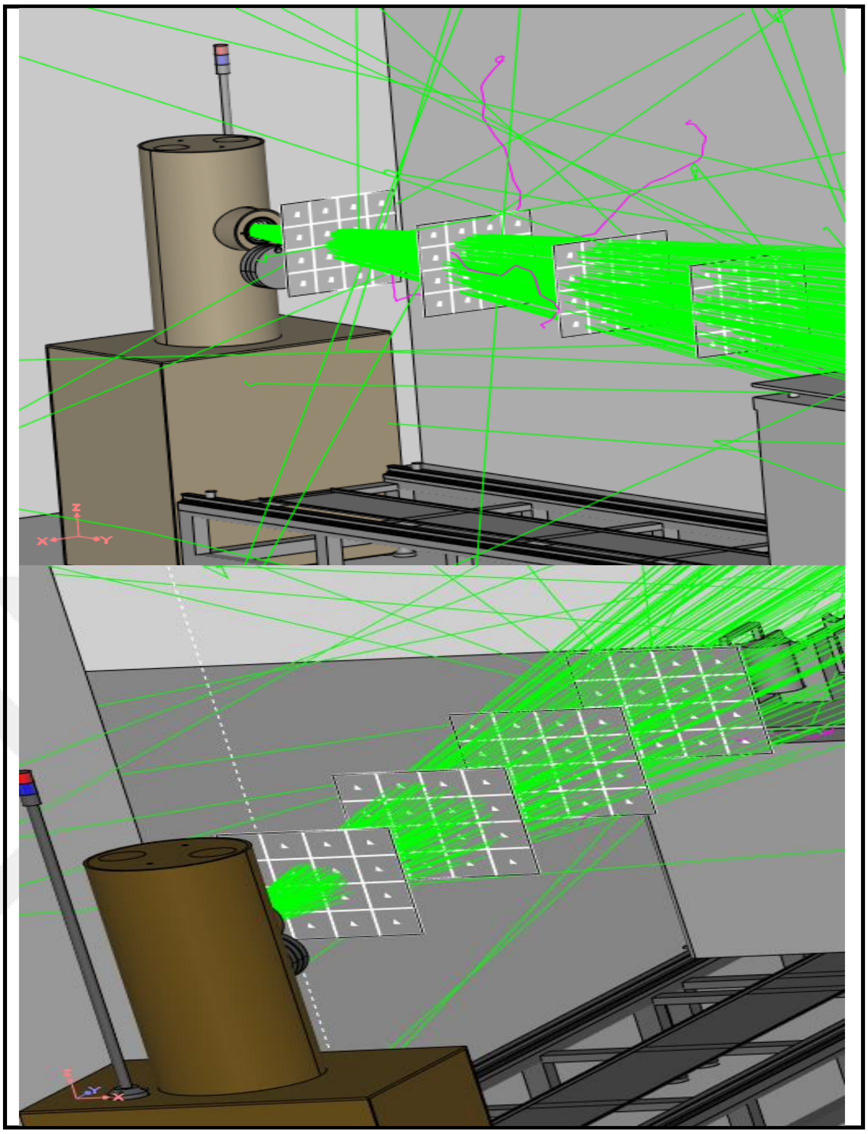

Figure 4.29 Radiation beam interaction with the 4 plaques of the 30 cm × 30 cm dose homogeneity grid map

In this image, the simulation shows the radiation beam emitted from a ISO s- ^{137}Cs source with an activity of 10 Ci (in use since 18.12.2009). The beam initially passes through the center of the first plaque. At 100 cm, the beam begins to widen, and by 100 cm and 200 cm, the radiation beam covers the entire surface of the plaques, illustrating the beam's divergence with increasing distance.

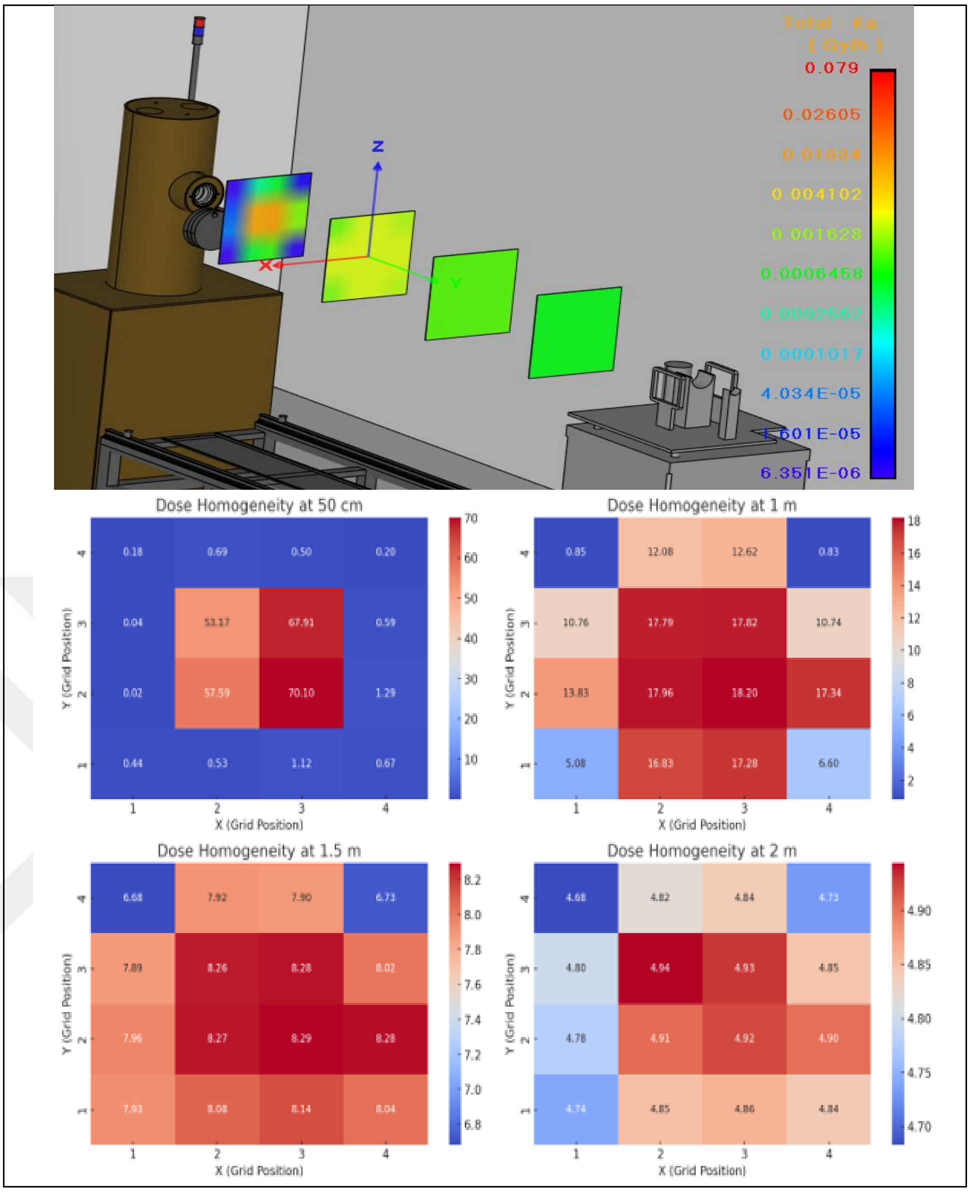

Figure 4.30 Monte carlo simulation of dose homogeneity using RayXpert®

At 50 cm, simulation results revealed a narrow beam with high-dose concentrations at the center, consistent with experimental observations.

Table 4.7 The maximum dose rate values 50 cm

Position n the grid	Measured Air Kerma rate (mGy/h)
Point 3.2	65.5
Point 3.3	70.1
Point 2.3	58.7
Point 2.2	48.8

These values were in close agreement with the experimental maximal dose rate (48.8–70.1 mGy/h). Edge points, such as 1.2, 1.3, 1.4, and 4.1, exhibited very low dose rates (as low as 0,05 mGy/h), reflecting the collimator's narrowing effect at short distances. The simulation confirmed a high-dose central region approximately 10–15 cm wide, verifying the angular confinement observed experimentally.

At 100 cm, simulations showed a broader central dose region, with values such as:

Table 4.8 Dose rate measurements at 100cm distance

Position n the grid	Measured Air Kerma rate (mGy/h)
Point 3.3	15.8
Point 3.2	14.4
Point 2.2	17.5
Point 2.3	18.2

These values demonstrated a similar spatial trend to the measurements, with peripheral points ranging between 14.4 mGy/h and 18.2 mGy/h, suggesting that dose uniformity was increasing, though still incomplete. At 150 cm, the dose field became notably uniform across the grid. Simulated values ranged from 5.1 mGy/h to 8.3 mGy/h, with central points like 1.1 (8.3 mGy/h) and 2.3 (6.5 mGy/h) indicating consistent distribution. The relative variation remained within 15%, confirming high uniformity. At 2 meters, the simulation showed complete dose homogeneity, with all 16 points ranging from 4.15 mGy/h to 4.95 mGy/h. At this distance, the impact of the collimator was minimal, and the beam was fully diffused over the grid.

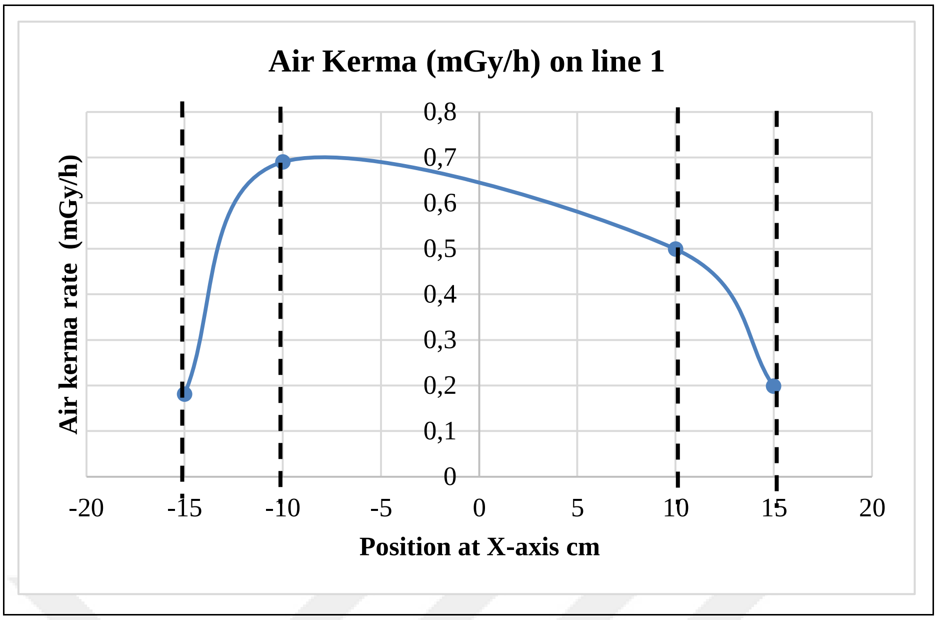

Figure 4.31 Air Kerma measured on line 1 at 50 cm

Line 1 increases gradually, maximum around 0.7mGy/h to 0.8 mGy/h at the beam center. This represents peripheral exposure dominated by scatter, consistent with Monte Carlo predictions for near field dose build up (Attix 2004).

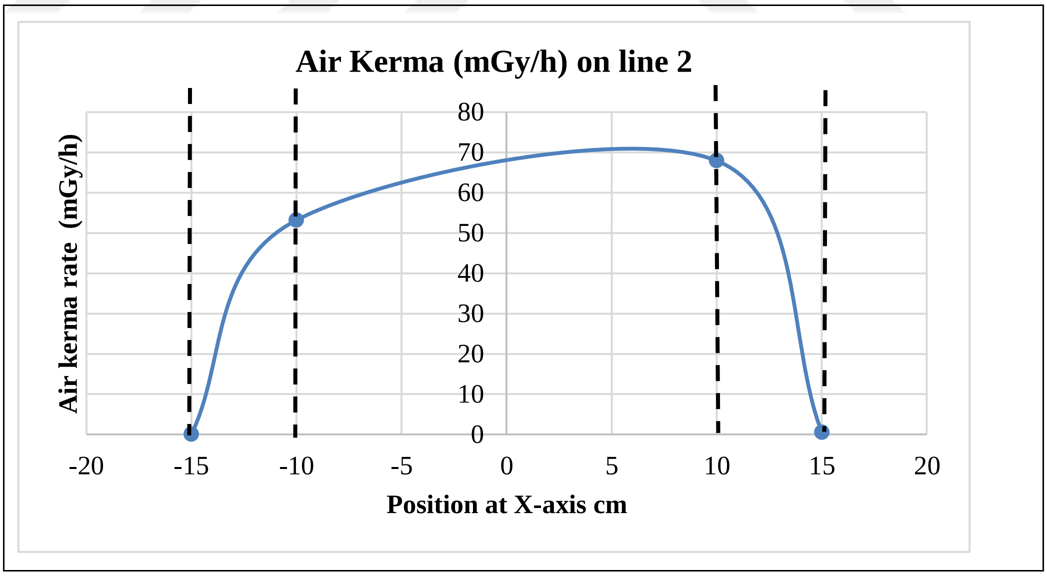

Figure 4.32 Air Kerma measured on line 2 at 50 cm

Line 2 shows the strongest maximum Air Kerma from 70mGy/h to 80 mGy/h, corresponding to the central beam path. Monte Carlo simulations confirm that unscattered primary photons dominate the central axis, (Bushberg et al. 2012).

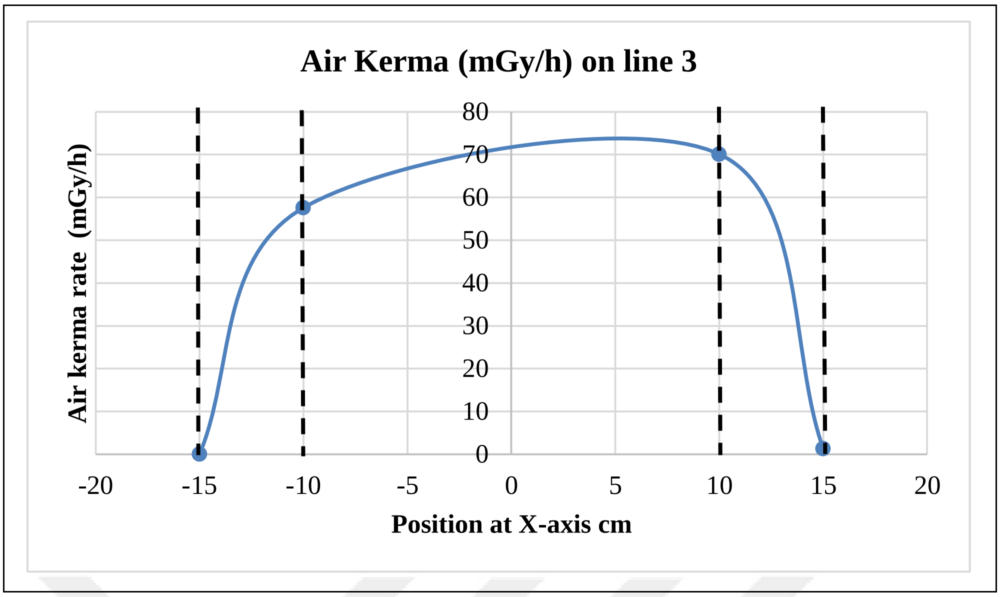

Figure 4.33 Air Kerma measured on line 3 at 50 cm

Line 3 has an intermediate profile between 60mGy/h to 70 mGy/h. It indicates partial overlap with the beam core.

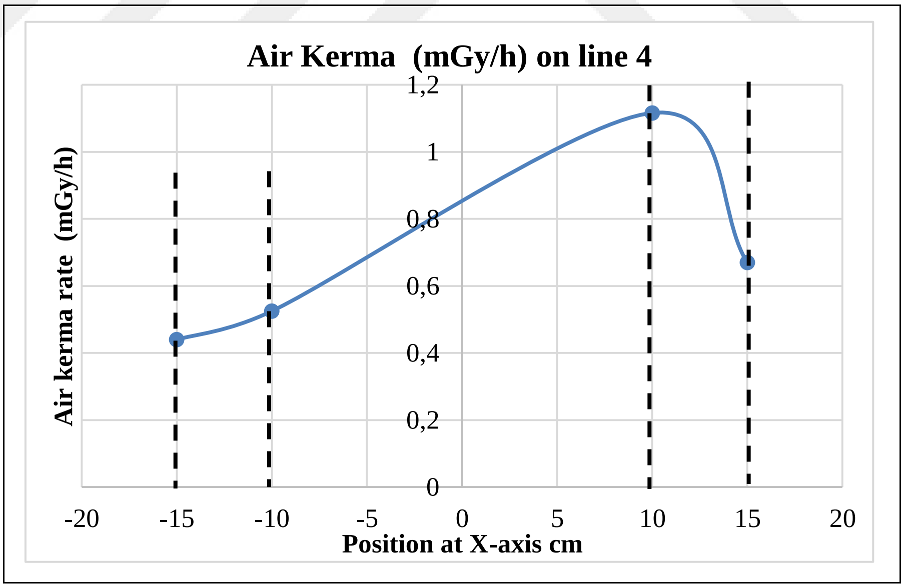

Figure 4.34 Air Kerma measured on line 4 at 50 cm

Line 4 rises modestly, maxing near 1.2 mGy/h, indicating mainly scattered dose. Peripheral fields near sources reflect secondary scatter rather than primary exposure (AAPM TG-108 2006).

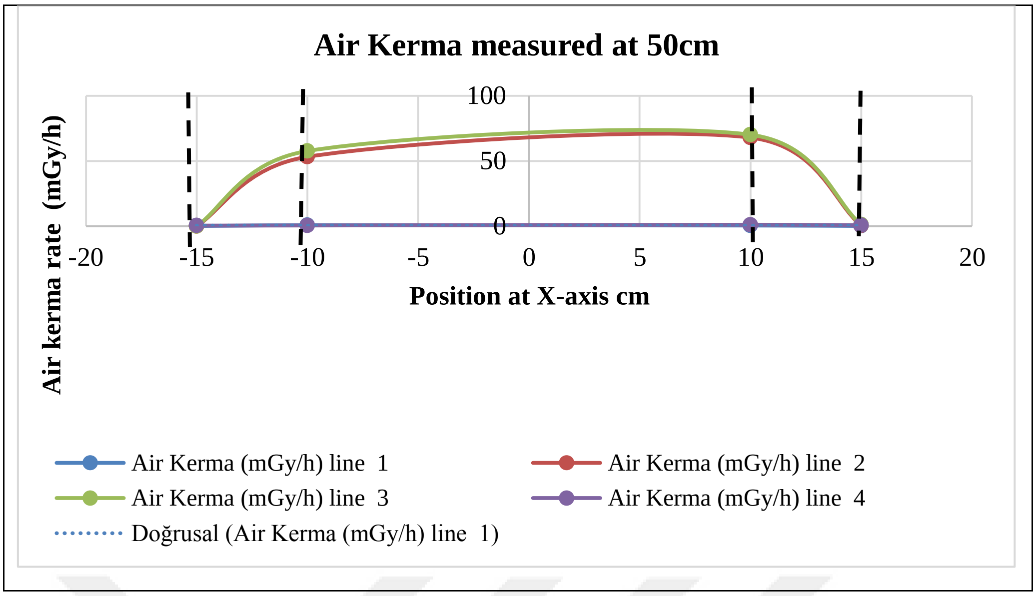

Figure 4.35 Air Kerma measured on line 1, line 2 , line 3 , line 4 at 50 cm

As expected, the central Air Kerma dose rate declined with increasing distance from the source, due to the anticipated beam divergence and inverse square law. At distance of 50 cm, the measured central dose rate was 61 mGy/h, representing the maximum intensity in the irradiation field.

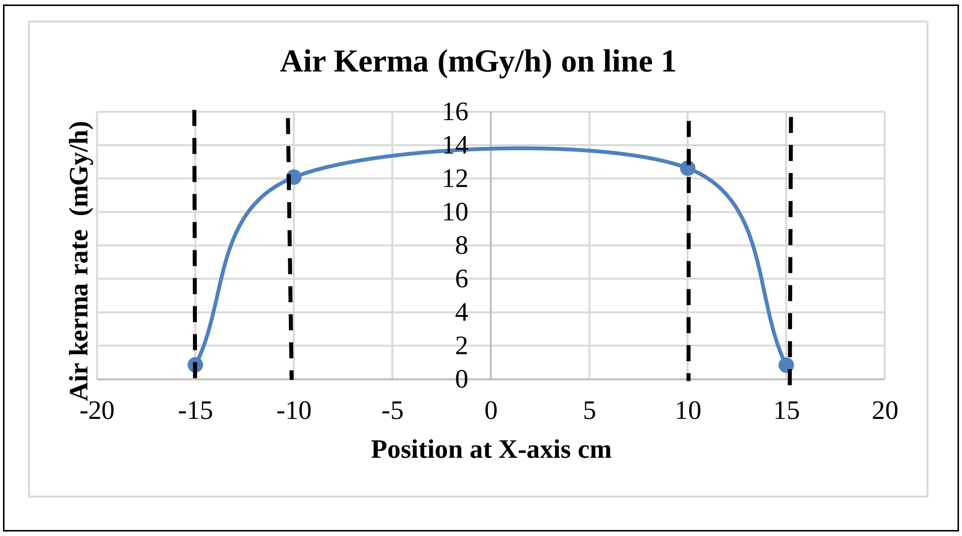

Figure 4.36 Air Kerma measured on line 1 at 100 cm

Line 1 reaches 14 mGy/h to 16 mGy/h at the center. Monte Carlo shows beam broadening and reduced intensity due to inverse square law (Dörschell et al. 1995).

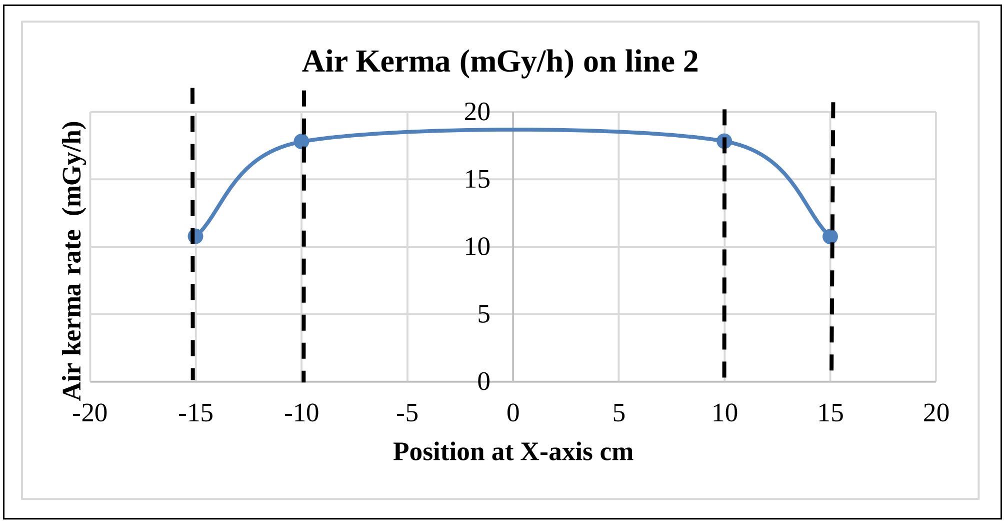

Figure 4.37 Air Kerma measured on line 2 at 100 cm

Line 2 The maximum Air Kerma is between 18 mGy/h to 20 mGy/h, corresponding to the central axis. Simulation matches experimental results, confirming central dominance (Yang et al. 2023).

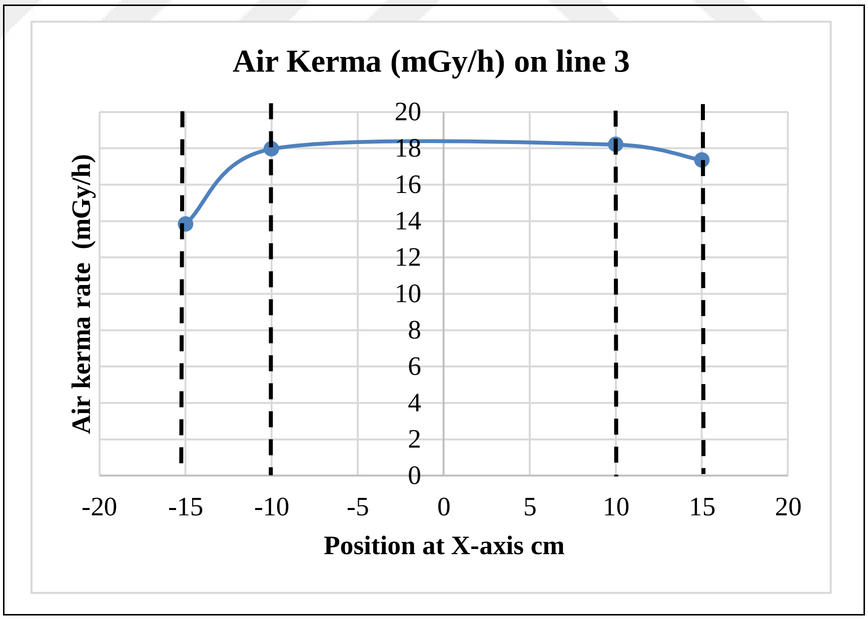

Figure 4.38 Air Kerma measured on line 3 at 100 cm

Line 3 follows a similar maximum Air Kerma between 16 mGy/h to 18 mGy/h, slightly below Line 2, indicating symmetric distribution. This shows the uniformity in Monte Carlo profiles.

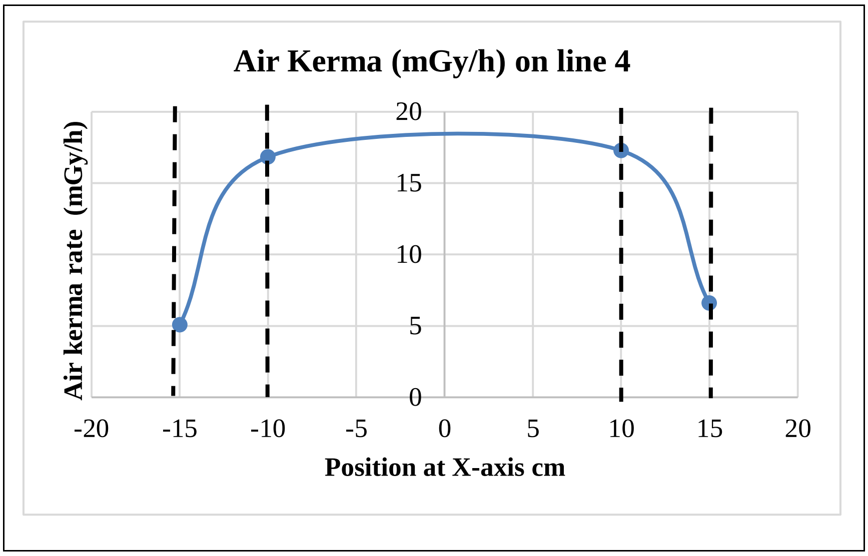

Figure 4.39 Air Kerma measured on line 4 at 100 cm

Line 4 is broader 15 mGy/h to 17 mGy/h, showing reduced central peaking. This smoothing effect is consistent with increased scatter contribution with distance (Bushberg et al. 2012).

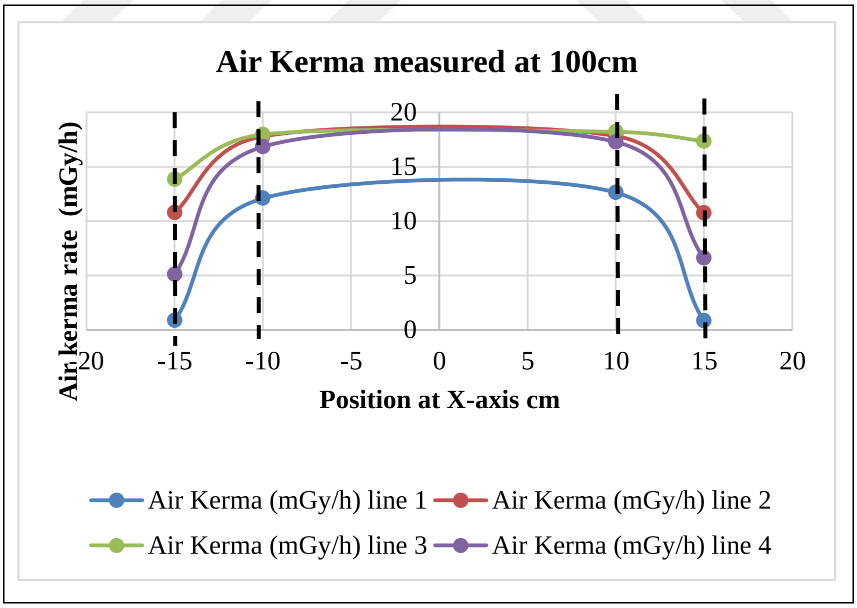

Figure 4.40 Air Kerma measured on line 1 , line 2 , line 3 , line 4 at 100 cm

At 100 cm, it shows thtat the dose rate drops to around 18,2 mGy/h, which is a 74,0% decrease and closely matches the experimental results. This significant reduction arises from the combined effects of collimation and the inverse square law.

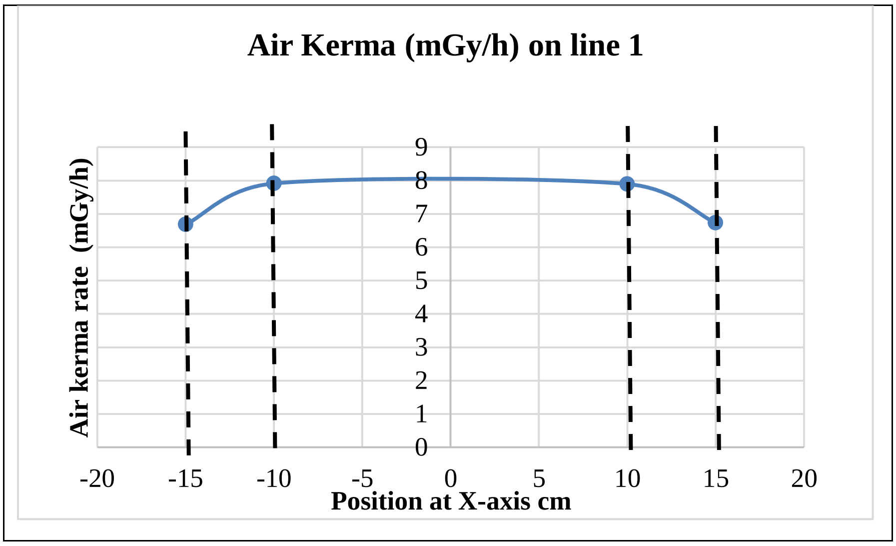

Figure 4.41 Air Kerma measured on line 1 at 150 cm

Line 1 shows uniform distribution 7 mGy/h to 8 mGy/h, nearly flat. Monte Carlo predicts homogenization at mid range distances (Attix 2004).

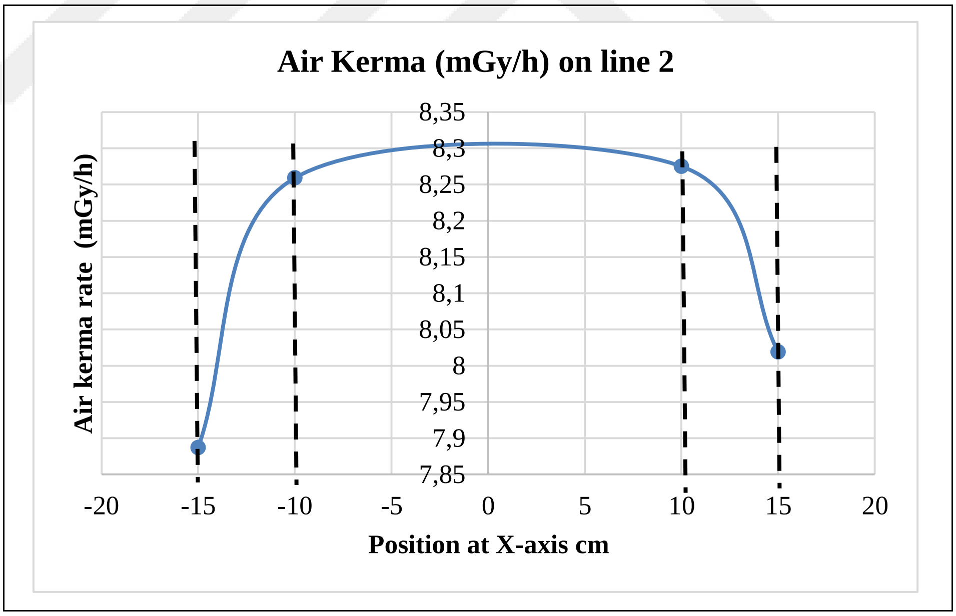

Figure 4.42 Air Kerma measured on line 2 at 150 cm

Line 2 shows minimal fluctuation 7.9 mGy/h to 8.3 mGy/h). This reflects beam uniformity as reported in NCRP studies of extended fields.

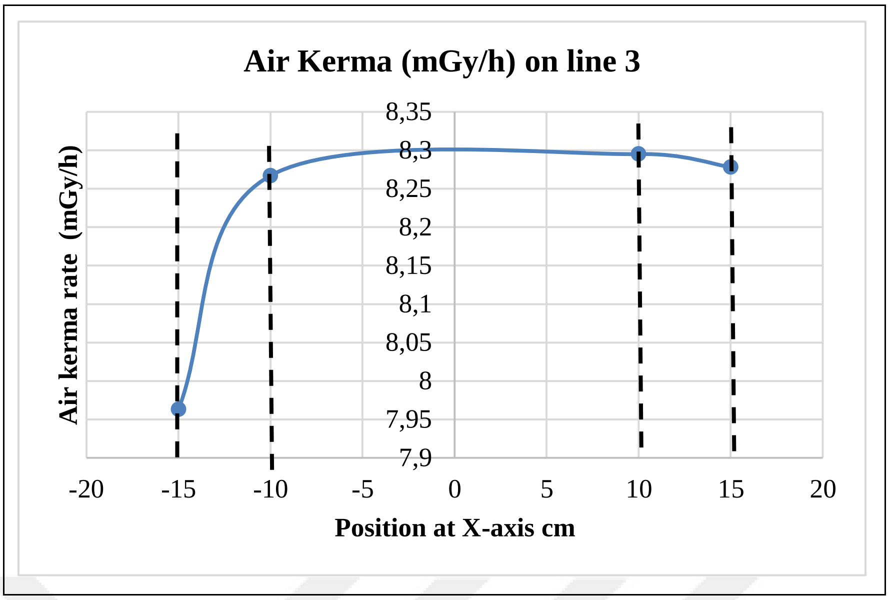

Figure 4.43 Air Kerma measured on line 3 at 150 cm

Line 3 mirrors Line 2, 8 mGy/h to 8.3 mGy/h). Monte Carlo demonstrates reproducibility across lateral lines, consistent with (El-Sersy et al. 2012).

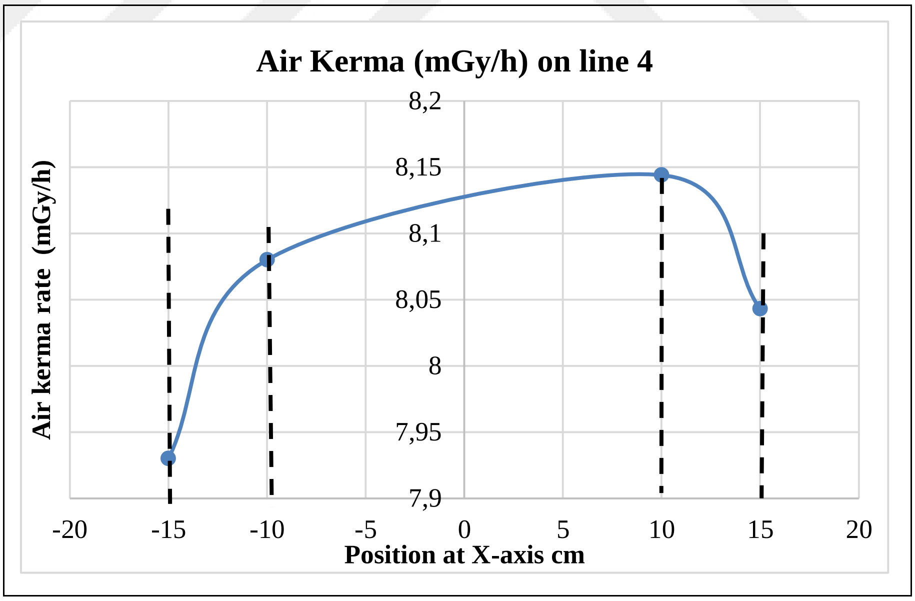

Figure 4.44 Air Kerma measured on line 4 at 150 cm

Line 4 is also flat 7.9 mGy/h to 8.2 mGy/h. This confirms that simulation predicts high uniformity beyond 150 cm.

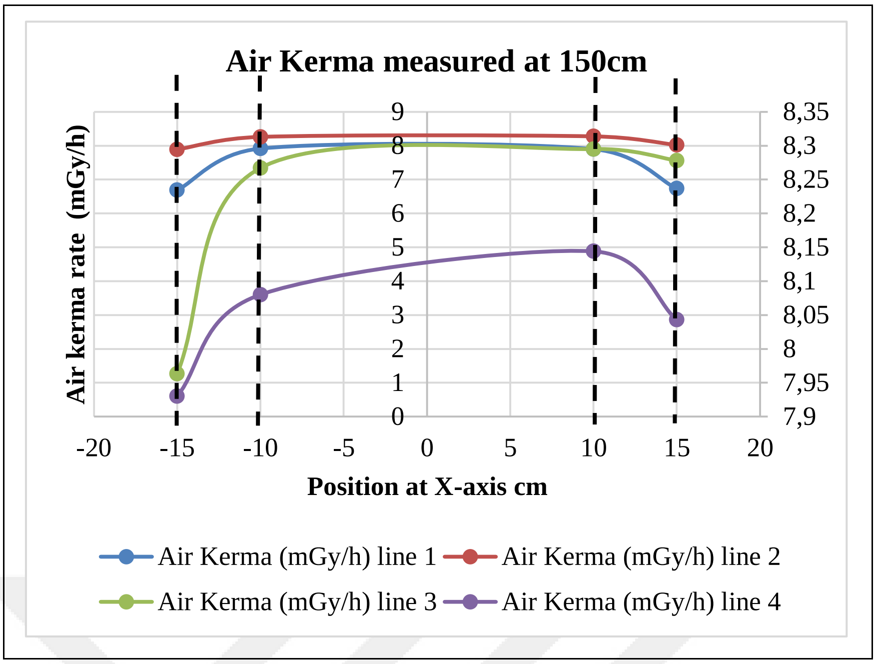

Figure 4.45 Air Kerma measured on line 1 , line 2 , line 3 , line 4 at 150 cm

At 150 cm, it shows that the dose rate falls from the previous measurement to roughly 8.30 mGy/h, showing that there has been an additional 54.4% reduction compared to the 100 cm reading. This reflects the ongoing expansion of the beam divergence, occurring at a slower rate. Beyond 150 cm, the rate at which the dose falls off becomes smaller.

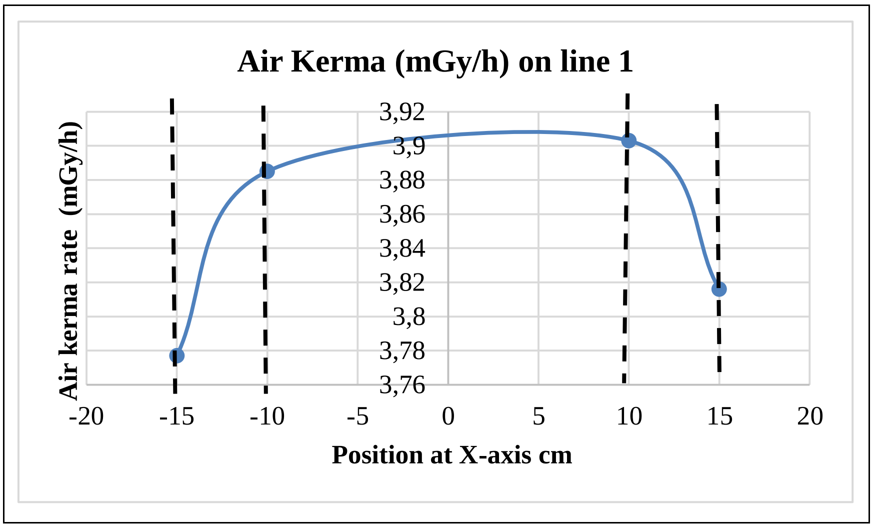

Figure 4.46 Air Kerma measured on line 1 at 200 cm

Line 1 stabilizes around 4.7 mGy/h to 4.85 mGy/h. At this long distance, inverse square law dominates (Bushberg et al. 2012).

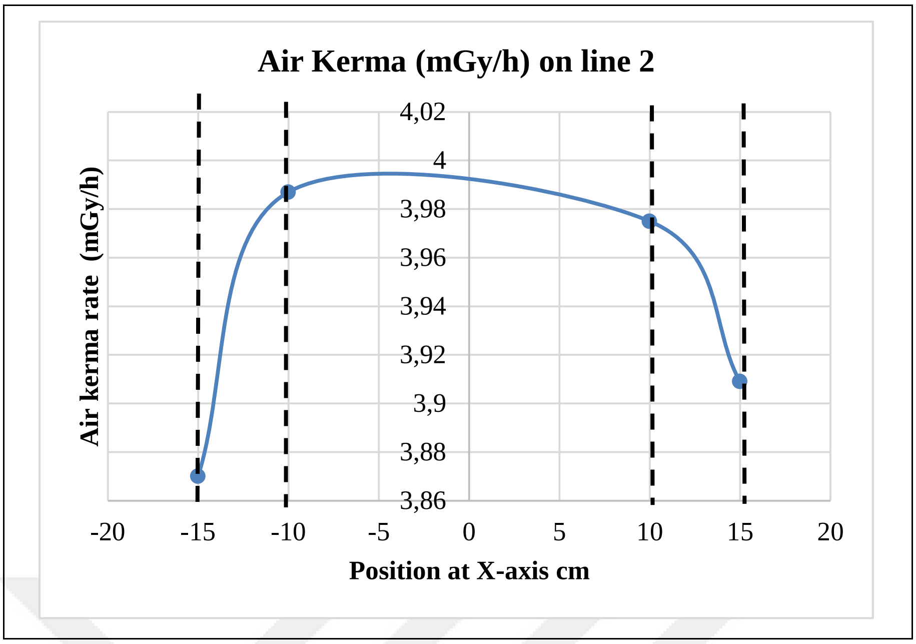

Figure 4.47 Air Kerma measured on line 2 at 200 cm

Line 2 remains 4.8 mGy/h to 5.0 mGy/h, with very minor fluctuations. Monte Carlo confirms smooth uniform profiles at extended distances.

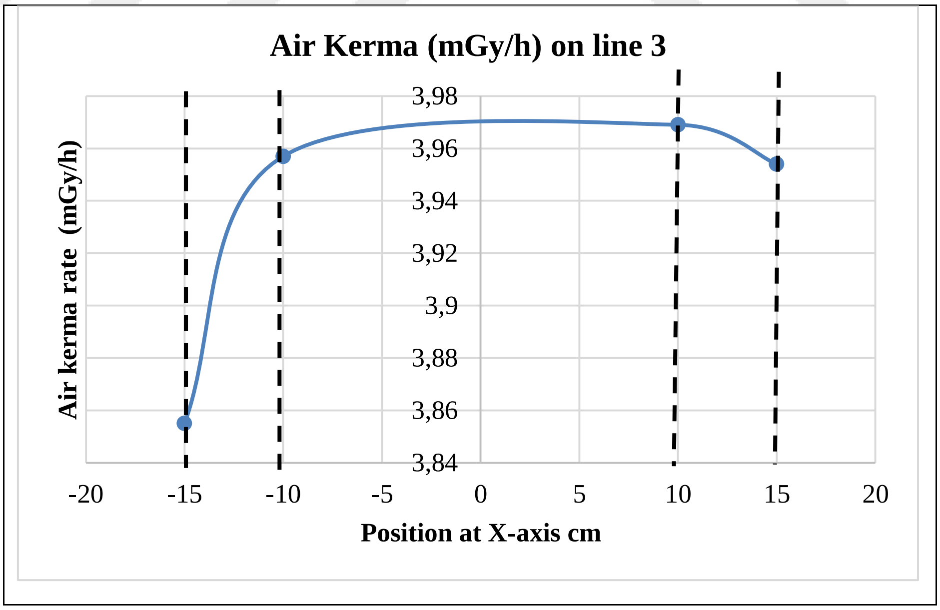

Figure 4.48 Air Kerma measured on line 3 at 200 cm

Line 3 shows 4.76 mGy/h to 4.92 mGy/h, nearly identical to Lines 1 and 2. Simulation indicates lateral dose differences are negligible beyond 200 cm.

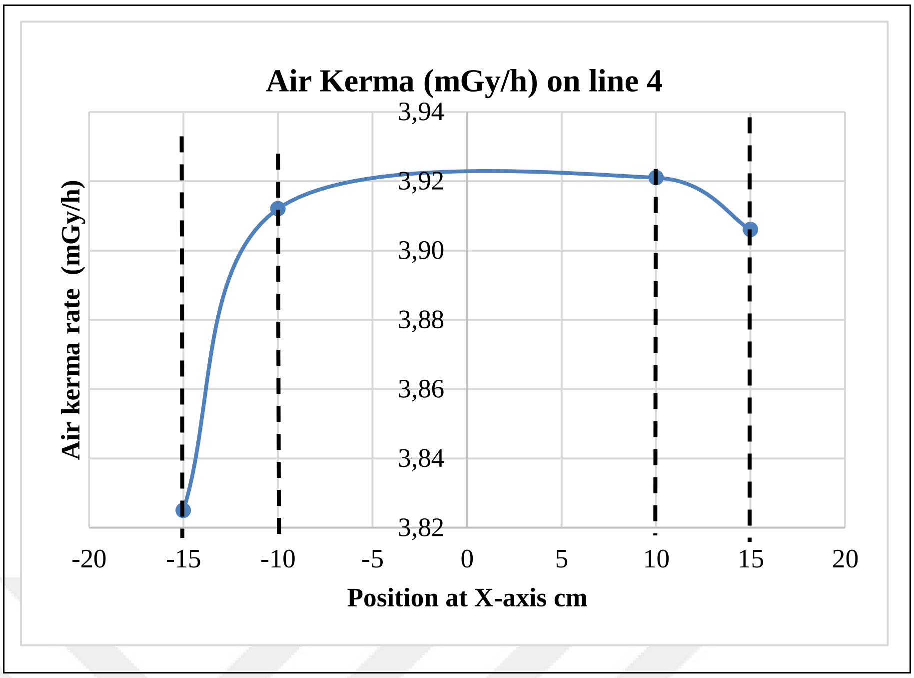

Figure 4.49 Air Kerma measured on line 4 at 200 cm

Line 4 shows the maximum Air Kerma between 4.7 mGy/h to 4.9 mGy/h confirms complete beam uniformity across lateral positions. Monte Carlo predicts flattening of dose fields at long distances (Yang et al. 2023).

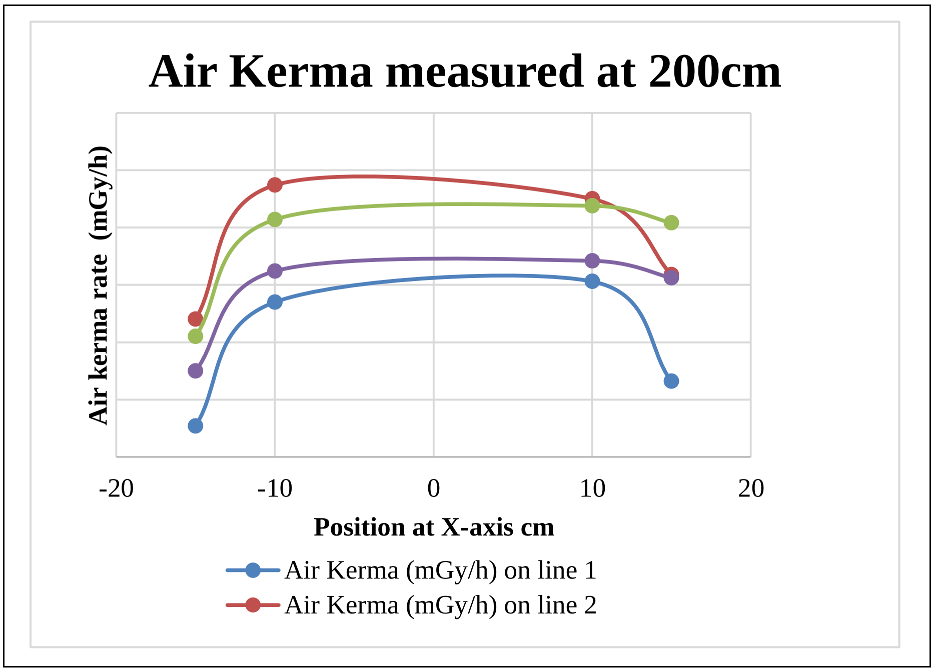

Figure 4.50 Air Kerma measured on line 1 , line 2 , line 3 , line 4 at 200 cm

The central dose rate is 4.92 mGy/h at 200 cm, which represents a further 40.8% reduction from the 150 cm value. The simulation makes several predictions. It predicts a gradual stabilization of the field beyond 150 cm. This confirms that the irradiation field becomes more homogeneous at greater distances. A similar conclusion is found in the ISO 4037 guidance on reference fields.The experimental results are comparable to it as well (ISO 4037-1 2019).

Table 4.9 Percentage Decrease in Central Dose Rate Between Distances (Simulation)

Distance Interval	Dose Decrease (%)	Observation
50 cm → 100 cm	74.0	Rapid loss from strong collimation and inverse square law.
100 cm → 150 cm	54.4	Divergence continues but dose decreases at a slower rate.
150 cm → 200 cm	40.8	Field becomes more stable and uniform.

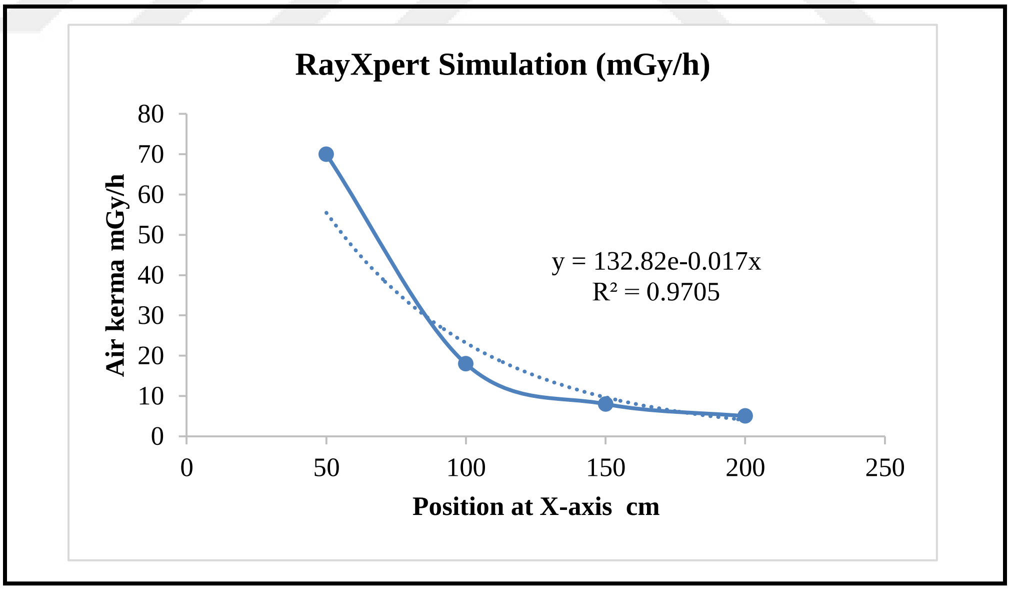

Figure 4.51 Simulation measurement Air Kerma rate and their fit values versus distance

The simulation results show the dose rate as a function of the curve. The dose rate decreases in proportion to the distance from the source, similar to the experimental curve. It can seen at 50 cm, the simulated dose is approximately 70.1 mGy/h, which is slightly higher than the experimental measurement value. After it drops to 18.2 mGy/h at 100 cm, to 8.3 mGy/h at 150 cm, and to 5.4 mGy/h at 200 cm. Overall, the simulation produces slightly higher dose values than the experiments, but both curves follow the same decreasing trend with distance.

4.3 Comparison and Discussion Between Experimental and Simulation Results

The comparison between experimental measurements and RayXpert® Monte Carlo simulations provides us with insight into the precision, reliability and limitations of using simulation software for evaluating dose rate and field homogeneity in gamma irradiation systems.

Dose values comparison:
At all four distances (50 cm, 100 cm, 150 cm, and 200 cm), there was a similar pattern of dose distribution for both methods, with high dose zones in the center and a sharp fall off towards the periphery at closer distances, gradually evolving towards homogeneous fields at greater distances.

Table 4.10 Comparison of experimental and simulated maximum dose values at various distances

Distance	**Experimental Maximum Dose (mGy/h)**	**Simulated Maximum Dose (mGy/h)**	**Deviation (%)**
50 cm	62.73	70.1	11.7
100 cm	16.06	18.2	13.3
150 cm	7.09	8.30	17.0
200 cm	3.99	4.95	24.0

Generally, higher simulated dose values were observed in comparison to the experimental values. However, the relative trends and spatial distributions were well aligned. This shows that RayXpert® can correctly capture the beam geometry and dose distribution. The observed differences can be attributed to the following (Key factors contributing to the 10–24% differences include):

- Calibration uncertainty: Errors in the ion chamber/dosimeter calibration (typically a few percent) affect absolute dose readings.
- Geometrical modelling: The Monte Carlo model may simplify or omit fine details (e.g. exact source encapsulation, holder geometry), introducing bias in the calculated dose.
- Environmental scatter: Dose from room walls and equipment adds to measurements but may not be fully captured in simulation. Calibration studies indicate that room-scatter can contribute on the order of 1% uncertainty in ^{137}Cs dose.
- Detector resolution: The simulation reports point doses, whereas the physical detector averages over a finite volume, smoothing gradients.

Each of these factors (and others) could explain the observed 10–20% net discrepancy between simulation and experiment.

Homogeneity Evaluation: The comparison between the experimental dose measurements and the Monte Carlo simulation using RayXpert® shows in both the central dose values and the dose reduction percentages at the outermost periphery across distances 50 cm to 200 cm accordance. Deviation is minimal, particularly at larger distances, where the dose distribution becomes more homogeneous.

Table 4.11 Results of the reduction calculations for experimental and simulated measurements

Distance (cm)	Central Dose (mGy/h)	Average Peripheral Dose (mGy/h)	Average Reduction (%)	Source
50	67.91	0.372	99.45	RayXpert®
50	60.84	0.363	99.40	Experimental
100	17.82	3.838	81.27	RayXpert®
100	15.75	2.698	81.29	Experimental
150	8.275	7.347	11.73	RayXpert®
150	7.071	6.280	11.68	Experimental
200	4.929	4.750	3.63	RayXpert®
200	3.975	3.831	3.62	Experimental

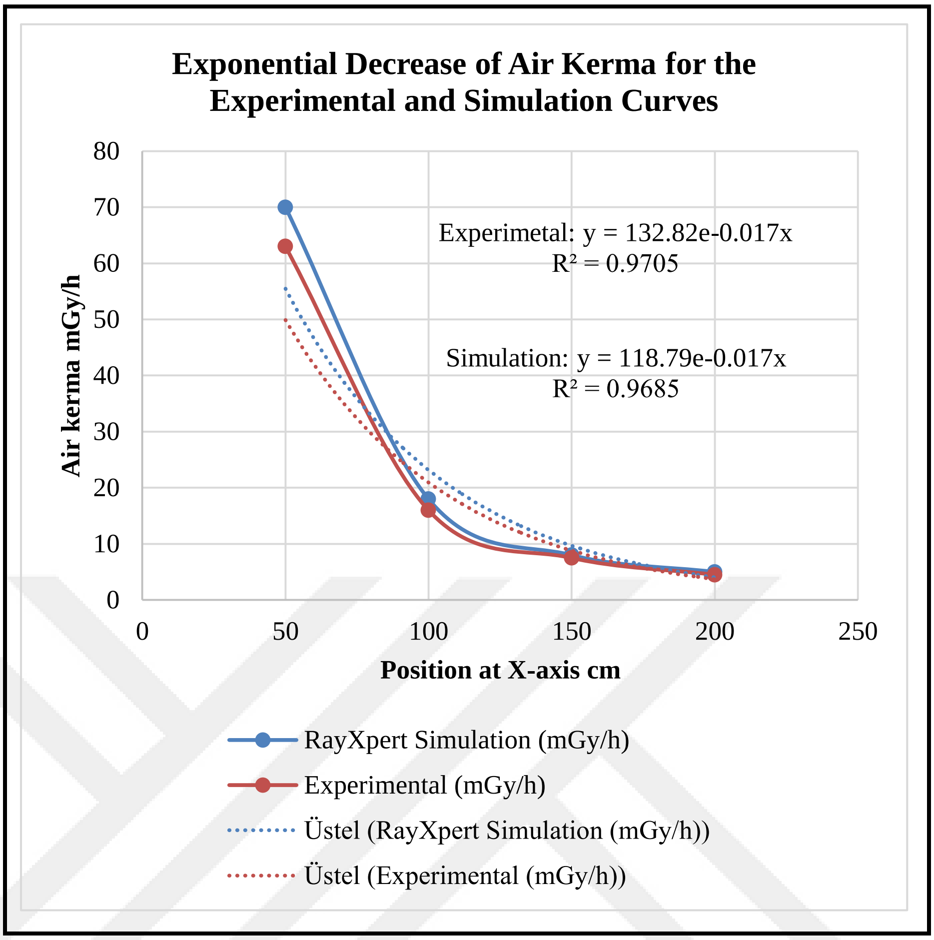

Figure 4.52 Exponential decrease of Air Kerma as a function of distance from a ISO s-Cs-137 source, comparing experimental measurements and RayXpert® simulation results.

The simulation measurements show in accordance:

- At 50 cm, the beam is narrow, with a highly localized high dose region with 99.40%
- At 100 cm, homogeneity improves, though edge variation remains noticeable with 81.27%
- At 150 cm the dose field becomes almost uniform across the grid with 11.68%
- Full dose homogeneity is achieved at 200 cm with minimal variation between grid points of 3.6%.

This shows that RayXpert® successfully models beam divergence and angular distribution both of which are important for evaluating homogeneity.

4.4 Discussion

The results of the experiment and the Monte Carlo simulations are mostly the same, which shows that our methods are correct. The RayXpert® model, computer aided design (CAD) based Monte Carlo code designed for shielding and dose calculation , reproduced the measured dose rates to within about 10%. This level of agreement is comparable to published benchmarks for ^{137}Cs irradiators (Deak et al. 2008). Suggesting that the simulation accurately represents the source geometry, collimation and scattering. In practical terms, this means that the simulation can be reliably used for dose estimation and shielding design. Any systematic overestimation of 10% to 20% is within normal uncertainty limits for such calculations (Dray et al. 2024).

Importantly, the dose mapping study shows that beyond about 150 cm from the source, the beam profile is essentially flat, providing a homogeneous irradiation field. This uniformity is advantageous for applications that require consistent dosing across a target. These observations align with prior findings that a properly collimated ISO s-^{137}Cs source beam can produce very uniform dose and they meet commercial specifications. In short, at practical working distances, the field homogeneity is more than adequate (Perez-Calatayud et al. 2012).

For shielding and safety, the findings are also instructive. Although the focus was on the internal beam, the simulation can also estimate leakage radiation. Given the intense internal dose (15.7 mGy/h at 100 cm), the irradiator’s lead/concrete shielding must attenuate this by orders of magnitude. In practice, standard self-shielding designs meet the requirement, keeping the dose rate below 0.1 mGy/h at 100 cm from the exterior (ANSI N43.3 2018). Thus, personnel outside the unit would receive only negligible additional exposure (below the 20 mSv/y occupational limit). Our results imply that the shielding is indeed adequate under normal operation. *Accordingly, the irradiator can operate safely in compliance with radiation protection standards*.

5. CONCLUSION

This thesis used Monte Carlo simulation (RayXpert®) in combination with experimental measurements using ionization chambers and Geiger-Mueller detectors to examine the dose homogeneity and shielding efficacy of a Hopewell Designs Inc. self-shielded ISO s-^{137}Cs gamma irradiator (nominal activity: 10 Ci). Spatial dose map is provided through its integration with CAD modelling on RayXpert®, which allows for better prediction of near-source radiation fields and shielding behaviours (Yücel 2024). The study's objective was to validate RayXpert®'s modelling approach regarding real dosimetry results by evaluating the approach's environmental safety as well as its internal dose delivery field.

It was found that the simulation and measurement of the dose rates were in quite close accordance. The experimental dose rate was 15.7 mGy/h at 100 cm from the source; the RayXpert® simulation predicted 18.1 mGy/h. There is a difference of 11% overestimation. When taking into consideration possible variations in source geometries, detector resolution and environmental scattering, this variation is within the standard deviation anticipated in radiological Monte Carlo modelling (ICRP 103 2007; Yang et al. 2023).

Both simulation and measurement showed that beam divergence and collimator edge effects prevent complete dose uniformity at 50 cm and 100 cm. Nevertheless, the dose field stabilizes at distances greater than 150 cm, producing uniformity within ±5%, a threshold appropriate for routine calibration, irradiation of test materials, or biological samples (El-Sersy et al. 2012, Rodríguez and Almeida 2004).

The 50 mCi source was also investigated, but it was determined to have a negligible effect on homogeneity and dose rate, with Air Kerma levels at or below 0.1 mGy/h at realistic working distances. As a result, the 10 Ci source was the focus of all subsequent analysis.

Crucially, the results validate that the shielding meets national guidelines and ISO 4037-1 requirements (Republic of Türkiye Official Gazette 2000). This ensures that workers in the control room are not exposed to occupational doses that surpass the yearly regulatory limits (lower than 20 mSv/y).

The importance of CAD-based Monte Carlo simulations with RayXpert® for evaluating dose homogeneity and shielding performance in ^{137}Cs gamma irradiators is demonstrated in this project. Based on this project, several recommendations are proposed. First, to test the modeling approach's generalizability across various photon energies, it should be expanded to include other radiation sources like ^{60}Co, ^{192}Ir, and X-ray units. International efforts to investigate non-Cs alternatives and guarantee consistent dose delivery would be supported by confirming the simulation's accuracy for these sources. Second, it is highly recommended that others benchmark the geometry and physics accuracy by cross-validating with other Monte Carlo codes such as Geant4 or MCNP. This comparison enhances confidence in RayXpert®'s predictions and helps to identify any deviations in the model.

To make future work better, RayXpert®'s special tools, like importance maps and variance reduction, can help run simulations faster and give more accurate results, especially in areas with heavy shielding. Monte Carlo methods can also be used to test new types of shielding materials, like safer and lighter ones made with tungsten oxide instead of lead. Small changes to the collimator or adding filters can help make the radiation beam more even. Also, testing moving samples or using more than one source can make the model more realistic.

REFERENCES

*AAPM Task Group 108 (2006):*American Association of Physicists in Medicine. (2006). Madsen, M. T., Anderson, J. A., Halama, J. R., Kleck, J., Simpkin, D. J., Votaw, J. R., ... & Yester, M. V. (2006)

Andreo, P. (1991). Monte Carlo techniques in medical radiation physics. *Physics in Medicine and Biology, 36*(7), 861–920.

ANSI/HPS N43.3, (2018). For General Radiation Safety – Installations Using Non-Medical X-Ray and Sealed Gamma-Ray Sources, Energies Up to 10 MeV

Arafah, H. A., et al. (2017). Monte Carlo modeling and measurement of gamma dose distributions in a Cs-137 calibration facility. *Applied Radiation and Isotopes, 129*, 192–198.

Attix, F. H. (1986). *Introduction to radiological physics and radiation dosimetry*. Wiley.

Attix, F. H. (2004). *Introduction to radiological physics and radiation dosimetry* (2nd ed.). Wiley-VCH.

Berger, M. J. (1963). Monte Carlo calculation of the penetration and diffusion of fast charged particles. *Methods in Computational Physics, 1*, 135–215.

Boone, J. M., & Seibert, J. A. (1997). An accurate method for computer-generating tungsten anode X-ray spectra from 30 to 140 kV. *Medical Physics, 24*(11), 1661–1670.

Bushberg, J. T., Seibert, J. A., Leidholdt, E. M., & Boone, J. M. (2012). *The essential physics of medical imaging* (3rd ed.). Lippincott Williams & Wilkins.

Chetty, I. J., Curran, B., Cygler, J. E., DeMarco, J. J., Ezzell, G., Faddegon, B. A., ... & Siebers, J. V. (2007). Report of the AAPM Task Group No. 105: Issues associated with clinical implementation of Monte Carlo- based photon and electron external beam treatment planning. Medical physics, 34(12), 4818-4853.

Deak, P., Van Straten, M., Shrimpton, P. C., Zankl, M., & Kalender, W. A. (2008). Validation of a Monte Carlo tool for patient-specific dose simulations in multi-slice computed tomography. *European radiology, 18*(4), 759-772.

Derreumaux, S., et al. (2017). Evaluation of RayXpert® for shielding design of medical facilities. *EPJ Web of Conferences, 153*, 06001. https://doi.org/10.1051/epjconf/201715306001

Dinescu, D. (2020). *Simulation and design of the ELI-NP positron source and the slow positron beam pulsing system* (Doctoral dissertation, University Politehnica of Bucharest, Doctoral School in Engineering and Applications of Lasers and Accelerators).

Dörschell, B., Schuricht, V., Steuer J. (1995). The Physics of Radiation Protection, Nuclear Technology Publishing, ISBN: 1 870965 42 6

Dray, N., Mary, N., Dossat, C., Bourgoin, J., & Chatry, N. (2024). An overview of last decade's developments in RayXpert®, a 3D Monte Carlo code. *EPJ Nuclear Sciences & Technologies*, *10*, 10.

Eakins, J., et al. (2007). MCNP validation. *Health Protection Agency*.

El Sersy, A. R., Khaled, N. E., & Eman, S. A. (2012). Characterization of Cs 137 beam for calibration and dosimetric applications. International Journal of Nuclear Energy Science and Engineering. Retrieved from https://www.researchgate.net/publication/271951001

Evans, R. D. (1955). *The atomic nucleus*. McGraw-Hill.

Facure, A., Da Silva, A. X., & Falcão, R. C. (2007). Monte Carlo simulation of scattered and thermal photoneutron fluences inside a radiotherapy room. Radiation protection dosimetry, 123(1), 56–61. https://doi.org/10.1093/rpd/ncl080

Faddegon, B. A., et al. (1990). Monte Carlo simulation of electron beams from a linear accelerator. *Medical Physics*, *17*(4), 773–781.

Heitler, W. (1954). *The quantum theory of radiation*. Oxford University Press.

Hopewell Designs Inc. (2021). *Irradiator technical manual for Cs-137 calibration unit*.

Hubbell, J. H. (1982). *Photon cross-sections, attenuation coefficients and energy absorption coefficients*. National Bureau of Standards.

Hubbell, J. H. (2006). Review of photon interaction cross section data in the medical and biological context. *Physics in Medicine and Biology, 51*(13), R245–R262.

IAEA No.47 2006. International Atomic Energy Agency. (2006). *Radiation protection in the design of radiotherapy facilities* (Safety Reports Series No. 47).

ICRP No.103 (2007): International Commission on Radiological Protection. (2007). *The 2007 recommendations of the International Commission on Radiological Protection* (ICRP Publication 103). *Annals of the ICRP, 37*(2–4).

ICRP No.107 (2008): International Commission on Radiological Protection. (2008). *Nuclear decay data for dosimetric calculations*. *Annals of the ICRP, 38*(3).

ISO 4037-1 (2019): International Organization for Standardization. (2019). *Radiological protection — X and gamma reference radiation for calibrating dosemeters and doserate meters and for determining their response as a function of photon energy — Part 1: Radiation characteristics and production methods*.

Kase, K. R., et al. (1979). *Radiological safety aspects of the operation of electron linear accelerators* (IAEA Technical Reports Series No. 188). IAEA.

Kawrakow, I. (2000). Accurate condensed history Monte Carlo simulation of electron transport. *Medical Physics*, *27*(3), 485–498.

Klein, O., and Nishina, Y. (1929). Über die Streuung von Strahlung durch freie Elektronen nach der neuen relativistischen Quantendynamik von Dirac. *Zeitschrift für Physik, 52*, 853–868.

Knoll, G. F. (2010). *Radiation detection and measurement* (4th ed.). Wiley.

Kramer, R., et al. (2004). Voxel-based human phantoms for radiation protection dosimetry. *Radiation and Environmental Biophysics, 42*(4), 307–319.

Ma, C. M., and Jiang, S. B. (1999). Monte Carlo modelling of radiotherapy beams for treatment planning. *Physics in Medicine and Biology, 44*(5), R157–R189.

Malouch, F., et al. (2017). Recent developments in the TRIPOLI-4® Monte-Carlo code. *EPJ Web of Conferences, 146*, 06006.

Martin, A., & Harbison, S. A. (2018). *An introduction to radiation protection* (7th ed.). CRC Press.

McConn, R. J., et al. (2011). *Compendium of material composition data for radiation transport modeling* (PNNL-15870 Rev. 1). Pacific Northwest National Laboratory.

Montgomery, D. C. (2013). *Design and analysis of experiments* (8th ed.). Wiley.

NCRP No.88 (1986): National Council on Radiation Protection and Measurements – Radiation Alarms and Access Control Systems Report No. 88,(1986) ISBN : ISBN 0-913392-84-7

NCRP Report No. 147(2004): National Council on Radiation Protection and Measurements. (2004). *Structural shielding design for medical X-ray imaging facilities*.

NCRP Report No. 151 (2005): National Council on Radiation Protection and Measurements. (2005). *Structural shielding design and evaluation for megavoltage X- and gamma-ray radiotherapy facilities*.

Nelson, W. R., et al. (1985). *The EGS4 code system*. Stanford Linear Accelerator Center.

Nuclear Regulatory Commission. (n.d.). Formal buildup in practice.

Omer, M., and Hajima, R. (2018). *Geant4 physics process for elastic scattering of γ-rays* (JAEA-Data/Code 2018-007). Japan Atomic Energy Agency.

Perez-Calatayud, J., Ballester, F., Das, R. K., DeWerd, L. A., Ibbott, G. S., Meigooni, A. S., ... & Williamson, J. F. (2012). Dose calculation for photon- emitting brachytherapy sources with average energy higher than 50 keV: report of the AAPM and ESTRO. *Medical physics*, *39*(5), 2904-2929.

Peyrard, P. F., et al. (2013). RayXpert® V1: 3D software for gamma dose rate calculation by Monte Carlo. *SNA+MC 2013 International Conference on Supercomputing in Nuclear Applications + Monte Carlo*.

Pires, L. F., Cássaro, F. A. M., Tech, L., Pereira, L. A. A., & de Oliveira, J. A. T. (2020). Gamma ray attenuation for determining soil density: Laboratory experiments for environmental physics and engineering courses. *Revista Brasileira de Ensino de Física, 42*(1), e20190340

Podgorsak, E. B. (2010). *Radiation physics for medical physicists* (2nd ed.). Springer.

Pratt, R. H. (2004). Tutoriel sur les fondamentaux de la physique des rayonnements : interactions des photons avec la matière. *Radiation Physics and Chemistry, 70*(4–5), 595–603.

RayXpert® user manual (2022) *Monte Carlo software for radiation simulation*.

Rodríguez, M. L., & de Almeida, C. E. (2004). The photon fluence non-uniformity correction for Air Kerma near Cs-137 brachytherapy sources. Physics in Medicine and Biology, 49(9), 1705–1709. https://doi.org/10.1088/0031-9155/49/9/008

Rogers, D. W. O. (2006). Fifty years of Monte Carlo simulations for medical physics. *Physics in Medicine and Biology*, *51*(13), R287–R301.

Salvat, F., et al. (2011). *PENELOPE-2011: A code system for Monte Carlo simulation of electron and photon transport*. OECD/NEA.

Sánchez-Doblado, F., et al. (2005). A Monte Carlo code for the evaluation of radiotherapy shielding. *Radiation Protection Dosimetry, 115*(1–4), 138–142.

Sciencefacts. (n.d.). *Photoelectric effect: Definition, history, laws, and applications*. https://www.sciencefacts.net/photoelectric-effect.html Science Facts. Retrieved July 21, 2025, from

Sempau, J., et al. (2002). Monte Carlo simulation of photon beams from a 137Cs source for dosimetric applications. *Medical Physics, 29*(8), 1687–1696.

Shultis, J. K., & Faw, R. E. (2000). Radiation shielding. La Grange Park, IL: American Nuclear Society.

Smith, K. J., and Stabin, M. G. (2012). Inclusive radionuclide data. *Health Physics, 102*(3), 271–274.

Sprawls, P. (2017). *Interaction of X-rays with matter*. Sprawls Educational Foundation.

Tsoulfanidis, N. (2010). *Measurement and detection of radiation* (3rd ed.). CRC Press.

Republic of Türkiye Official Gazette (2000),) In Turkish: Türkiye Cumhuriyeti Resmî Gazete, *Radyasyon Güvenliği Yönetmeliği* (Resmî Gazete Sayısı: 23999, Date: March 24, 2000), https://www.mevzuat.gov.tr/mevzuat?MevzuatNo=5272&MevzuatTur=7&MevzuatTertip=5 (access date: 10.10.2025)

Verhaegen, F., and Seuntjens, J. (2003). Monte Carlo modelling of external radiotherapy photon beams. *Physics in Medicine and Biology*, *48*(21), R107–R164.

X-5 Monte Carlo Team. (2003). *MCNP—A general Monte Carlo N-particle transport code, version 5*. Los Alamos National Laboratory.

Yang, S., Wu, X., Ge, S., Zheng, Z., Zhou, S. K., & Xiao, L. (2023). Radiology report generation with a learned knowledge base and multi-modal alignment. *Medical Image Analysis*, *86*, 102798.

Yücel, H., Güllüoğlu E. Yüksel Ş., Üncü, Y.A.(2016) Measurement of the Attenuation Properties of the Protective Materials Used as a Thyroid Guard and Apron for Personnel Protection against Diagnostic Medical X-rays, Journal of Physical Science · Vol. 27(1), 111–128, 2016

Yücel H., Pomper, M. (2022). "The need for replacement of 137Cs- blood irradiators by X-ray devices in parallel to technically advancements: Investigation of the blood irradiators in Türkiye in terms of source safety and security," CN-295/EVT2001738 "International Conference on Safety and Security of Radioactive Sources: Accomplishments and Future Endeavours , Vienna, Austria, 2022, Abstract ID:185

Yücel, H. (2024). *Radiation protection lecture notes*. Ankara University Institute of Nuclear Sciences.

Yücel, H. (2024a). *101516 Radiation detection and measurement methods lecture notes*. Retrieved June 9, 2024., f